Manganese–driven oxidation of aminopolyphosphonates studied by compound–specific carbon isotope analysis

Dissertation
der Mathematisch–Naturwissenschaftlichen Fakultät
der Eberhard Karls Universität Tübingen
zur Erlangung des Grades eines
Doktors der Naturwissenschaften
(Dr. rer. nat.)

vorgelegt von
Philipp Rafael Martin
aus Stuttgart

Tübingen
2021

Gedruckt mit Genehmigung der Mathematisch–Naturwissenschaftlichen Fakultät der Eberhard Karls Universität Tübingen.

Tag der mündlichen Qualifikation:	21.03.2022
Dekan:	Prof. Dr. Thilo Stehle
1. Berichterstatter:	Prof. Dr. Stefan B. Haderlein
2. Berichterstatter:	Prof. Dr. Torsten C. Schmidt

Abstract

Aminopolyphosphonates (APPs) are strong chelating agents within the group of anthropogenic organophosphorus compounds and are increasingly used in various industrial and household applications e.g., as antiscaling agents or bleaching stabilizers. Due to an incomplete removal in wastewater treatment plants, increasing emissions into the environment along with potential (eco–)toxicological risks are predicted. However, knowledge on the environmental fate of APPs is scarce, hampering a comprehensive environmental risk assessment. While APPs are believed to be mainly removed from the aqueous phase via sorption, the detection of their transformation products in the effluent of wastewater treatment plants indicates that they are also oxidized under environmentally relevant conditions. Processes likely contributing to the oxidation of APPs in technical and environmental systems are homogeneous Mn(II)–catalyzed oxidation by molecular oxygen and heterogeneous oxidation at manganese dioxide surfaces (MnO_2). The investigation of these processes solely by concentration analysis is hampered because the transformation products formed by oxidation of APPs are partially unspecific for different precursor substances as well as processes. In such cases, isotopic investigations by compound–specific carbon isotope analysis (carbon CSIA) can serve as valuable complementary tools, as they allow to gain information on the environmental fate of organic contaminants based on the isotopic composition of the precursor substance only.

The first goal of this work was the development of a liquid chromatography/ isotope ratio mass spectrometry (LC–IRMS) method for widely used (A)PPs. The chromatographic separation of 1–hydroxyethane 1,1–diphosphonate (HEDP), aminotrismethylene phosphonate (ATMP) and ethylenediaminetetramethylene phosphonate (EDTMP) was achieved on an anion exchange column under acidic conditions. The investigated APPs were quantitatively oxidized within the LC–IRMS interface with instrument typical limits of precise isotope analysis (around 200 ng carbon on column). In batch experiments we showed that equilibrium sorption of the model compound ATMP onto goethite did not cause a significant isotope effect. The manganese(II)–catalyzed oxidation of ATMP by molecular oxygen however, was associated with a kinetic isotope effect, leading to an enrichment in ^{13}C. Consequently, carbon CSIA is a promising approach to study transformation processes of APPs in aqueous system and thus get a more comprehensive understanding on their environmental fate.
In the second part of the work, a detailed investigation of the homogeneous manganese(II)–catalyzed oxidation of ATMP by dissolved oxygen was conducted to gain a better understanding of the role of potential Mn(III)ATMP intermediates. Therefore, the dependency of the kinetic carbon isotope fractionation (expressed as carbon isotope enrichment factor ε_C) and

Mn(II)ATMP–normalized reaction rate on the complexed ATMP fraction was investigated in batch experiments. As ATMP oxidation only by complex self–decomposition could not explain the decreasing normalized reaction rates and ε_C–values with the complexed ATMP fraction, transformation via two competing reaction pathways was hypothesized: oxidation of free ATMP by Mn(III)ATMP–intermediates at low complexed fractions and complex self–decomposition for low concentrations of free ATMP. This so far not known reaction pathway involving Mn(III)ATMP as oxidant has significant implications for the environmental fate of APPs. In natural waters, Mn(III)APP–intermediates are likely reduced to Mn(II)APP by natural reductants (e.g., natural organic matter) present at higher concentrations than the APPs. This entails to a diminished potential of Mn(II)–catalyzed oxidation for the transformation of APPs. Besides homogeneous Mn(II)–catalyzed oxidation, the heterogeneous transformation at MnO_2 surfaces was proposed as potentially relevant removal process for APPs. So far, studies investigating this process in terms of environmental relevance as well as underlying reaction mechanisms are lacking. In order to narrow this knowledge gap, the transformation of the model compound iminodimethylene phosphonate (IDMP) at MnO_2 was studied under varying environmental conditions (MnO_2 mineralogy, pH) in part three of this work. First–order reaction kinetics, as well as the relatively low ε_C–values indicated electron transfer from the mineral surface to the IDMP as rate–limiting step in the overall reaction, rather than sorption or bond cleavage. However, slightly but statistically significant lower ε_C–values (more pronounced observable kinetic isotope effects) at acidic pH and Mn(III)–enriched MnO_2, implied facilitated electron transfer under these conditions. Thus, while a qualitative proof of IDMP oxidation at MnO_2 by carbon CSIA was feasible under all tested experimental conditions, the variability of the ε_C–values hampers a clear identification of the underlying process.

This work demonstrates the potential of carbon CSIA as a valuable tool to study sources and fate of APPs in technical and environmental systems. First applications of the method resulted in an improved understanding of homogeneous and heterogeneous manganese–driven oxidation of APPs and subsequently the role of these processes for the environmental fate of APPs. In future studies, the developed method can be applied to investigate further relevant sorption and transformation processes. These findings contribute to a more comprehensive understanding of the environmental chemistry of APPs.

Kurzfassung

Aminopolyphosphonate (APPs) sind starke Chelatbildner innerhalb der Gruppe der anthropogenen Organophosphorverbindungen und werden zunehmend in verschiedenen Industrie– und Haushaltsanwendungen eingesetzt, z.B. als Entkalkungsmittel oder Bleichstabilisatoren. Aufgrund der unvollständigen Entfernung in Kläranlagen werden zunehmende Emissionen in die Umwelt und damit verbundene potenzielle (öko–)toxikologischen Risiken vorhergesagt. Allerdings ist das Wissen über den Verbleib von APPs in der Umwelt spärlich, was eine umfassende Bewertung der Umweltrisiken erschwert. Während angenommen wird, dass APPs hauptsächlich durch Sorption aus der wässrigen Phase entfernt werden, weißt der Nachweis ihrer Transformationsprodukte im Abwasser von Kläranlagen darauf hin, dass sie unter umweltrelevanten Bedingungen ebenfalls oxidiert werden. Prozesse, die wahrscheinlich zur Oxidation von APPs in technischen und Umweltsystemen beitragen, sind die homogene Mn(II)–katalysierte Oxidation durch molekularen Sauerstoff und die heterogene Oxidation an Mangandioxid–Oberflächen (MnO_2). Die Untersuchung dieser Prozesse allein durch Konzentrationsanalyse wird jedoch dadurch erschwert, dass die bei der Oxidation von APPs gebildeten Transformationsprodukte teilweise sowohl für verschiedene Vorläuferverbindungen als auch für verschiedene Oxidationsprozesse unspezifisch sind. In solchen Fällen können Isotopenuntersuchungen mittels substanzspezifischer Kohlenstoffisotopenanalyse (engl.: compound–specific carbon isotope analysis, carbon CSIA) als wertvolles ergänzendes Instrument dienen, da sie es ermöglichen, Informationen über den Verbleib organischer Schadstoffe in der Umwelt auf der Grundlage der Isotopenzusammensetzung der Vorläufersubstanz zu gewinnen.

Das erste Ziel dieser Arbeit war die Entwicklung einer Flüssigchromatographie/ Isotopenverhältnis–Massenspektrometrie–Methode (LC–IRMS) für weit verbreitete (A)PPs. Die chromatographische Trennung von 1–Hydroxyethan–1,1–diphosphonat (HEDP), Aminotrismethylenphosphonat (ATMP) und Ethylendiamintetramethylenphosphonat (EDTMP) wurde auf einer Anionenaustauschersäule unter sauren Bedingungen erzielt. Die untersuchten APPs wurden innerhalb der LC–IRMS–Schnittstelle quantitativ oxidiert, wobei die instrumententypischen Grenzen der präzisen Isotopenanalyse (etwa 200 ng Kohlenstoff auf der Säule) erzielt wurden. In Batch–Experimenten zeigten wir, dass die Gleichgewichtssorption der Modellverbindung ATMP an Goethit keinen Isotopeneffekt verursachte. Die Mangan(II)–katalysierte Oxidation von ATMP durch molekularen Sauerstoff war jedoch mit einem kinetischen Isotopeneffekt verbunden, der zu einer Anreicherung von ^{13}C führt. Folglich ist die Kohlenstoff–CSIA ein vielversprechender Ansatz, um Transformationsprozesse von APPs in wässrigen Systemen zu untersuchen und somit ein umfassenderes Verständnis ihres Verbleibs in der Umwelt zu

erhalten.
Im zweiten Teil der Arbeit wurde eine detaillierte Untersuchung der homogenen Mangan(II)–katalysierten Oxidation von ATMP durch gelösten Sauerstoff durchgeführt, um ein besseres Verständnis der Rolle potenzieller Mn(III)ATMP–Intermediate zu gewinnen. Hierfür wurde die Abhängigkeit der kinetischen Kohlenstoffisotopenfraktionierung (ausgedrückt als Kohlenstoffisotopenanreicherungsfaktor ε_C) und der Mn(II)ATMP–normalisierten Reaktionsgeschwindigkeit von der komplexierte ATMP Fraktion in Batch–Experimenten untersucht. Da die ATMP–Oxidation ausschließlich durch Zerfall des Komplexes die abnehmenden normalisierten Reaktionsraten und ε_C–Werte mit der komplexierten ATMP–Fraktion nicht erklären konnten, wurde eine Transformation von ATMP über zwei konkurrierende Reaktionswege postuliert: Oxidation von freiem ATMP durch Mn(III)ATMP–Intermediate bei niedrigen komplexierten Fraktionen und Zerfall des Komplexes bei niedrigen Konzentrationen von freiem ATMP. Dieser zuvor nicht bekannte Reaktionsweg, an dem Mn(III)ATMP als Oxidationsmittel beteiligt ist, hat erhebliche Auswirkungen auf das Umweltverhalten von APPs. In natürlichen Gewässern werden Mn(III)APP–Intermediate wahrscheinlich von natürliche Reduktionsmittel (z.B. natürlichem organischen Material), die in höheren Konzentrationen als die APPs vorhanden sind, zu Mn(II)APP reduziert. Dies hat ein vermindertes Potenzial der Mn(II)–katalysierten Oxidation für deren Transformation zur Folge.
Neben der homogenen Mn(II)–katalysierten Oxidation wurde die heterogene Umwandlung an MnO_2–Oberflächen als potenziell relevanter Entfernungsprozess für APPs postuliert. Bisher fehlen Studien, die diesen Prozess im Hinblick auf seine Umweltrelevanz und die zugrunde liegenden Reaktionsmechanismen untersuchen. Um diese Wissenslücke zu schließen, wurde im dritten Teil dieser Arbeit die Umwandlung der Modellverbindung Iminodimethylenphosphonat (IDMP) an MnO_2 unter variierenden Umweltbedingungen (MnO_2–Mineralogie, pH–Wert) untersucht. Eine Reaktionskinetik erster Ordnung sowie relativ niedrige ε_C–Werte deuteten auf Elektronentransfer von der Mineraloberfläche auf das IDMP als den geschwindigkeitsbestimmenden Schritt in der Gesamtreaktion hin und nicht die Sorption oder die Bindungsspaltung. Geringfügig, aber statistisch signifikant niedrigere ε_C–Werte (größere zu beobachtende kinetische Isotopeneffekte) bei saurem pH–Wert und Mn(III)–angereichertem MnO_2 deuten jedoch auf einen beschleunigten Elektronentransfer unter diesen Bedingungen hin. Während also ein qualitativer Nachweis der IDMP–Oxidation an MnO_2 durch Kohlenstoff–CSIA unter allen getesteten Versuchsbedingungen möglich war, erschwert die Variabilität der ε_C–Werte eine eindeutige Identifizierung des zugrunde liegenden Prozesses.

Diese Arbeit zeigt das Potenzial der Kohlenstoff–CSIA als wertvolles Instrument um die Quellen und den Verbleib von APPs in technischen und Umweltsystemen zu untersuchen. Erste Anwendungen der Methode führten zu einem verbesserten Verständnis der homogenen und heterogenen Mangan–getriebenen Oxidation von APPs und somit der Rolle dieser Prozesse für das Umweltverhalten von APPs. In zukünftigen Studien kann die entwickelte Methode eingesetzt werden um weiterer Sorptions– und Umwandlungsprozesse zu untersuchen. Diese Erkenntnisse tragen zu einem umfassenderen Verständnis der Umweltchemie von APPs bei.

Contents

List of Figures

List of Tables

1 General introduction

1.1 Phosphonates in nature – Properties and relevance

Organo–phosphonates are the corresponding anions of phosphonic acids, which are characterized by a $R-C-PO_3H_2$ moiety. The first synthetic and naturally occurring representatives described are aminomethyl phosphonate (AMPA) and 2–aminoethyl phosphonate (2–AEP), which were isolated in the 1940s and 1950s, respectively.[1,2] Since then, numerous (bio–)synthetic phosphonates were identified, ranging from small compounds (e.g., 2–AEP) to macromolecules, such as phosphonolipids.[1,3] One major interest to study the (bio–)chemistry of phosphonates was (and still is) their similarity regarding structure and physico–chemical properties to phosphate (mono–)esters ($R-O-PO_3^{2-}$), the widest spread group of natural phosphorus–containing organics.[4] Essential for biochemical processes, for instance as part of genetic material (DNA and RNA) or as biochemical "battery" (ATP), phosphate esters can be seen as a compound class with an – or even the most – outstanding biological importance in earth's history amongst all biomolecules.[5,6] Phosphate mono–esters and phosphonates have in common that they are diprotic and thus tend to form complexes with di– and trivalent cations.[7,8] A crucial difference however, is the stability of the $C-P$ bond in comparison to its counterpart in phosphate esters.[3] While the hydrolysis of $R-O-P$ bonds is readily catalyzed by enzymes, the $R-C-P$ bond in phosphonates is stable against hydrolysis, as well as thermal degradation and photolysis due to a high activation energy needed for its cleavage.[9,10] This stability in combination with the similar steric configuration compared to phosphate esters and amino (carboxylic) acids result in the biochemical activity of phosphonates.[1] Phosphonates and amino–phosphonates in particular are able to compete with phosphate esters and amino acids for active sites of enzymes.[4,11,12] Due to the chemical stability of phosphonates, they often cannot be utilized by enzymes, leading to the inhibition of the enzyme.[13,14] As a consequence, microbially synthesized phosphonates comprise amongst others small biomolecules acting as antibiotics and herbicides.[1]

Despite their stability, specialized microorganisms are able to utilize phosphonates as phosphorus source by cleaving the $C-P$ bond, catalyzed by various enzyme families, for instance by $C-P$ lyase–type enzymes.[9,10] Considering that phosphonates are believed to contribute substantially to the total dissolved P pool in the environment (e.g., up to 25 % in oceans), they likely represent an important organic phosphorus source in some environments.[15]

Due to the chemical stability and (bio–)chemical activity of natural phosphonates, synthetic analogues making use of these beneficial properties are of growing commercial importance. The most prominent representatives are phosphonate–based pesticides, foremost glyphosate (N–(phosphonomethyl)glycine), the quantitatively most applied herbicide worldwide.[16] Moreover, phosphonates are used as flame retardants and antiviral drugs.[17,18] Polyphosphonates (i.e., representatives containing multiple phosphonic acid moieties) are increasingly used as antiscalants and bleaching stabilizers in industrial and household applications and will be discussed hereafter.[19]

1.2 Polyphosphonate chelating agents – Properties and usage

Polyphosphonate chelating agents (PPs) are a group of synthetic phosphonates characterized by three or more ($R-C-PO_3^{2-}$) moieties. The quantitatively most important polyphosphonates are 1–hydroxyethane–1,1–diphosphonate (HEDP), 2–phosphonobutane–1,2,4–tricarboxylate (PBTC), aminotrismethylene phosphonate (ATMP), ethylenediaminetetramethylene phosphonate (EDTMP) and diethylenetriaminepentamethylene phosphonate (DTPMP) (see **Figure 1.1**). ATMP, EDTMP and DTPMP are characterized by at least one tertiary amine group and therefore called aminopolyphosphonates (APPs).

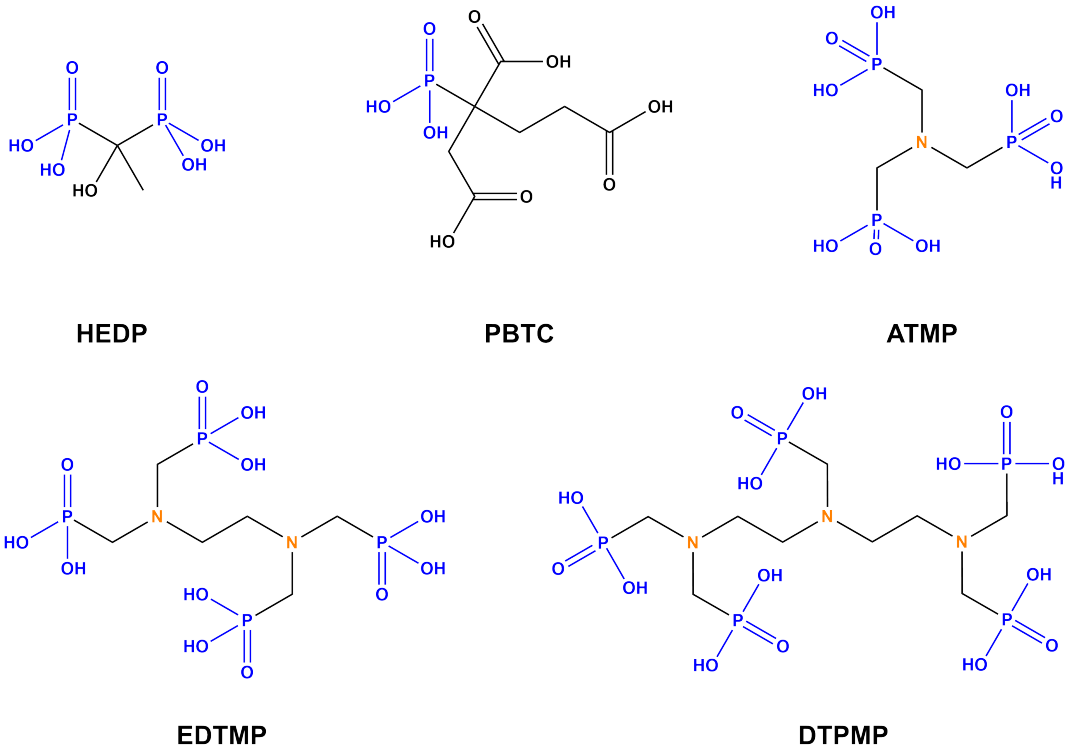

Figure 1.1: Chemical structures of the polyphosphonic acids 1–hydroxyethane–1,1–diphosphonic acid (HEDP), 2–phosphonobutane–1,2,4–tricarboxylic acid (PBTC), aminotrismethylene phosphonic acid) (ATMP), ethylenediaminetetramethylene phosphonic acid (EDTMP) and diethylenetriaminepentamethylene phosphonic acid (DTPMP). Phosphonic acid and amine groups are marked in blue and orange, respectively.

PPs and their salts are highly soluble in water ($\geqslant 21\,g\,L^{-1}$), consequently have very low Henry constants (1×10^{-18} atm m^3 mol^{-1} to 1×10^{-17} atm m^3 mol^{-1}) and low tendency to partition into organic phases ($\log(K_{ow})$ -3.4 for DTPMP and -4.1 for EDTMP).[19] They exhibit high complex formation constants (K_{compl}) with di– and trivalent cations due to their ability to act as chelates. The complex formation constants are in most cases (slightly) higher than the constants for the corresponding polycarboxylates. Exemplified by ATMP (compared to its analogue NTA), $\log(K_{compl})$–values range from 7.2 (NTA: 6.4) for magnesium to 16.4 (NTA: 10.7) for zinc.[20] As a rule of thumb, the complex formation constant for polyphosphonates increases with (i) the number of phosphonic acid moieties and (ii) the cations tendency for

hydrolysis, i.e., its acidity.[20,21] Consequently, K_{compl}–values are (i) highest for DTPMP among the aforementioned polyphosphonates and (ii) lower for (earth) alkali metals compared to transition and heavy metals.[20] The tendency of PPs to form stable complexes with essential (trace) metals is the reason for their indirect toxicity towards some aquatic and soil organisms, such as algea.[22] However, high no–observed–effect concentrations (NOEC) of PPs in the mg L^{-1}–range imply a low acute toxicity. These findings in combination with low (predicted) environmental concentrations of PPs indicate a low environmental risk for acute (eco–)toxicity so far.[19,23]

The combination of their (i) high complex formation constants for di– and trivalent cations (e.g., Ca(II) and Fe(III)), (ii) resilience towards chemical degradation and (iii) low toxicity led to the growing commercial importance of polyphosphonates over the last decades. PPs are mainly applied as scale inhibitors and anti–fouling agents in membrane filtration and cooling waters, as stone formation inhibitors in oil drilling as well as bleaching stabilizers in the textile and paper industry. In household and industrial cleaners, they are increasingly used as complexing agents and bleaching stabilizers.[24,25] Further applications include cosmetics (as bleaching stabilizers), concrete and cement (as high temperature solidification delaying agents) and pharmaceutical products (as Ca(II) chelating agents in medication for the treatment of bone diseases).[19] The global consumption of polyphosphonates increased from 56 kt a^{-1} in 1998 to 96 kt a^{-1} in 2012 (and from 15 kt a^{-1} to 49 kt a^{-1} in Europe).[19] More recent data emphasize the use of phosphonates in cleaning agents and detergents in Germany, which increased from 1.9 kt a^{-1} in 1994 to 7.6 kt a^{-1} in 2019.[26] Since the 1980s, they replaced structurally similar amino–polycarboxylates (e.g., ethylenediaminetetra acetate, EDTA) and polyphosphates, which showed adverse environmental effects such as remobilization of heavy metals from sediments and surface water eutrophication.[27,28]

1.3 Environmental chemistry and fate of (amino–)polyphosphonates

Due to their high complex formation constants with di– and trivalent metal cations, PPs strongly adsorb onto metal (hydr–)oxides via surface–complexation at environmentally relevant pH–values.[29,30] The formation of ternary surface–calcium–phosphonate complexes can further enhance the sorption of PPs.[31,32] The interaction with natural sorbents other than (hydr–)oxide is less studied. ATMP was shown to sorb onto immobilized humic acid, with highly pH dependent sorption capacity. Sorption was strong at acidic conditions (pH 3.6 – 4.8) but negligible at pH–values higher than 6.[29] Sorption to clay minerals has not been investigated so far for APPs. For HEDP however, the affinity to bentonite clay was found to be in the same order of magnitude as for goethite. Complexation to surface functional groups as well as intercalation were proposed as sorption mechanisms.[30,33] For clay minerals a correlation between the sorption capacity and the amount of (hydr–)oxidic bound metals was found.[33] This observation supports the assumption that PPs mainly interact with clay minerals via functional surface groups. Similar observations were made for the sorption of ortho–phosphate onto clay minerals

with varying acid–extractable contents of iron, aluminium, manganese, and calcium.[34] Various studies investigated the sorption of PPs onto complex sorbent matrices, such as activated/ digested sewage sludge or sediments. Metal oxides, clay minerals and organic matter were proposed as most important sorbents.[29,35] However, many of these studies lack detailed information on the composition of the sorbent matrix (e.g., mineral composition) and therefore do not allow to draw conclusions on the sorption mechanism.[19]

Besides adsorption, several pathways leading to oxidative breakdown of complexed PPs are described in literature, although PPs in freely dissolved (i.e., non–complexed) form are considered to be resistant towards biodegradation as well as abiotic degradation.[19,23] Investigated oxidation processes include photodegradation of Fe(III)–complexes, Mn(II)–catalyzed oxidation by dissolved oxygen and advanced oxidation processes (AOPs, e.g., Fenton's reaction and ozonation). Most studies indicated that APPs are more prone to oxidation in comparison to amine–free PPs, emphasizing the role of the amine functional group for electron transfer.[36–39] As a consequence, more studies on the oxidation of APPs are available in literature. Iron–catalyzed photo–degradation is considered the most important transformation pathway for APPs in surface waters, due to the high reactivity of Fe(III)–APP complexes.[23,25] For EDTMP, an averaged half–life of 26 h for central European surface waters was calculated, based on lab–determined quantum yields of the Fe(III)–EDTMP complex.[40] The degradation scheme was similar to the photodegradation of EDTA. However, in contrast to EDTA, the final product of EDTMP degradation (N–methyl–aminomethylene phosphonate) was stable under the investigated conditions, as it did not form a strong iron–complex.[40] Although other complexing metal ions or competing ligands likely affect the degradation rates of APPs, further data are not available. The photo–transformation of the Fe(III)–complexes of ATMP, EDTMP and DTPMP under irradiation of a middle–pressure mercury lamp revealed ortho–phosphate and AMPA as transformation products, with AMPA yields of up to 7 %.[41] Hence, APP oxidation might be a significant source for AMPA, which so far is considered to originate primarily from the degradation of the herbicide glyphosate.[42] Consequently, AMPA formation from APP oxidation could challenge the interpretation of AMPA concentrations in water bodies as an indicator for glyphosate (bio–)degradation. Another transformation pathway for APPs hypothesized to be relevant in soils and sediments is manganese–driven oxidation. Nowack and Stone reported the degradation of ATMP, EDTMP and DTPMP in the presence of Mn(II) and dissolved oxygen, as well as the degradation of ATMP by manganite (Mn(III)OOH) under oxic and anoxic conditions.[37,43,44] The amino–monophosphonates glyphosate and AMPA were also shown to be oxidized at manganese oxide surfaces, while Mn(II)–catalyzed oxidation in homogeneous aqueous solution was not observed.[45] Nitrogen–free PPs, such as HEDP were not oxidized.[37] Iminomethylene phosphonate (IDMP), N–formyl–iminomethylene phosphonate (FIDMP), formaldehyde, as well as ortho–phosphate were identified as transformation products of ATMP oxidation. Bis(phosphonomethyl) carbamate – formed via the oxidation of FIDMP – was proposed as a further transformation product but was not identified so far. The proposed reaction mechanism of ATMP oxidation comprises (i) the formation of a methylene radical,

resulting from C−P bond cleavage and (ii) the rapid oxidation of the radical to either IDMP or FIDMP. The fact that these two primary transformation products were detected in the effluent of a Swiss waste water treatment plants (WWTP) implies that this pathway also takes place in technical systems.[44] A more detailed discussion on the general role of manganese as potent oxidant and catalyst in environmental and technical systems follows below.

In summary, PPs are considered to be removed from the aqueous phase mainly via sorption due to their strong interaction with various sorbents.[46] Consequently, high elimination rates of 80 % to 90 % determined in WWTP were attributed mainly to sorption onto sewage sludge. Based on these numbers, a discharge of 1.2 kt a^{-1} to 4.9 kt a^{-1} of PPs to receiving waters in Europe was estimated.[19] Accordingly, dissolved polyphosphonate concentrations in selected German rivers in the ng L^{-1} to low µg L^{-1} range were found.[47–49] PPs were detected on suspended matter in WWTP effluent, thus contributing also to the particulate phosphorous fraction.[19,49] Although (partial) transformation of this emitted polyphosphonate fraction is likely, knowledge on transformation rates and the formation of transformation products such as phosphate and AMPA is scarce. However, these processes are of high relevance due to possible adverse effects on receiving surface waters and sediments with respect to eutrophication or ecotoxicology. The earlier discussed oxidation processes have in common that they finally lead to the release of ortho–phosphate after C−P bond cleavage. Hence, it can be assumed that polyphosphonates represent a significant phosphorous source in WWTP effluent receiving surface waters.[19] This applies in particular to APPs, which are more prone to oxidative breakdown than N–free PPs. Consistently, it was shown recently that concentrations of the amino–free PPs HEDP and PBTC are significantly higher than APP concentrations in the effluent of two German WWTPs and in the sediments of the receiving rivers, implying a faster breakdown of APPs.[48,49] Yet, no identification or even quantification of potential transformation products was conducted in these studies. As identified transformation products include also potentially problematic compounds such as AMPA, a better understanding on the environmental fate PPs is needed.

1.4 The role of manganese as environmental oxidant and catalyst

Manganese makes up 0.1 % by weight of the earth's crust and is considered the second most important transition metal in biogeochemical cycles following iron.[50,51] Manganese exhibits a complex redox chemistry and is found in various redox states, ranging from +II (e.g., manganese chloride), over +IV (e.g., manganese dioxide) to +VII (e.g., permanganate). Among these, Mn(+II) to Mn(+IV) species are the most common ones under environmentally relevant conditions, i.e., within the stability range of water.[52,53] Mn(II) is the predominant dissolved manganese species due to (i) the high solubility of most Mn(II)–salts and (ii) the slow abiotic oxidation by molecular oxygen at pH–values below 9. Various microbial strains however, effectively catalyze Mn(II)–oxidation by molecular oxygen, leading to the formation of manganese(III/IV) oxides.[54,55] This group of minerals belongs to the most potent natural oxidants, with standard oxidation potentials (E^0) in the range of 1.2 V to 1.5 V and around 0.6 V for

environmentally relevant concentrations at pH 7 (E^w).[56,57] These properties, in combination with their low crystallinity and resulting high surface area, make manganese oxides – despite their low concentration in soils and sediments – substantially involved in the biogeochemical cycling of various soil and water constituents.[58,59] Manganese oxides are considered an important driver in the carbon cycle, because they are able to both stabilize and destabilize natural organic matter (NOM) in soils and sediments depending on the governing reaction process, such as adsorption/complexation, oxidative breakdown or polymerisation.[60] Furthermore, manganese oxides are able to adsorb and oxidize organic contaminants, as well as heavy metals and therefore influence their mobility and toxicity in the environment.[61,62]

Manganese(III) is known for its important biochemical role as active center of enzymes, such as (i) the Mn(II/III) superoxide dismutase family or (ii) the photosystem II, in which Mn(III/IV) is part of the oxygen–evolving centre.[63–65] Due to a lack of studies however, knowledge on the distribution and reactivity of dissolved Mn(III)–complexes in the environment was limited until a few years ago and dissolved manganese was presumed to be exclusively Mn(II).[66,67] Owing to the thermodynamic instability of free Mn(III) (aquo–complexes) and the resulting rapid disproportionation to Mn(II)/Mn(IV), manganese(III) was an overlooked redox state and only assumed to be stable under controlled laboratory conditions, for instance when complexed with an excess of pyrophosphate.[54,55] However, in the last decade several studies showed that Mn(III) can also be stabilized under environmental conditions by complexation with natural ligands like (i) siderophores (i.e., biologically synthesized chelating agents) such as desferrioxamine B (DFOB) or (ii) complex natural organic matter (NOM).[66,68–70] Manganese(III)–complexes were identified in oxic and suboxic environmental water samples by spectroscopic and electrochemical methods and it could be shown that up to 90 % of dissolved manganese in suboxic marine environments was bound in Mn(III)–complexes.[70–72] These findings underlined that Mn(III) is a so far overlooked redox buffer in aquatic environments as it can act as oxidant as well as reductant and thus stabilize suboxic conditions.[70]

Besides its role in biogeochemical cycles, the potential of Mn(III)(–complexes) as AOP oxidants for the transformation of organic contaminants is increasingly being investigated in recent years.[73,74] Manganese(III) generated *in–situ* by the (electro–)chemical reduction of persulfate or manganese oxides was shown to effectively oxidize various compounds, including diclofenac, bisphenols, atrazine and 4–chlorophenol via an one–electron transfer.[74–76] Obtained reaction rates were considerably higher (factor 10^3 to 10^5) than those of non–activated MnO_4^- and MnO_2. When Mn(III) was only weakly stabilized by bisulfite (HSO_3^-), higher reaction rate constants than for hydroxyl radicals were obtained in some cases.[74,77] While only shown in laboratory model systems so far, these studies emphasize the potential role of Mn(III)(–complexes) as strong one–electron oxidant for organic contaminants in environmental and technical systems.[52]

1.5 Compound–specific isotope analysis (CSIA) and stable isotope fractionation

Compound–specific isotope analysis (CSIA) is increasingly used in the field of environmental chemistry to track origin and fate of organic contaminants in the environment.[78] CSIA has been applied for (i) contaminant source identification, (ii) detection and (iii) quantification of *in–situ* (bio–)degradation and (iv) identification of reaction pathways and (v) the underlying reaction mechanisms.[79,80]

As compound–specific isotope ratio mass spectrometry traditionally was coupled to gas–chromatographic separation (GC–IRMS), the range of target analytes was restricted to (semi–)volatile or derivatizable analytes for a long time.[78] Today, a liquid–chromatography interface for carbon isotope ratio mass spectrometry (LC–IRMS) is available, allowing carbon CSIA of water–soluble, non–volatile compounds. The system is based on (i) the chromatographic separation of the analytes by an inorganic, carbon–free eluent, (ii) the (semi–)quantitative wet–chemical oxidation of the analytes to carbon dioxide by heat–activated persulfate (i.e., sulfate radicals) in the eluent stream and a subsequent transfer of the CO_2 into the carrier gas stream and finally (iii) detection of the CO_2–isotopologues in the IRMS, from which the isotopic signature of the analytes are calculated (see **Figure 1.2**).[81]

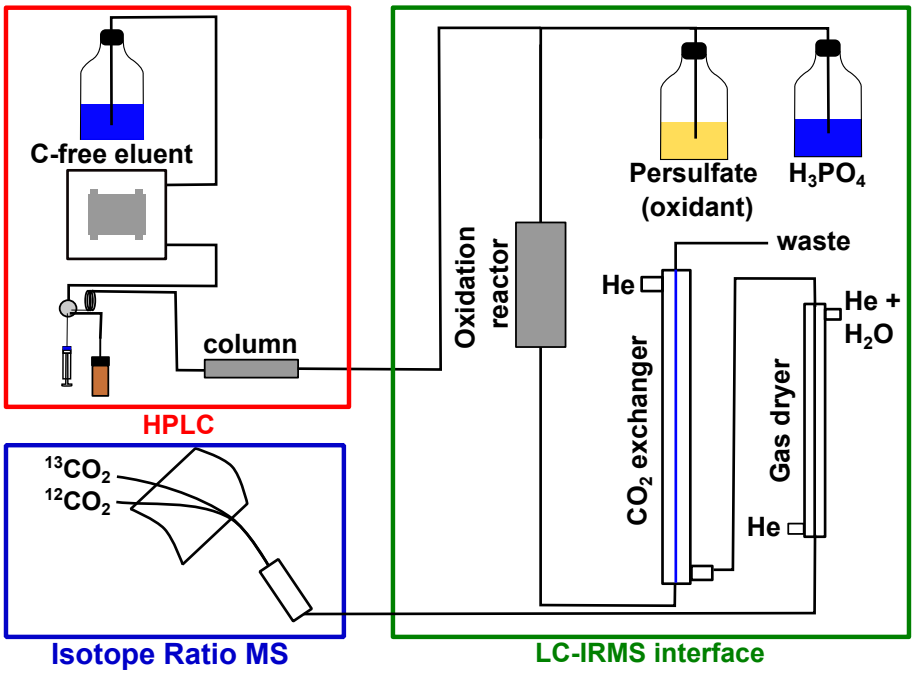

Figure 1.2: Scheme of the liquid chromatography/ isotope ratio mass spectrometry (LC–IRMS) coupling, comprising of (i) a HPLC for analyte separation, (ii) the interface for the wet–chemical oxidation of organic carbon to CO_2 and (iii) IRMS for detection of the CO_2 isotopologues.

Despite the limitations of this approach, especially the restriction to inorganic, carbon–free eluents and buffers hampering chromatographic separation, LC–IRMS methods for several compound classes were developed in recent years including amino acids, halogenated organic

acids, antibiotics and herbicides.[82–85] Applied separation techniques include size–exclusion, ion exchange, mixed–mode, as well as high–temperature liquid chromatography.[86,87]

The investigation of the environmental fate of organic compounds by CSIA is based on the analysis of their stable isotopic composition (at natural abundance).[88] In general, organic compounds comprise a mixture of molecules possessing either a heavy (^{13}C for carbon) or light (^{12}C) isotope of the element of interest – so called isotopologues. The relative abundances of two stable isotopes in a compound are reported as isotopic ratio R (e.g., $R_C = {}^{13}C/{}^{12}C$ for carbon) which is usually converted to a delta–value (e.g., δ^{13}C for carbon) by normalizing R to an international standard (see **Equation 1.1**). In the case of carbon, the standard material is represented by the carbonate Vienna Peedee belemnite (VPDB) with an isotopic ratio of $R_{C,VPDB} = 0.011180$.[89] As physical and chemical processes lead only to small isotopic shifts in the order of 10^{-5} to 10^{-4}, the delta–value is usually expressed in per mil (‰).

$$\delta^{13}C = \left(\frac{R_{comp}}{R_{std}} - 1\right) \times 1000\,‰ \tag{1.1}$$

(Bio–)chemical transformation processes often discriminate between the isotopologues exhibiting a heavy isotope at the reactive position and those exhibiting a light isotope, resulting in slightly different reaction rate constants. The ratio between these isotopologue–specific reaction rates is termed kinetic isotope effect (KIE = $^{l}k/^{h}k$). In most cases, the KIE is greater than unity, i.e., leads to gradual enrichment of the lighter isotopologues in the product pool, while the heavier isotopologues accumulate in the remaining reactant pool ("normal" KIE). The extent of the observed shift in the isotopic composition can be expressed by an isotope enrichment factor, ε. In closed systems, the Rayleigh distillation equation (**Equation 1.2**) can be used to determine ε–values from measured isotope ratios and the remaining fraction (i.e., normalized concentration) of the reactant.[90]

$$\ln\left(\frac{R(t)}{R(0)}\right) = \ln\left(\frac{\delta^{13}C(t)+1}{\delta^{13}C(t)+1}\right) = \varepsilon_C \times \ln\left(f(t)\right) \tag{1.2}$$

$R(0)$ and δ^{13}C(0) is the initial, $R(t)$ and δ^{13}C(t) the actual measured (normalized) isotope ratio and $f(t)$ is the remaining substrate fraction (i.e., $c(t)/c(0)$) at a certain time point.

So far, carbon isotope fractionation has been successfully used to identify (bio–)degradation of legacy contaminants such as chlorinated ethenes at field sites, and under favourable conditions, to quantify the extent of (bio–)degradation.[80,91] Furthermore, isotope fractionation provides information on the underlying reaction pathways, or even mechanisms.[90,92] This is possible, as the measured ε–value is indirectly linked to the KIE of the underlying reaction. However, as all carbon atoms of the target analyte are measured after it has been quantitatively oxidized to CO_2, not the intrinsic isotope fractionation at the reactive (i.e., cleaved) bond, but rather an averaged ("diluted") isotope fractionation over the complete molecule is measured. Nevertheless, an apparent (i.e., observed) kinetic isotope effect (AKIE) referring to the intrinsic KIE associated

with bond cleavage can be determined from CSIA data, by correcting for non–reactive carbon atoms. For a symmetric molecule with all carbon atoms chemically equal and positioned at the reactive bond, the $AKIE_C$ at the reacting position can be approximated by means of **Equation 1.3**.[90]

$$AKIE_C \approx \frac{1}{n_C \times \varepsilon_C + 1} \tag{1.3}$$

Here, n_C denotes the total number of carbon atoms.

AKIE values can be compared to theoretical semi–classical Streitwieser limits to elucidate the underlying reaction mechanisms. The Streitwieser limit represents the maximum intrinsic kinetic isotope effect for the cleavage of a chemical bond. Its calculation is based on the difference in the vibrational energies of the reactive bonds involving either the light or heavy isotope of the element of interest. Thus, the Streitwieser limit represents a simplified situation, as other factors contributing to the KIE are neglected (e.g., effects of additional bonds). Furthermore, it is assumed that the bond–cleavage at the reactive position is the rate–limiting step of the overall reaction.[88] However, this simplified assumption usually does not necessarily hold in environmentally relevant transformation processes, as they do not only comprise the bond cleavage step but may also include preceding steps such as mass transfer of the reactant to the reaction site or formation of a precursor complex.[93] These steps are typically not associated with a pronounced isotope effect, as they affect the whole molecule and/ or usually do not lead to bond–cleavage or formation.[88] Within such multistep reactions, the slowest (i.e., rate–limiting) step typically dominates the observed isotope effect.[90] Consequently, in reactions where non–fractionating steps are slower than the bond–cleavage step (which is assumed to fractionate), the observed isotope fractionation gets diminished, as the intrinsic KIE of bond–cleavage gets masked.[90] Therefore, information on rate–limiting steps within a reaction cascade can be obtained by CISA. However, as in many cases the underlying mechanisms of a reaction are not fully understood, masking also complicates the deciphering of the reaction mechanism, as the observed KIE might be ambiguous, pointing to either (i) a mechanism associated with a low KIE, or (ii) a mechanism associated with a high, but masked KIE. This obstacle can be overcome by dual (2D) CSIA, i.e., combining two isotope systems (e.g., $\delta^{13}C/\delta^{15}N$).[94] As masking steps such as phase transfer processes typically affect the complete molecule (i.e., both investigated isotope systems), they are cancelled out in 2D isotope plots, allowing a more reliable differentiation of reaction pathways by 2D CSIA.[90,95]

The absence of significant isotope fractionation for phase transfer processes (e.g., sorption or volatilization) furthermore implies that isotopic investigations can be used to differentiate between transformation and sorption/ volatilization as case for a concentration decrease of contaminants in the aqueous phase. For non–polar organic contaminants, such as aromatic or halogenated hydrocarbons this was already demonstrated in various studies.[96,97] However, the

assumption of the absence of significant isotope fractionation during sorption might not hold in the case of polyphosphonates. In contrast to non–polar organics, which are sorbing via weak, unspecific van der Waals forces, phosphonates are considered to sorb via the formation of strong inner–sphere surface–complex between one (monodentate complex) or two (bidentate complex) phosphonic acid group and the mineral.[31,98–100] So far, knowledge on the isotope fractionation associated with chemical sorption of ionic organics such as polyphosphonates is scarce. However, various studies on inorganic anions are available, which are assumed to sorb via similar mechanisms. Sorption of ortho–phosphate to ferrihydrite showed significant oxygen isotope fractionation.[101] Preferential sorption of light isotopologues was also observed for various oxyanions, e.g., Si–isotope fractionation in ortho–silicate and Bo–isotope fractionation in ortho–borate.[102,103] Based on these findings, an oxygen isotope fractionation is also conceivable for the sorption polyphosphonates onto mineral (hydr–)oxides. According to the proposed mechanism however, no carbon–containing functional groups are involved in the complex formation. Hence, carbon can only be subjected to a secondary isotope effect, which occurs at positions in the vicinity of the reactive bond and arise for instance from coordination geometry changes within the molecule. These secondary isotope effects are around one order of magnitude lower than primary ones caused by vibrational energy differences.[90]

Summarizing, significant carbon isotope effects during sorption of polyphosphonates are unlikely. However, in order to allow a profound interpretation of natural processes governed by superimposed transformation and sorption (e.g, transformation at mineral surfaces) by stable isotope analysis, sorption–associated isotope effects should be addressed in future studies.

1.6 Objectives and structure of the thesis

Despite their growing consumption in industrial and household applications, knowledge on the environmental fate of amino–polyphosphonates with respect to the significance of sorption and transformation for their removal from the aqueous phase is limited. The use of concentration analysis to get deeper insights into these processes is hampered by the fact that the potential transformation products such as IDMP, AMPA or phosphate are unspecific. A promising, but so far unexploited tool to overcome these obstacles is compound–specific isotope analysis (CSIA), which allows to gain insights into the aforementioned processes solely based on the analysis of the parent compound. Prerequisites for this are defined laboratory experiments under controlled conditions in order develop a comprehensive understanding of the isotope fractionation associated with sorption as well as transformation processes. For this reason, the presented work aimed to (i) set the analytical foundation for carbon CSIA of APPs by developing a LC–IRMS method as well as (ii) apply this method to get deeper insights into environmentally relevant transformation processes of APPs in the presence of manganese (oxides) and dissolved oxygen.

The presented research work is organized in five chapters. In **chapter 1**, an introduction to phosphonates in general and the environmental chemistry of (amino–)polyphosphonates

in particular, as well as the role of manganese as oxidant and catalyst in the environment is provided. Furthermore, the concepts of stable isotope fractionation and compound–specific isotope analysis (CSIA) are discussed, with focus on carbon CSIA of ionic, water–soluble analytes by liquid–chromatography/ isotope ratio mass spectrometry (LC–IRMS). **Chapter 2** describes the development of a LC–IRMS method for HEDP, ATMP and EDTMP, which represents the indispensable prerequisite for further investigation of polyphosphonates by carbon CSIA. The method development comprised of (i) the chromatographic separation of the analytes, as well as (ii) optimization of the wet–chemical oxidation conditions for a quantitative mineralization of the analytes to CO_2. The optimized method was evaluated with respect to the limit of precise isotope analysis, i.e., the detection limit for the analysis of true and precise δ^{13}C–values. Finally, the potential of isotope analysis to differentiate between concentration loss of ATMP from the aqueous phase by either equilibrium sorption onto goethite or Mn(II)–catalyzed oxidation was investigated. In **chapter 3**, a study on the mechanisms of homogeneous Mn(II)–catalyzed oxidation of ATMP by dissolved oxygen is presented. Previous work hypothesized Mn(III)–complexes as key intermediates for the oxidation of ATMP via inner–sphere electron transfer. Furthermore, side reactions involving Mn(III)ATMP–species as oxidants cannot be excluded based on the described reactivity of Mn(III)(–complexes). Yet, information on this potential pathway is lacking. To narrow this knowledge gap, the Mn–to–ATMP speciation was systematically varied in laboratory batch experiments by changing (i) the initial Mn–to–ATMP ratio and (ii) the pH value in order to unravel potential reactions between Mn(III)ATMP–intermediates and free ATMP and thus get a more comprehensive understanding of the system. To this end, the reaction kinetics and observed kinetic isotope fractionation were related to the Mn–to–ATMP speciation, which was described quantitively by equilibrium speciation modeling. In **chapter 4**, the focus is shifted from the homogeneous Mn(II)–catalyzed oxidation to the heterogeneous oxidation at manganese dioxide surfaces. In order to allow an isolated investigation of the heterogeneous reaction, the amino–biphosphonate iminodimethylene phosphonate (IDMP) was used as model compound, which is resilient towards homogeneous Mn(II)–catalyzed oxidation. IDMP oxidization was investigated in laboratory batch experiments under varying conditions, such as MnO_2 mineralogy and pH. The experimental data was evaluated with respect to reaction order, reaction rate constant and observed kinetic isotope fractionation. Finally, a reaction scheme including putative rate–limiting steps should be developed based on the findings obtained. Combined with the findings from chapter 3, the study therefore sets the basis needed for a comprehensive investigation of systems with superimposed homogeneous and heterogeneous manganese–driven oxidation of amino–polyphosphonates. Lastly, **chapter 5** summarizes the major findings of the presented research work, discusses their environmental implications and provides suggestions for the design of follow–up studies.

References

(1) Metcalf, W. W.; van der Donk, W. A. Biosynthesis of phosphonic and phosphinic acid natural products. *Annual Review of Biochemistry* **2009**, *78*, 65–94.

(2) Hilderbrand, R. L., *The role of phosphonates in living systems*; CRC Press: 2018.

(3) Horsman, G. P.; Zechel, D. L. Phosphonate Biochemistry. *Chemical Reviews* **2017**, *117*, 5704–5783.

(4) Engel, R. Phosphonates as analogues of natural phosphates. *Chemical Reviews* **1977**, *77*, 349–367.

(5) Westheimer, F. H. Why nature chose phosphates. *Science* **1987**, *235*, 1173–1178.

(6) Bowler, M. W.; Cliff, M. J.; Waltho, J. P.; Blackburn, G. M. Why did Nature select phosphate for its dominant roles in biology? *New Journal of Chemistry* **2010**, *34*, 784–794.

(7) Galezowska, J.; Gumienna-Kontecka, E. Phosphonates, their complexes and bio-applications: A spectrum of surprising diversity. *Coordination Chemistry Reviews* **2012**, *256*, 105–124.

(8) Murugavel, R.; Choudhury, A.; Walawalkar, M. G.; Pothiraja, R.; Rao, C. N. R. Metal complexes of organophosphate esters and open-framework metal phosphates: synthesis, structure, transformations, and applications. *Chemical Reviews* **2008**, *108*, 3549–3655.

(9) Ternan, N. G.; Mc Grath, J. W.; Mc Mullan, G.; Quinn, J. P. Organophosphonates: occurrence, synthesis and biodegradation by microorganisms. *World Journal of Microbiology and Biotechnology* **1998**, *14*, 635–647.

(10) Kononova, S.; Nesmeyanova, M. Phosphonates and their degradation by microorganisms. *Biochemistry (Moscow)* **2002**, *67*, 184–195.

(11) Fields, S. C. Synthesis of natural products containing a C-P bond. *Tetrahedron* **1999**, *55*, 12237–12273.

(12) Kafarski, P.; LeJczak, B. Biological activity of aminophosphonic acids. *Phosphorus, Sulfur, and Silicon and the Related Elements* **1991**, *63*, 193–215.

(13) Naydenova, E. D.; Todorov, P. T.; Troev, K. D. Recent synthesis of aminophosphonic acids as potential biological importance. *Amino Acids* **2010**, *38*, 23–30.

(14) Orsini, F.; Sello, G.; Sisti, M. Aminophosphonic acids and derivatives. Synthesis and biological applications. *Current Medicinal Chemistry* **2010**, *17*, 264–289.

(15) McGrath, J. W.; Chin, J. P.; Quinn, J. P. Organophosphonates revealed: new insights into the microbial metabolism of ancient molecules. *Nature Reviews Microbiology* **2013**, *11*, 412–419.

(16) Duke, S. O.; Powles, S. B. Glyphosate: a once-in-a-century herbicide. *Pest Management Science* **2008**, *64*, 319–325.

(17) Wendels, S.; Chavez, T.; Bonnet, M.; Salmeia, K. A.; Gaan, S. Recent developments in organophosphorus flame retardants containing PC bond and their applications. *Materials* **2017**, *10*, 784.

(18) De Clercq, E.; Li, G. Approved antiviral drugs over the past 50 years. *Clinical Microbiology Reviews* **2016**, *29*, 695–747.

(19) Rott, E.; Steinmetz, H.; Metzger, J. W. Organophosphonates: A review on environmental relevance, biodegradability and removal in wastewater treatment plants. *Science of the Total Environment* **2018**, *615*, 1176–1191.

(20) Knepper, T. P. Synthetic chelating agents and compounds exhibiting complexing properties in the aquatic environment. *TRAC Trends in Analytical Chemistry* **2003**, *22*, 708–724.

(21) Popov, K.; Rönkkömäki, H.; Lajunen, L. H. J. Critical evaluation of stability constants of phosphonic acids (IUPAC Technical Report). *Pure and Applied Chemistry* **2001**, *73*, 1641–1677.

(22) Schowanek, D.; McAvoy, D.; Versteeg, D.; Hanstveit, A. Effects of nutrient trace metal speciation on algal growth in the presence of the chelator [S, S]-EDDS. *Aquatic Toxicology* **1996**, *36*, 253–275.

(23) Jaworska, J.; Van Genderen-Takken, H.; Hanstveit, A.; van de Plassche, E.; Feijtel, T. Environmental risk assessment of phosphonates, used in domestic laundry and cleaning agents in the Netherlands. *Chemosphere* **2002**, *47*, 655–665.

(24) Greenlee, L. F.; Testa, F.; Lawler, D. F.; Freeman, B. D.; Moulin, P. Effect of antiscalants on precipitation of an RO concentrate: metals precipitated and particle characteristics for several water compositions. *Water Research* **2010**, *44*, 2672–2684.

(25) Nowack, B. Environmental chemistry of phosphonates. *Water Research* **2003**, *37*, 2533–2546.

(26) German Cosmetic Toiletry Perfumery Detergent Association *Sustainability in the laundry, home care and cleaning products industry in Germany* (*Nachhaltigkeit in der Wasch-, Pflege- und Reinigungsmittelbranche in Deutschland*); Report; Industrieverband Körperpflege- und Waschmittel e. V, 2021.

(27) Jarvie, H. P.; Neal, C.; Withers, P. J. Sewage-effluent phosphorus: a greater risk to river eutrophication than agricultural phosphorus? *Science of the Total Environment* **2006**, *360*, 246–253.

(28) Wu, L. H.; Luo, Y. M.; Christie, P.; Wong, M. H. Effects of EDTA and low molecular weight organic acids on soil solution properties of a heavy metal polluted soil. *Chemosphere* **2003**, *50*, 819–822.

(29) Nowack, B. Aminopolyphosphonate removal during wastewater treatment. *Water Research* **2002**, *36*, 4636–4642.

(30) Nowack, B.; Stone, A. T. Adsorption of Phosphonates onto the Goethite-Water Interface. *Journal of Colloid and Interface Science* **1999**, *214*, 20–30.

(31) Martinez, R. J.; Farrell, J. Understanding Nitrilotris(methylenephosphonic acid) reactions with ferric hydroxide. *Chemosphere* **2017**, *175*, 490–496.

(32) Nowack, B.; Stone, A. T. The Influence of Metal Ions on the Adsorption of Phosphonates onto Goethite. *Environmental Science & Technology* **1999**, *33*, 3627–3633.

(33) Fischer, K. Sorption of chelating agents (HEDP and NTA) onto mineral phases and sediments in aquatic model systems: Part I: Sorption onto clay minerals. *Chemosphere* **1991**, *22*, 15–27.

(34) Edzwald, J. K.; Toensing, D. C.; Leung, M. C.-Y. Phosphate adsorption reactions with clay minerals. *Environmental Science & Technology* **1976**, *10*, 485–490.

(35) Fischer, K. Sorption of chelating agents (HEDP and NTA) onto mineral phases and sediments in aquatic model systems: Part II: Sorption onto sediments and sewage sludges. *Chemosphere* **1992**, *24*, 51–62.

(36) Sun, S.; Wang, S.; Ye, Y.; Pan, B. Highly efficient removal of phosphonates from water by a combined Fe(III)/UV/co-precipitation process. *Water Research* **2019**, *153*, 21–28.

(37) Nowack, B.; Stone, A. T. Degradation of Nitrilotris(methylenephosphonic Acid) and Related (Amino)Phosphonate Chelating Agents in the Presence of Manganese and Molecular Oxygen. *Environmental Science & Technology* **2000**, *34*, 4759–4765.

(38) Kuhn, R.; Jensch, R.; Bryant, I. M.; Fischer, T.; Liebsch, S.; Martienssen, M. The influence of selected bivalent metal ions on the photolysis of diethylenetriamine penta(methylenephosphonic acid). *Chemosphere* **2018**, *210*, 726–733.

(39) Rott, E.; Minke, R.; Bali, U.; Steinmetz, H. Removal of phosphonates from industrial wastewater with UV/Fe(II), Fenton and UV/Fenton treatment. *Water Research* **2017**, *122*, 345–354.

(40) Matthijs, E.; de Oude, N. T.; Bolte, M.; Lemaire, J. Photodegradation of ferric ethylenediaminetetra(methylenephosphonic acid) (EDTMP) in aqueous solution. *Water Research* **1989**, *23*, 845–851.

(41) Lesueur, C.; Pfeffer, M.; Fuerhacker, M. Photodegradation of phosphonates in water. *Chemosphere* **2005**, *59*, 685–691.

(42) Grandcoin, A.; Piel, S.; Baures, E. AminoMethylPhosphonic acid (AMPA) in natural waters: Its sources, behavior and environmental fate. *Water Research* **2017**, *117*, 187–197.

(43) Nowack, B.; Stone, A. T. Homogeneous and heterogeneous oxidation of nitrilotrismethylenephosphonic acid (NTMP) in the presence of manganese (II, III) and molecular oxygen. *The Journal of Physical Chemistry B* **2002**, *106*, 6227–6233.

(44) Nowack, B.; Stone, A. T. Manganese-catalyzed degradation of phosphonic acids. *Environmental Chemistry Letters* **2003**, *1*, 24–31.

(45) Barrett, K. A.; McBride, M. B. Oxidative degradation of glyphosate and aminomethylphosphonate by manganese oxide. *Environmental Science & Technology* **2005**, *39*, 9223–9228.

(46) Rott, E.; Happel, O.; Armbruster, D.; Minke, R. Behavior of PBTC, HEDP, and Aminophosphonates in the Process of Wastewater Treatment. *Water* **2020**, *12*, 53.

(47) Schmidt, C. K.; Raue, B.; Brauch, H.-J.; Sacher, F. Trace-level analysis of phosphonates in environmental waters by ion chromatography and inductively coupled plasma mass spectrometry. *International Journal of Environmental Analytical Chemistry* **2013**, *94*, 385–398.

(48) Armbruster, D.; Rott, E.; Minke, R.; Happel, O. Trace-level determination of phosphonates in liquid and solid phase of wastewater and environmental samples by IC-ESI-MS/MS. *Analytical and Bioanalytical Chemistry* **2020**, *412*, 4807–4825.

(49) Rott, E.; Happel, O.; Armbruster, D.; Minke, R. Influence of wastewater discharge on the occurrence of PBTC, HEDP, and aminophosphonates in sediment, suspended matter, and the aqueous phase of rivers. *Water* **2020**, *12*, 803.

(50) Howe, P.; Malcolm, H.; Dobson, S., *Manganese and its compounds: environmental aspects*; World Health Organization: 2004.

(51) Post, J. E. Manganese oxide minerals: Crystal structures and economic and environmental significance. *Proceedings of the National Academy of Sciences* **1999**, *96*, 3447–3454.

(52) Li, H.; Santos, F.; Butler, K.; Herndon, E. A Critical Review on the Multiple Roles of Manganese in Stabilizing and Destabilizing Soil Organic Matter. *Environmental Science & Technology* **2021**, *55*, 12136–12152.

(53) Qian, A.; Zhang, W.; Shi, C.; Pan, C.; Giammar, D. E.; Yuan, S.; Zhang, H.; Wang, Z. Geochemical stability of dissolved Mn (III) in the presence of pyrophosphate as a model ligand: Complexation and disproportionation. *Environmental Science & Technology* **2019**, *53*, 5768–5777.

(54) Luther, G. W. Manganese(II) Oxidation and Mn(IV) Reduction in the Environment—Two One-Electron Transfer Steps Versus a Single Two-Electron Step. *Geomicrobiology Journal* **2005**, *22*, 195–203.

(55) Tebo, B. M.; Bargar, J. R.; Clement, B. G.; Dick, G. J.; Murray, K. J.; Parker, D.; Verity, R.; Webb, S. M. Biogenic manganese oxides: properties and mechanisms of formation. *Annual Review of Earth and Planetary Sciences* **2004**, *32*, 287–328.

(56) Stone, A. T. Reductive dissolution of manganese (III/IV) oxides by substituted phenols. *Environmental Science & Technology* **1987**, *21*, 979–988.

(57) Canfield, D.; Kristensen, E.; Thamdrup, B., *Aquatic Geomicrobiology*; Advances in Marine Biology, Vol. 48; Academic Press Inc: 2005.

(58) Negra, C.; Ross, D. S.; Lanzirotti, A. Oxidizing behavior of soil manganese: interactions among abundance, oxidation state, and pH. *Soil Science Society of America Journal* **2005**, *69*, 87–95.

(59) Luther, G. W.; Karolewski, J. S.; Sutherland, K. M.; Hansel, C. M.; Wankel, S. D. The Abiotic Nitrite Oxidation by Ligand-Bound Manganese (III): The Chemical Mechanism. *Aquatic Geochemistry* **2021**, 1–14.

(60) Li, H.; Santos, F.; Butler, K.; Herndon, E. A Critical Review on the Multiple Roles of Manganese in Stabilizing and Destabilizing Soil Organic Matter. *Environmental Science & Technology* **2021**, *55*, 12136–12152.

(61) Remucal, C. K.; Ginder-Vogel, M. A critical review of the reactivity of manganese oxides with organic contaminants. *Environmental Science: Processes and Impacts* **2014**, *16*, 1247–66.

(62) Borch, T.; Kretzschmar, R.; Kappler, A.; Cappellen, P. V.; Ginder-Vogel, M.; Voegelin, A.; Campbell, K. Biogeochemical redox processes and their impact on contaminant dynamics. *Environmental Science & Technology* **2010**, *44*, 15–23.

(63) Archibald, F. S.; Fridovich, I. The scavenging of superoxide radical by manganous complexes: in vitro. *Archives of Biochemistry and Biophysics* **1982**, *214*, 452–463.

(64) Iranzo, O. Manganese complexes displaying superoxide dismutase activity: a balance between different factors. *Bioorganic Chemistry* **2011**, *39*, 73–87.

(65) Armstrong, F. A. Why did Nature choose manganese to make oxygen? *Philosophical Transactions of the Royal Society B: Biological Sciences* **2008**, *363*, 1263–1270.

(66) Madison, A. S.; Tebo, B. M.; Mucci, A.; Sundby, B.; Luther, G. W. Abundant porewater Mn (III) is a major component of the sedimentary redox system. *Science* **2013**, *341*, 875–878.

(67) Kostka, J. E.; Luther, G. W.; Nealson, K. H. Chemical and biological reduction of Mn (III)-pyrophosphate complexes: Potential importance of dissolved Mn (III) as an environmental oxidant. *Geochimica et Cosmochimica Acta* **1995**, *59*, 885–894.

(68) Oldham, V. E.; Mucci, A.; Tebo, B. M.; Luther III, G. W. Soluble Mn (III)–L complexes are abundant in oxygenated waters and stabilized by humic ligands. *Geochimica et Cosmochimica Acta* **2017**, *199*, 238–246.

(69) Duckworth, O. W.; Sposito, G. Siderophore-manganese(III) interactions. I. Air-oxidation of manganese(ll) promoted by desferrioxamine B. *Environmental Science & Technology* **2005**, *39*, 6037–6044.

(70) Trouwborst, R. E.; Clement, B. G.; Tebo, B. M.; Glazer, B. T.; Luther, G. W. Soluble Mn (III) in suboxic zones. *Science* **2006**, *313*, 1955–1957.

(71) Klewicki, J. K.; Morgan, J. J. Kinetic Behavior of Mn(III) Complexes of Pyrophosphate, EDTA, and Citrate. *Environmental Science & Technology* **1998**, *32*, 2916–2922.

(72) Webb, S. M.; Dick, G. J.; Bargar, J. R.; Tebo, B. M. Evidence for the presence of Mn (III) intermediates in the bacterial oxidation of Mn (II). *Proceedings of the National Academy of Sciences* **2005**, *102*, 5558–5563.

(73) Jiang, J.; Pang, S.-Y.; Ma, J. Role of ligands in permanganate oxidation of organics. *Environmental Science & Technology* **2010**, *44*, 4270–4275.

(74) Sun, B.; Guan, X.; Fang, J.; Tratnyek, P. G. Activation of Manganese Oxidants with Bisulfite for Enhanced Oxidation of Organic Contaminants: The Involvement of Mn(III). *Environmental Science & Technology* **2015**, *49*, 12414–12421.

(75) Gao, Y.; Jiang, J.; Zhou, Y.; Pang, S.-Y.; Ma, J.; Jiang, C.; Wang, Z.; Wang, P.-X.; Wang, L.-H.; Li, J. Unrecognized role of bisulfite as Mn(III) stabilizing agent in activating permanganate (Mn(VII)) for enhanced degradation of organic contaminants. *Chemical Engineering Journal* **2017**, *327*, 418–422.

(76) Zhu, Y.; Wang, X.; Zhang, J.; Ding, L.; Li, J.; Zheng, H.; Zhao, C. Generation of active Mn (III) aq by a novel heterogeneous electro-permanganate process with manganese (II) as promoter and stabilizer. *Environmental Science & Technology* **2019**, *53*, 9063–9072.

(77) Hu, E.; Zhang, Y.; Wu, S.; Wu, J.; Liang, L.; He, F. Role of dissolved Mn(III) in transformation of organic contaminants: Non-oxidative versus oxidative mechanisms. *Water Research* **2017**, *111*, 234–243.

(78) Elsner, M.; Jochmann, M. A.; Hofstetter, T. B.; Hunkeler, D.; Bernstein, A.; Schmidt, T. C.; Schimmelmann, A. Current challenges in compound-specific stable isotope analysis of environmental organic contaminants. *Analytical and Bioanalytical Chemistry* **2012**, *403*, 2471–2491.

(79) Schmidt, T. C.; Jochmann, M. A. Origin and fate of organic compounds in water: characterization by compound-specific stable isotope analysis. *Annual Review of Analytical Chemistry* **2012**, *5*, 133–155.

(80) Thullner, M.; Centler, F.; Richnow, H.-H.; Fischer, A. Quantification of organic pollutant degradation in contaminated aquifers using compound specific stable isotope analysis – Review of recent developments. *Organic Geochemistry* **2012**, *42*, 1440–1460.

(81) Krummen, M.; Hilkert, A. W.; Juchelka, D.; Duhr, A.; Schlüter, H.-J.; Pesch, R. A new concept for isotope ratio monitoring liquid chromatography/mass spectrometry. *Rapid Communications in Mass Spectrometry* **2004**, *18*, 2260–2266.

(82) Gilevska, T.; Gehre, M.; Richnow, H. H. Performance of the wet oxidation unit of the HPLC isotope ratio mass spectrometry system for halogenated compounds. *Analytical Chemistry* **2014**, *86*, 7252–7257.

(83) Godin, J. P.; Hau, J.; Fay, L. B.; Hopfgartner, G. Isotope ratio monitoring of small molecules and macromolecules by liquid chromatography coupled to isotope ratio mass spectrometry. *Rapid Communications in Mass Spectrometry* **2005**, *19*, 2689–2698.

(84) Kujawinski, D. M.; Zhang, L.; Schmidt, T. C.; Jochmann, M. A. When other separation techniques fail: compound-specific carbon isotope ratio analysis of sulfonamide containing pharmaceuticals by high-temperature-liquid chromatography-isotope ratio mass spectrometry. *Analytical Chemistry* **2012**, *84*, 7656–7663.

(85) Kujawinski, D. M.; Wolbert, J. B.; Zhang, L.; Jochmann, M. A.; Widory, D.; Baran, N.; Schmidt, T. C. Carbon isotope ratio measurements of glyphosate and AMPA by liquid chromatography coupled to isotope ratio mass spectrometry. *Analytical and Bioanalytical Chemistry* **2013**, *405*, 2869–2878.

(86) Godin, J. P.; McCullagh, J. S. Review: Current applications and challenges for liquid chromatography coupled to isotope ratio mass spectrometry (LC/IRMS). *Rapid Communications in Mass Spectrometry* **2011**, *25*, 3019–3028.

(87) Zhang, L.; Kujawinski, D. M.; Jochmann, M. A.; Schmidt, T. C. High-temperature reversed-phase liquid chromatography coupled to isotope ratio mass spectrometry. *Rapid Communications in Mass Spectrometry* **2011**, *25*, 2971–2980.

(88) Elsner, M.; Zwank, L.; Hunkeler, D.; Schwarzenbach, R. P. A new concept linking observable stable isotope fractionation to transformation pathways of organic pollutants. *Environmental Science & Technology* **2005**, *39*, 6896–6916.

(89) Coplen, T. B.; Böhlke, J. K.; De Bievre, P.; Ding, T.; Holden, N.; Hopple, J.; Krouse, H.; Lamberty, A.; Peiser, H.; Revesz, K. Isotope-abundance variations of selected elements (IUPAC Technical Report). *Pure and Applied Chemistry* **2002**, *74*, 1987–2017.

(90) Elsner, M. Stable isotope fractionation to investigate natural transformation mechanisms of organic contaminants: principles, prospects and limitations. *Journal of Environmental Monitoring* **2010**, *12*, 2005–2031.

(91) Hohener, P.; Elsner, M.; Eisenmann, H.; Atteia, O. Improved constraints on in situ rates and on quantification of complete chloroethene degradation from stable carbon isotope mass balances in groundwater plumes. *Journal of Contaminant Hydrology* **2015**, *182*, 173–182.

(92) Schmidt, T. C.; Zwank, L.; Elsner, M.; Berg, M.; Meckenstock, R. U.; Haderlein, S. B. Compound-specific stable isotope analysis of organic contaminants in natural environments: a critical review of the state of the art, prospects, and future challenges. *Analytical and Bioanalytical Chemistry* **2004**, *378*, 283–300.

(93) Schwarzenbach, R. P.; Gschwend, P. M.; Imboden, D. M., *Environmental Organic Chemistry*; John Wiley & Sons: 2002.

(94) Hofstetter, T. B.; Berg, M. Assessing transformation processes of organic contaminants by compound-specific stable isotope analysis. *TrAC Trends in Analytical Chemistry* **2011**, *30*, 618–627.

(95) Tobler, N. B.; Hofstetter, T. B.; Schwarzenbach, R. P. Carbon and hydrogen isotope fractionation during anaerobic toluene oxidation by Geobacter metallireducens with different Fe (III) phases as terminal electron acceptors. *Environmental Science & Technology* **2008**, *42*, 7786–7792.

(96) Schüth, C.; Taubald, H.; Bolaño, N.; Maciejczyk, K. Carbon and hydrogen isotope effects during sorption of organic contaminants on carbonaceous materials. *Journal of Contaminant Hydrology* **2003**, *64*, 269–281.

(97) Slater, G. F.; Ahad, J. M.; Lollar, B. S.; Allen-King, R.; Sleep, B. Carbon isotope effects resulting from equilibrium sorption of dissolved VOCs. *Analytical Chemistry* **2000**, *72*, 5669–5672.

(98) Barja, B. C.; Tejedor-Tejedor, M. I.; Anderson, M. A. Complexation of Methylphosphonic Acid with the Surface of Goethite Particles in Aqueous Solution. *Langmuir* **1999**, *15*, 2316–2321.

(99) Zenobi, M. C.; Luengo, C. V.; Avena, M. J.; Rueda, E. H. An ATR-FTIR study of different phosphonic acids adsorbed onto boehmite. *Spectrochimica Acta Part A: Molecular and Biomolecular Spectroscopy* **2010**, *75*, 1283–1288.

(100) Calvet, R. Adsorption of organic chemicals in soils. *Environmental Health Perspectives* **1989**, *83*, 145–177.

(101) Jaisi, D. P.; Blake, R. E.; Kukkadapu, R. K. Fractionation of oxygen isotopes in phosphate during its interactions with iron oxides. *Geochimica et Cosmochimica Acta* **2010**, *74*, 1309–1319.

(102) Delstanche, S.; Opfergelt, S.; Cardinal, D.; Elsass, F.; André, L.; Delvaux, B. Silicon isotopic fractionation during adsorption of aqueous monosilicic acid onto iron oxide. *Geochimica et Cosmochimica Acta* **2009**, *73*, 923–934.

(103) Lemarchand, E.; Schott, J.; Gaillardet, J. How surface complexes impact boron isotope fractionation: Evidence from Fe and Mn oxides sorption experiments. *Earth and Planetary Science Letters* **2007**, *260*, 277–296.

2 Stable carbon isotope analysis of polyphosphonate complexing agents by anion chromatography coupled to isotope ratio mass spectrometry: method development and application

Philipp R. Martin, Daniel Buchner, Maik A. Jochmann, Stefan B. Haderlein

Author	Author position	Scientific ideas	Data generation*	Analysis & interpretation	Paper writing
P. Martin	1	40 %	90 %	50 %	50 %
D. Buchner	2	10 %	0 %	30 %	30 %
M. Jochmann	3	40 %	0 %	10 %	10 %
S. Haderlein	4	10 %	0 %	10 %	10 %

Title of the paper:
Stable carbon isotope analysis of polyphosphonate complexing agents by anion chromatography coupled to isotope ratio mass spectrometry:
method development and application

Status in the publication process:
published in *Analytical and Bioanalytical Chemistry*

* Experiments were conducted with the help of Melanie Schüßler (see acknowledgments)

Reprinted (adapted) by permission from Springer Nature Customer Service Centre GmbH:
Martin, P. R., Buchner, D., Jochmann, M. A., & Haderlein, S. B.
Analytical and Bioanalytical Chemistry, **2020**, 412(20), 4827–4835.
DOI: 10.1007/s00216-019-02251-w

2.1 Abstract

Compound–specific carbon isotope analysis (carbon CSIA) by liquid chromatography/ isotope ratio mass spectrometry (LC–IRMS) is a novel and promising tool to elucidate the environmental fate of polar organic compounds such as polyphosphonates, strong complexing agents for di– and trivalent cations with growing commercial importance over the last decades. Here, we present a LC–IRMS method for the three widely used polyphosphonates 1–hydroxyethane 1,1–diphosphonate (HEDP), amino tris(methylenephosphonate) (ATMP) and ethylenediamine tetra(methylenephosphonate) (EDTMP). Separation of the analytes, as well as ATMP and its degradation products was carried out on an anion exchange column under acidic conditions. Quantitative wet–chemical oxidation inside the LC–IRMS interface to CO_2 was achieved for all three investigated polyphosphonates at a comparatively low sodium persulfate concentration despite the described resilience of HEDP towards oxidative breakdown. The developed method has proven to be suitable for the determination of carbon isotope fractionation of ATMP transformation due to manganese catalyzed reaction with molecular oxygen, as well as for equilibrium sorption of ATMP to goethite. A kinetic isotope effect was associated with the investigated reaction pathway, whereas no detectable isotope fractionation could be observed during sorption. Thus, CSIA is an appropriate technique to distinguish between sorption and degradation processes that contribute to a concentration decrease of ATMP in laboratory batch experiments. Our study highlights the potential of carbon CSIA by LC–IRMS to gain a process–based understanding of the fate of polyphosphonate complexing agents in environmental as well as technical systems.

2.2 Introduction

Compound–specific isotope analysis (CSIA) of light elements (H, C, N) has become a versatile, well established tool in environmental chemistry in the last two decades.[1] CSIA was successfully applied for source identification, product authenticity, detection and quantification of in situ (bio–) degradation as well as identification of the underlying reaction mechanisms.[2–4] However, in the early days of CSIA the only instrumentation commercially available was gas chromatography/isotope ratio mass spectrometry and was therefore restricted to (semi–) volatile, thermostable or derivatizable compounds. This restriction contrasts with the growing importance of non–volatile, polar and thermolabile organic pollutants, such as pharmaceuticals and pesticides in the last years.[5] For carbon CSIA this gap was recently closed owing to the development of a commercially available interface to couple liquid chromatography and isotope ratio mass spectrometry (LC–IRMS). This approach is based on a chromatographic separation of the analytes by means of a carbon free, inorganic eluent followed by (semi–) quantitative wet–chemical oxidation of the analytes to CO_2 in the aqueous phase and subsequent transfer of the CO_2 into a helium stream, which is finally introduced into the IRMS.[6] Nowadays, a variety of applications of LC–IRMS can be found in the food authenticity sector, e.g., to proof honey adulteration or identify the origin of ethanol in wine and sweeteners in chewing gums.[7–9]

However, routine LC–IRMS applications to investigate the environmental fate of water–soluble organic xenobiotics are scarce. This partially can be explained by the restriction of the available LC–IRMS interface to eluents free of organic modifiers, hampering the chromatographic separation of most analytes routinely separated on reversed–phase and porous graphitized carbon columns.[10] To overcome these problems high–temperature (HT–)LC–IRMS, which makes use of the decreased polarity of water at elevated temperatures, was successfully applied for the separation on reversed–phase columns.[11–13] On the other hand, ionic contaminants, which can be separated on ion exchange or mixed–mode columns without the need of organic modifiers gained growing attention over the last years. Two prominent examples for such compounds are the widely used herbicide glyphosate (N–(phosphonomethyl)glycine) and its degradation product (aminomethyl) phosphonic acid (AMPA), for which a LC–IRMS method based on cation exchange chromatography using an acidic phosphate buffer was developed recently.[14]

A compound class structurally related to the monophosphonate glyphosate is the group of polyphosphonic acids, which are characterized by two or more $C-PO(OH)_2$ moieties and are strong complexing agents for di– and trivalent cations.[15] Polyphosphonates are increasingly used as substitutes for polyphosphates and aminopolycarboxylates (e.g., ethylenediamine (tetra)acetic acid, EDTA) in industrial and household applications, as these compound classes are associated with environmental problems, such as surface water eutrophication and heavy metal remobilization.[16,17] Consequently, this increasing usage brings up the question, how polyphosphonates behave in technical and natural systems. Due to their strong affinity for mineral surfaces, sorption mainly at iron (oxyhxdr) oxides is considered as predominant process for polyphosphonate removal from water. In wastewater treatment plants elimination rates in the range of 90 % were calculated, at neutral pH mainly attributed to sorption onto amorphous iron hydroxides.[18,19] Furthermore, various abiotic degradation pathways are known, for instance manganese catalyzed oxidation by molecular oxygen or iron catalyzed photolysis.[20,21] However, so far only little is known about the importance of these degradation processes for the fate of polyphosphonates in natural and technical systems.[15,19]

This study presents (i) a LC–IRMS method for compound–specific carbon isotope analysis of three widely used polyphosphonates (1–hydroxyethane 1,1–diphosphonate (HEDP), amino tris(methylenephosphonate) (ATMP), ethylenediamine tetra(methylenephosphonate) (EDTMP)) and (ii) a first application investigating carbon isotope fractionation of ATMP for sorption onto the iron oxyhydroxide goethite as well as for Mn(II)–catalyzed oxidation with molecular oxygen.

2.3 Materials and methods

Chemicals and reagents

All solutions and suspensions were prepared from ultra–pure water obtained from a Barnstead™GenPure™system (Thermo Fisher Scientific, Germany). ATMP ($\geqslant$ 97 % (T)), HEDP ($\geqslant$ 95 % (T)) and oxalic acid ($\geqslant$ 99 % (RT)) were purchased from Sigma–Aldrich (Steinheim, Germany) and EDTMP was synthesized and purified by Zschimmer & Schwarz (Lahnstein, Germany). The eluent for concentration and carbon isotope analysis was prepared from sulfuric acid 95 % to 97 %, EMSURE®, Merck Millipore, Darmstadt, Germany). $Na_2S_2O_8$ ($\geqslant$ 98 %, Sigma–Aldrich, Steinheim, Germany) andH_3PO_4 (85 %, EMSURE®, Merck Millipore, Darmstadt, Germany) were used as reactants for LC–IRMS analysis. For carbon isotope analysis, all solutions were degassed before use for 30 min within an ultrasonic bath under reduced pressure obtained by a water–jet vacuum pump to remove dissolved CO_2. During the analysis all solutions were purged with helium (grade 5.0, Westfalen AG, Münster, Germany) to minimize re–dissolution of atmospheric carbon dioxide. Sodium nitrate ($NaNO_3$, $\geqslant$ 99 %, Carl Roth, Karlsruhe, Germany) was used as background electrolyte for all experiments, $Mg(NO_3)_2$ and $Ca(NO_3)_2$ (both $\geqslant$ 99 %, Carl Roth, Karlsruhe, Germany) were used during the sorption experiments. The pH was adjusted with 1 M NaOH. Manganese(II)chloride ($\geqslant$ 99 %, Merck Millipore, Darmstadt, Germany) and Na_2EDTA ($\geqslant$ 99 %, Sigma–Aldrich, Steinheim, Germany) were used for the degradation experiments. For the sorption experiments a commercially available goethite (α–FeOOH, Bayferrox 920Z, Lanxess GmBH, Cologne, Germany) was used.

Stable carbon isotope analysis

Separation of the analytes was conducted on an UltiMate3000 HPLC–system (Thermo Fisher Scientific, Germering, Germany). A volume of 50 µL was injected and separation was achieved on an IC NI–424 column (4.6 mm $\times$ 100 mm, Shodex, Munich, Germany), operated at constant temperature of 40 °C. As eluent 4 mM sulfuric acid was used, delivered at a flow rate of 500 µL min^{-1}.

Analysis of carbon isotope ratios was conducted on a Delta V Plus IRMS, which was hyphenated to the HPLC via a LC Isolink interface (both Thermo Fisher Scientific, Bremen, Germany). If not stated otherwise, the eluent stream was mixed within a mixing–tee with 1.5 M phosphoric acid and 30 g L^{-1} sodium persulfate, which were delivered at flow rates of 50 µL min^{-1} and 75 µL min^{-1}, respectively. This resulted in a pH–value of $\approx$ 1.5 and an oxygen background in the ion source of around 15 V (at $3 \times 10^8\,\Omega$). The oxidation reactor was operated at a temperature of 99.9 °C. After cooling the eluent stream down to room temperature, the CO_2 was transferred into the gas phase by a counter–stream of helium at a flow rate of 1.9 mL min^{-1}. Three CO_2 reference gas peaks were injected at the beginning of each measurement to monitor the ion source performance. The second monitoring gas peak (set value: 0 ‰) was used for the calculation of δ^{13}C–values of the analytes. The individual background algorithm was used

based on the stable CO_2 backgrounds during a run. During method validation, uncorrected δ^{13}C–value were used, as the focus was set on their robustness, rather than on their trueness. The δ^{13}C–values of ATMP in the samples from the degradation and sorption experiments were obtained using concentration adjusted ATMP reference standards (measured by EA–IRMS as described elsewhere[8] with δ^{13}C–value = -44.5 ± 0.1 ‰ (n = 3) in VPDB scale) bracketing six samples by duplicate standards. Samples were diluted to the same concentration before analysis. The uncertainty of the measurements was $\leqslant 0.5$ ‰ (n = 2).

Concentration analysis

For the quantification of remaining ATMP in solution, the UltiMate3000 HPLC–system (Thermo Fisher Scientific, Germering, Germany) equipped with an IC NI–424 anion exchange column (4.6 mm × 100 mm, Shodex, Munich, Germany), held at 40 °C was connected to a refraction index detector (RI–101, Shodex, Munich, Germany), held at 35 °C. A sample volume of 50 µL was injected and 4 mM H_2SO_4 at a flow rate of 700 µL min^{-1} was used as eluent. External standards were used for quantification ($R^2 \geqslant 0.99$) and an error of 5 % was estimated for the measurements.

Degradation batch experiments

Manganese catalyzed oxidation of ATMP by molecular oxygen was conducted in duplicates at an initial pH of 7.2 ± 0.1 at room temperature under constant stirring. First, 30 mL of a 1 mM ATMP–solution in 10 mM $NaNO_3$ was added to a 50 mL serum bottle and 2 mL were withdrawn for t0–sampling. The sample was equally distributed into two 1.5 mL amber–glass HPLC–vials, containing 25 µL of a 10 mM EDTA–solution, resulting in a final EDTA concentration of 0.25 mM. Afterwards, the reaction was started by adding a $MnCl_2$ stock solution (1 % (v/v), resulting in a nominal concentration of 0.1 mM). Further sampling was conducted as described above. ATMP oxidation was stopped by re–complexation with EDTA[20] and samples were stored at 4 °C if analyzed the next day, or at −20 °C for longer storage times. Samples stored according to this procedure were stable with regard to ATMP concentrations, as well as δ^{13}C–values.

Sorption batch experiments

Sorption of ATMP onto goethite was investigated in duplicates in 15 mL polypropylene centrifuge tubes containing 5 mL of a 50 g L^{-1} goethite suspension and 5 mL ATMP solution with varying concentrations (0.3 mM to 2 mM), both adjusted to pH 7.0 ± 0.1. To ensure constant ionic strength, the ATMP solution contained additionally 20 mM $NaNO_3$. In two experiments 2 mM $Mg(NO_3)_2$ or 2 mM $Ca(NO_3)_2$ were additionally added to investigate the influence of ternary surface complex formation on the isotope fractionation.[22] To achieve equilibrium conditions, the samples were shaken overhead for 23 h. After the reaction time, the tubes were centrifuged at 7200 rcf for 10 min and the supernatant was filtered through a 0.22 µm PTFE

syringe–filter (BGB Analytics, Rheinfelden, Germany). The filtered samples were stored at 4 °C in the dark until analysis.

Calculations

The resolution for two neighboring peaks was calculated according to **Equation 2.1**.[23]

$$R = 1.18 \times \frac{t_R(\text{peak 2}) - t_R(\text{peak 1})}{w_{1/2}(\text{peak 1}) + w_{1/2}(\text{peak 2})} \tag{2.1}$$

With the retention time t_R and the full width at half maximum $w_{1/2}$.

The carbon isotope enrichment factor (ε_C) for the degradation experiment was calculated by fitting the experimental data according to the Rayleigh model:[24]

$$\ln\left(\frac{\delta^{13}C(t)+1}{\delta^{13}C(0)+1}\right) = \varepsilon_C \times \ln\left(\frac{c(t)}{c(0)}\right) \tag{2.2}$$

With the isotopic signature $\delta^{13}C$ and the concentration c at time point t and at the beginning of the experiment.

2.4 Results and discussion

Chromatographic separation and limits of precise isotope analysis

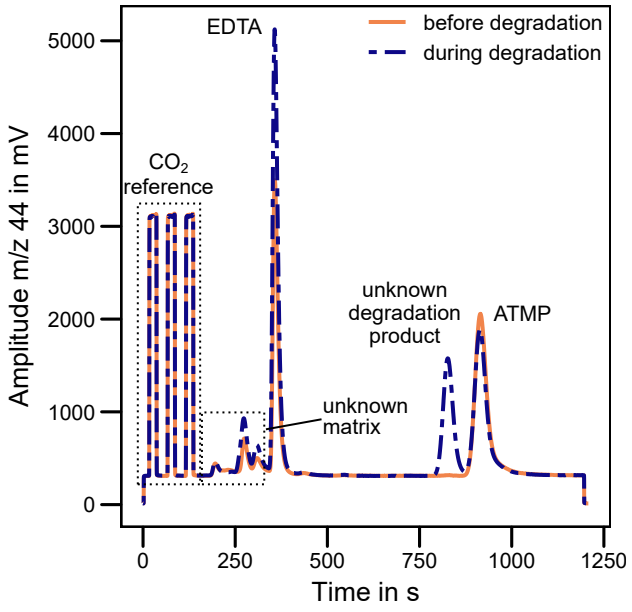

Figure 2.1: LC–IRMS chromatogram of ATMP, its unknown degradation products and EDTA (used as reaction quencher) from an ATMP degradation experiment. The samples were diluted to an ATMP concentration of 50 mg L^{-1}.

The separation of the three investigated polyphosphonates HEDP, ATMP and EDTMP was

achieved by anion exchange chromatography under acidic conditions using a 4 mM H_2SO_4 eluent at pH 2.1 (see **Figure A.1** for a representative chromatogram). The separation of all three analytes was achieved within 25 min at a resolution greater three between HEDP and ATMP, as well as between ATMP and EDTMP.

The chosen elution conditions were also suitable to separate ATMP and its degradation products in samples from laboratory batch degradation experiments (see **Figure 2.1**). Three unknown peaks, as well as EDTA (used as reaction quencher) were well separated from ATMP. One of the unknown peaks (t_r = 270 s) eluted with a retention time comparable to iminodi(methylenephosphonic acid) (IDMP, see **Figure A.2** for chromatogram), which is one degradation product of ATMP during manganese catalyzed oxidation.[20] However, the fact that the compound was detected also before degradation started and its response did not change over time contradicted with this possible peak assignment. The peak eluting at 830 s could be identified as degradation product as its area increased while reaction proceeded. This peak might result from the formation of either formyl–iminodi(methylenephosphonic acid) (FIDMP) or bis–(phosphonomethyl) carbamic acid, which were proposed as further degradation products during manganese catalyzed oxidation of ATMP.[25] However, as none of the two compounds was commercially available an identification was not possible. Peak separation between the unknown degradation product (t_r = 830 s) and ATMP (t_r = 910 s) was achieved with a calculated resolution of > 1.5. A distortion of the δ^{13}C–value obtained for ATMP by slight peak overlapping could be excluded, as a manual stepwise integration of the peak resulted in robust δ^{13}C–values (see **Figure A.3**). This observation was explained by the lower number of theoretical plates in liquid chromatography in comparison to gas chromatography and consequently a smaller isotope effect during separation. Furthermore, coelution of ATMP with impurities or degradation products could be ruled out based on the stepwise integration, as underlying peaks are likely to adulterate the obtained δ^{13}C–values to a different extent, depending on the integration boundaries.

Limits of precise isotope analysis (LPIA) for the developed method were determined using the moving mean approach described by Jochmann et al.[26] analyzing standards in the range of 25 mg L^{-1} to 100 mg L^{-1} in triplicates. Measured isotopic signatures were concentration independent from 100 mg L^{-1} to 30 mg L^{-1} (HEDP and ATMP) and at least to 25 mg L^{-1} (EDTMP) (see **Figure 2.2**). Hence, for all analytes a minimum of 200 ng carbon on column was needed for precise isotope analysis. This is within the range of published LPIA values for other compound classes analyzed by LC–IRMS, such as the monophosphonates glyphosate and AMPA or phenol and cresols.[14,27] Even though for HEDP and ATMP the 25 mg L^{-1} standards were outside the linear range of the instrument, the standard deviations at this concentration were below the accepted error of 0.5 ‰ and the δ^{13}C–value deviated by $\leqslant$ 0.5 ‰ from the moving mean. Hence, for HEDP and ATMP isotope measurements below the determined LPIA might be possible by a correction with compound–specific and concentration adjusted standards.

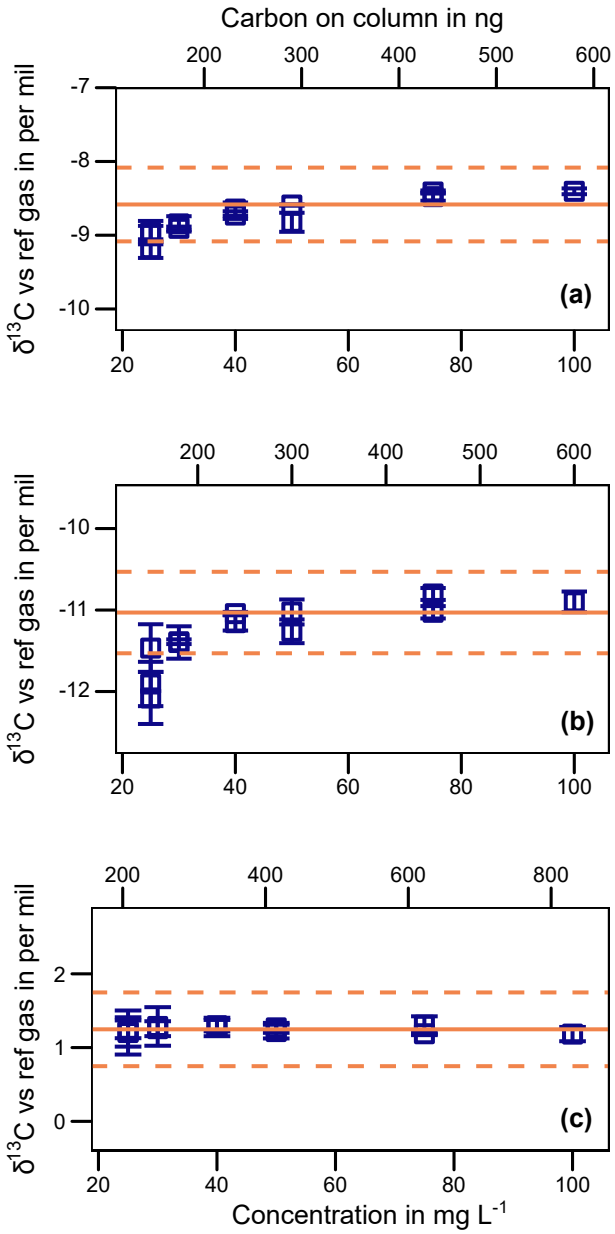

Figure 2.2: Linearity plots for (a) HEDP, (b) ATMP and (c) EDTMP, showing the dependency of the measured isotopic signature on the concentration and the amount of carbon on column, respectively. The solid line represents the mean isotopic signature of the four highest concentrations (40 mg L^{-1} to 100 mg L^{-1}) and the dashed lines marking the 0.5 ‰–range around this value, equal to the accepted error of the method. Error bars correspond to the standard deviations of triplicate measurements.

Systematic evaluation of oxidation efficiencies

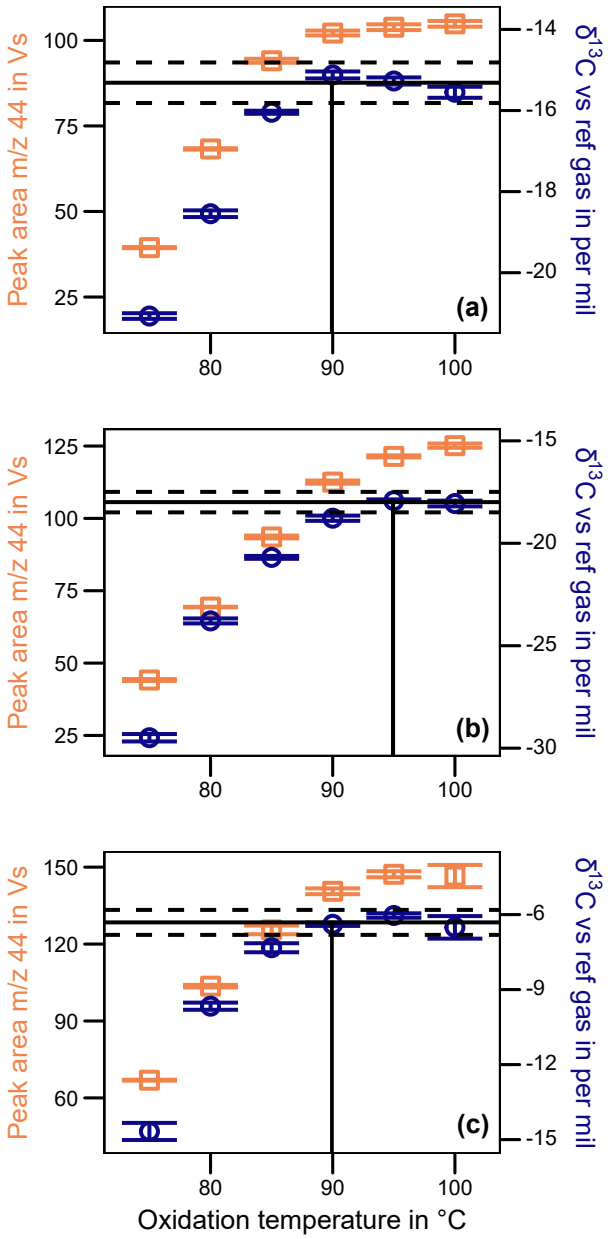

Figure 2.3: Peak area (orange squares, left axis) and uncorrected isotopic signature (blue circles, right axis) of HEDP (a), ATMP (b) and EDTMP (c) (n = 3) over the oxidation temperature (30 g L^{-1} persulfate at 75 µL min^{-1}). Concentration of the polyphosphonates was 50 mg L^{-1}, each. The horizontal lines correspond to the mean isotopic signature (including a 0.5 ‰ error) for the range with temperature independent isotopic signatures (marked by a vertical line).

Besides the chromatographic separation, the oxidation conditions inside the interface have to be evaluated with care during LC–IRMS method development. Incomplete oxidation was shown for compound classes resilient towards oxidation processes (e.g., caffeine, sulfonamides and halogenated acetic acids) and may bias the obtained δ^{13}C–values in comparison to the "true" EA–IRMS values.[11,12,28] Incomplete oxidation also results in decreased sensitivity due to

smaller peak areas. On the other hand, a high persulfate concentration leads to high oxygen background in the ion source and thus a reduced filament lifetime.[29] Therefore, oxidation conditions in the conversion–interface need to be carefully evaluated. To proof complete oxidation of a compound, a normalization of the measured δ^{13}C–values against easy oxidizable or inorganic international reference materials is conducted in many cases, which is an easy and fast procedure in the flow injection analysis (FIA) mode.[30] However, it might be impracticable in HPLC mode, in case the reference materials do not elute with acceptable retention times and/ or peak shapes from the used chromatographic column. Thus, for verification of complete oxidation in the established LC–IRMS method, two recently proposed procedures were adopted. First, the effect of the oxidation temperature on the obtained isotopic signatures and peak areas was investigated. Therefore, standards with concentrations of 50 mg L^{-1} were measured in triplicates for oxidation temperatures between 75 °C and 99.9 °C, while keeping persulfate concentration and flow rate constant. This procedure results in varying sulfate radical concentrations and thus changes the oxidation capacity of the system without any influence on the chromatographic separation.[31] The results of the oxidation temperature test for a persulfate concentration of 30 g L^{-1} and flow rate of 75 µL min^{-1} (corresponding to an oxygen background of around 15 V at $3 \times 10^8\,\Omega$) are shown in **Figure 2.3**. Temperature independent peak areas and δ^{13}C–values (standard deviations $\leqslant$ 0.3 ‰) were obtained at temperatures above 90 °C for HEDP & EDTMP and above 95 °C for ATMP, implying stable oxidation conditions. At lower temperature, decreasing peak areas and shifts of δ^{13}C–values to more negative values were observed, likely to be caused by incomplete oxidation of the analytes to CO_2. Changing persulfate concentration to 60 g L^{-1} and flow rate to 50 µL min^{-1} (corresponding to an oxygen background of around 22 V at $3 \times 10^8\,\Omega$) stable peak areas and δ^{13}C–values were obtained already at 85 °C for HEDP, EDTMP and 90 °C for ATMP (see **Figure A.4**), which was explained by the higher oxidation capacity of the system resulting from a higher concentration of sulfate radicals.

Hence, stable oxidation conditions at 99.9 °C could be obtained with a persulfate concentration of 30 g L^{-1}, which corresponds to 14.5 mM of persulfate in the oxidation reactor after mixing (and a residence time in the reactor, i.e., a reaction time of 19 s). This is considerably lower than concentrations in most published LC–IRMS methods, in which concentrations of 30 mM to 210 mM were applied (with corresponding reaction times of 20 s to 29 s, respectively).[28,32] Based on these findings, an unnecessarily high oxygen background within the ion source can be avoided and the filament life time can be increased.[29]
However, as demonstrated recently for caffeine, the oxidation temperature test is not a suitable indicator for complete oxidation of a compound. Although complete wet–chemical oxidation of caffeine is hampered by the stability of its N–heteroatomic ring system (resulting in oxidation efficiencies of less than 75 %), stable peak areas and δ^{13}C–values down to an oxidation temperature of 95 °C were obtained.[31] The limitations of the temperature test can be overcome by determining the compound–specific IRMS sensitivity. This test compares the slope of the carbon normalized calibration curve of a target compound with inorganic carbon (DIC) or a

complete oxidizable reference compound. While incomplete oxidation to CO_2 results in slopes deviating from DIC, complete conversion lead to comparable sensitivities, as shown for easy oxidizable compounds such as glucose or vanillin. Comparison to inorganic carbon is the most appropriate approach, as no oxidation is needed and quantitative CO_2 transfer from the liquid phase into the helium stream at the low pH values applied in the interface can be assumed. Hence, the slope of DIC can be used as a proxy for the absolute sensitivity of the LC–IRMS system. However, a direct comparison with carbonate in HPLC mode is not always possible due to problems arising from retention time and peak shape when using a chromatographic column. Thus, oxalate was chosen as reference compound, which showed a retention time between HEDP and ATMP. Based on the lack of heteroatoms oxalate was assumed to be completely oxidizable in the LC–IRMS system, which was confirmed by comparing its carbon normalized slope with the slope of DIC in FIA mode (see **Figure A.5**). In order to allow a better comparison between the different measurements, all peak areas were normalized to the average peak area of the monitoring gas pulses of one sequence. This procedure allowed to correct for the influence of variable ion source sensitivity on the slope of the regression curves (provided that the monitoring gas flow is constant).

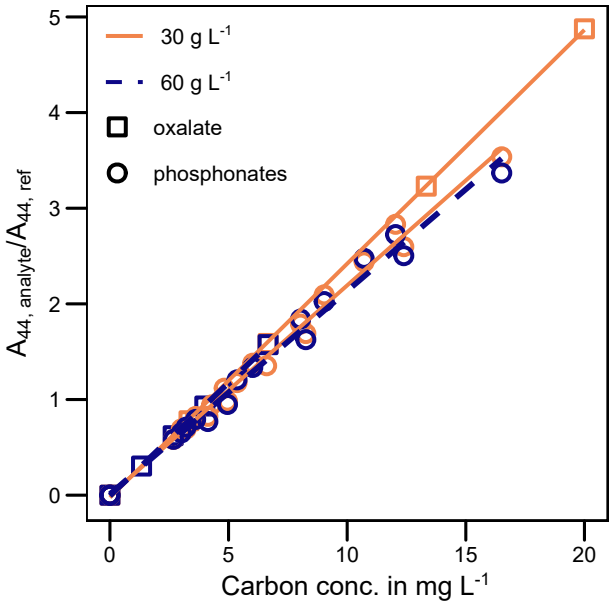

Figure 2.4: Sensitivities for oxalate (squares) and polyphosphonates (circles) at persulfate concentrations of 30 g L^{-1} (blue dashed lines) and 60 g L^{-1} (orange solid lines). The obtained peak areas were normalized to the average peak area of the monitoring gas pulses to account for varying ion source performance.

The slopes obtained for oxalate in HPLC mode of 0.244 ± 0.004 (95 % CI) for the lower and 0.236 ± 0.004 for the higher persulfate concentration ($R^2 \geqslant 0.999$, see **Figure 2.4**) were comparable with the slope obtained for oxalate (0.237 ± 0.001) and DIC (0.235 ± 0.004) in FIA mode, suggesting complete mineralization of oxalate under the tested HPLC conditions. The slopes for the investigated polyphosphonates were in the range of 0.206 to 0.235 ($R^2 \geqslant 0.999$,

see **Figure A.6**). In accordance to oxalate, no correlation between sensitivity and persulfate concentration was observed, as the slopes for ATMP and EDTMP were higher for the lower persulfate concentration. Due to the low variation of the slopes for polyphosphonates, the data for each persulfate concentration were pooled, yielding slopes of 0.219 ± 0.009 for the lower and 0.210 ± 0.010 for the higher persulfate concentration, respectively ($R^2 \geqslant 0.9889$, see **Figure 2.4**).

These results indicate that the higher oxidation capacity of the system had only a minor influence on the oxidation of oxalate as well as polyphosphonates, which is consistent with the oxidation temperature tests. Compared to recent work, in which slopes differing by a factor of approximately two for easy and partially oxidizable compounds were shown, the variations for polyphosphonates and oxalate can be considered as insignificant, suggesting (almost) complete mineralization.[31] This conclusion is noteworthy, as it was shown that HEDP is significantly more resilient towards ozonation and manganese catalyzed oxidation by molecular oxygen than ATMP and EDTMP, which was attributed to its lack of amino groups.[20,33] Complete oxidation of the analytes was further suggested by almost identical offsets between the $\delta^{13}C$–values obtained by EA–IRMS and LC–IRMS for the polyphosphonates, as well as for oxalate (see **Table 2.1**). As incomplete oxidation of the investigated polyphosphonates results in biased $\delta^{13}C$–values (see **Figure 2.3**), a comparable offset indicates quantitative oxidation of the polyphosphonates.

Table 2.1: Influence of LC–IRMS oxidation parameters on the measured offset ($\Delta\delta^{13}C_{LC-EA}$) between the "true" isotopic signature measured by EA–IRMS and the value measured by LC–IRMS (against monitoring gas with a $\delta^{13}C$ set-value of 0 ‰) for the investigated polyphosphonates and oxalate.

Oxidation conditions			$\Delta\delta^{13}C_{LC-EA}$ in ‰			
Persulfate conc. in $g\,L^{-1}$	Persulfate flow in $\mu L\,min^{-1}$	O_2 ($3 \times 10^8\,\Omega$) in V	HEDP	ATMP	EDTMP	oxalate
30	75	15	26.6 ± 0.3	26.3 ± 0.4	26.9 ± 0.1	27.0 ± 0.1
60	50	22	26.7 ± 0.1	26.1 ± 0.4	27.0 ± 0.2	26.5 ± 0.3

Based on various tests conducted under realistic measurement conditions in HPLC mode, it was shown that the investigated polyphosphonates are quantitatively oxidized in the LC–IRMS interface at a comparatively low persulfate concentration. This emphasizes the advantage of a detailed investigation of the oxidation conditions during LC–IRMS method development. Especially in systems not optimized to remove excess oxygen by an additional reduction reactor,[29] this helps to prevent unnecessarily high oxygen backgrounds and consequently reduce instrument downtime and costs per analysis.

Application: Differentiation of sorption and degradation of ATMP based on CSIA

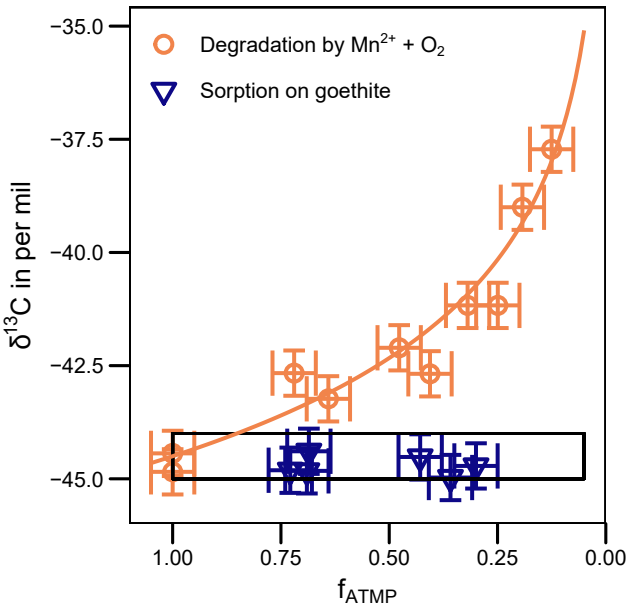

Figure 2.5: Isotopic signature ($\delta^{13}C$) over the remaining aqueous fraction of ATMP during sorption onto goethite (blue triangles) and manganese catalyzed degradation by molecular oxygen (orange circles), including the fit according to the Rayleigh model. The black rectangle represents the initial isotopic signature of ATMP (−44.5 ‰) including the typical measurement uncertainty of 0.5 ‰. For the fraction an error of 7 % was estimated.

The developed and evaluated method was applied to study potential isotope fractionation of ATMP during (i) equilibrium sorption onto the iron oxyhydroxide goethite and (ii) manganese catalyzed oxidation – processes that are likely relevant for the environmental fate of polyphosphonates.

The sorption of ATMP onto iron (oxyhydr–) oxides was investigated extensively in previous studies, which were based on experimental data, as well as on molecular modelling.[22,34,35] Surface complex formation between the phosphonic acid groups and the mineral surface was proposed as the underlying sorption mechanism. In the absence of calcium these bonds are formed directly between one or two oxygen of a phosphonic acid group and iron central atoms of the mineral, whereas calcium acts as a bridging complex leading to the formation of ternary surface complexes. Although, no data for the influence of dissolved magnesium on the sorption of ATMP is available yet, a mechanism as for calcium is conceivable based on the similarity of physicochemical properties of magnesium and calcium.

In accordance with these studies, equilibrium sorption of ATMP onto goethite could be described by a saturation–type Langmuir isotherm (see **Figure A.7(a)**). Carbon isotope analysis was conducted for samples spanning a range of adsorbed ATMP fractions from 25 % to 75 %. Neither in the absence, nor in the presence of dissolved calcium or magnesium significant carbon isotope fractionation ($\leqslant 0.5$ ‰) was observed, resulting in an average $\delta^{13}C$–value of -44.7 ± 0.2 ‰ (n = 6) (see **Figure 2.5**). Taking the proposed sorption mechanisms into account,

these results can be explained by the fact that carbon is not directly involved in the bond–formation steps and thus only secondary isotope effects (i.e. isotope effects at non–reactive positions) come into consideration.[24]

Degradation of ATMP by molecular oxygen was investigated in detail in studies by Nowack & Stone.[20,25] The authors proposed a reaction scheme consisting of (i) an initial complex formation step between manganese and ATMP, (ii) the oxidation of this complex by molecular oxygen to Mn(III)ATMP and (iii) the oxidation of ATMP by Mn(III) leading to a C–P bond cleavage in the ATMP and a corresponding reduction of the manganese to Mn(II). Consequently, manganese is acting as a catalyzed in this reaction.

Consistent with this scheme, ATMP could be completely degraded in the presence of dissolved oxygen and 0.1 mM Mn^{2+} (initial manganese to ATMP ratio of 0.1) within 8 h (see **Figure A.7(b)**). As can be seen in **Figure 2.5**, significant enrichment of ^{13}C in the remaining ATMP fraction was observed during the reaction, implying that the reaction is associated with a normal kinetic isotope effect. The data could be fitted using the Rayleigh model ($R^2 = 0.95$), yielding a carbon isotope enrichment factor of -3.3 ± 0.6 ‰ (95 % CI). This value is considerably lower than the theoretically value calculated from the semi–classical Streitwieser limit for C–P bond cleavage of -14.4 % (see appendix A for calculations). This difference points towards a masking of the kinetic isotope effect associated with the bond cleavage by a preceding non–fractionating step, likely the formation of the MnATMP complex.[24] This hypothesis is supported by the observations made in the sorption experiments, which implied that the complex formation step is not associated with a significant carbon isotope effect. Moreover, the initial formation of the MnATMP complex was identified in previous studies as the rate–limiting step for manganese to ATMP ratios below one, as applied here.[20]

Overall, the results showed that carbon CSIA is a suitable tool to assign a concentration decrease of ATMP either to adsorption or degradation under the given conditions owing to the shift of the $\delta^{13}C$–signature to more positive values during degradation. Based on the obtained isotope enrichment factor this shift becomes significant ($\geqslant 2$ ‰) when at least 47 % of the initial ATMP is degraded, which then allows the qualitative proof of degradation.[36]

Conclusion

Although compound–specific carbon isotope analysis by LC–IRMS is a promising tool to investigate the fate of polar organic xenobiotics in environmental and technical systems, only a small number of methods are available. With this study we broaden the range of possible applications by presenting the first LC–IRMS method for the three widely used polyphosphonate complexing agents HEDP, ATMP and EDTMP. An elaborate investigation of the wet–chemical oxidation conditions proofed complete oxidation of the three investigated compounds inside the LC–IRMS interface. Applying the developed method, surface complex formation (no detectable isotope effect) can be differentiated from manganese catalyzed oxidation of ATMP (normal kinetic isotope effect with $\varepsilon_C = -3.3 \pm 0.6$ ‰), highlighting the potential of CSIA to

investigate the fate of polyphosphonate complexing agents in technical and environmental systems. As not all transformation products formed during manganese catalyzed oxidation of ATMP are identified yet or have multiple possible sources (e.g. IDMP production during photolysis of EDTMP and DTPMP[37,38]) CSIA offers a straightforward and robust method to (qualitatively) proof ATMP degradation.[25]

In further studies we will investigate the influence of different parameters such as the pH on the kinetic isotope effect for manganese catalyzed ATMP–degradation, which might help to get deeper insights into the underlying reaction mechanism and therefore into the environmental behavior of polyphosphonates. In order to apply the developed method to environmental samples, enrichment techniques have to be developed in the future, as shown recently for the quantification of polyphosphonates in river water.[39,40] Although high pre–concentration factors in the order of 1×10^4 are needed for LC–IRMS analysis due to the high amount of injected carbon needed, it was shown recently for a set of pesticides that a solid–phase enrichment step prior to LC–IRMS analysis allowed detection limits in the sub–$\mu g\,L^{-1}$ range, hence in environmentally relevant concentrations.[41]

References

(1) Elsner, M.; Imfeld, G. Compound-specific isotope analysis (CSIA) of micropollutants in the environment - current developments and future challenges. *Current Opinion in Biotechnology* **2016**, *41*, 60–72.

(2) Elsner, M.; Zwank, L.; Hunkeler, D.; Schwarzenbach, R. P. A new concept linking observable stable isotope fractionation to transformation pathways of organic pollutants. *Environmental Science & Technology* **2005**, *39*, 6896–6916.

(3) Schmidt, T. C.; Zwank, L.; Elsner, M.; Berg, M.; Meckenstock, R. U.; Haderlein, S. B. Compound-specific stable isotope analysis of organic contaminants in natural environments: a critical review of the state of the art, prospects, and future challenges. *Analytical and Bioanalytical Chemistry* **2004**, *378*, 283–300.

(4) Thullner, M.; Centler, F.; Richnow, H.-H.; Fischer, A. Quantification of organic pollutant degradation in contaminated aquifers using compound specific stable isotope analysis – Review of recent developments. *Organic Geochemistry* **2012**, *42*, 1440–1460.

(5) Loos, R.; Carvalho, R.; António, D. C.; Comero, S.; Locoro, G.; Tavazzi, S.; Paracchini, B.; Ghiani, M.; Lettieri, T.; Blaha, L. EU-wide monitoring survey on emerging polar organic contaminants in wastewater treatment plant effluents. *Water Research* **2013**, *47*, 6475–6487.

(6) Krummen, M.; Hilkert, A. W.; Juchelka, D.; Duhr, A.; Schlüter, H.-J.; Pesch, R. A new concept for isotope ratio monitoring liquid chromatography/mass spectrometry. *Rapid Communications in Mass Spectrometry* **2004**, *18*, 2260–2266.

(7) Cabanero, A. I.; Recio, J. L.; Ruperez, M. Liquid chromatography coupled to isotope ratio mass spectrometry: a new perspective on honey adulteration detection. *Journal of Agricultural and Food Chemistry* **2006**, *54*, 9719–9727.

(8) Köster, D.; Wolbert, J. B.; Schulte, M. S.; Jochmann, M. A.; Schmidt, T. C. Origin of Xylitol in Chewing Gum: A Compound-Specific Isotope Technique for the Differentiation of Corn- and Wood-Based Xylitol by LC-IRMS. *Journal of Agricultural and Food Chemistry* **2018**, *66*, 2015–2020.

(9) Cabanero, A. I.; Recio, J. L.; Ruperez, M. Isotope ratio mass spectrometry coupled to liquid and gas chromatography for wine ethanol characterization. *Rapid Communications in Mass Spectrometry* **2008**, *22*, 3111–3118.

(10) Godin, J. P.; McCullagh, J. S. Review: Current applications and challenges for liquid chromatography coupled to isotope ratio mass spectrometry (LC/IRMS). *Rapid Communications in Mass Spectrometry* **2011**, *25*, 3019–3028.

(11) Kujawinski, D. M.; Zhang, L.; Schmidt, T. C.; Jochmann, M. A. When other separation techniques fail: compound-specific carbon isotope ratio analysis of sulfonamide containing pharmaceuticals by high-temperature-liquid chromatography-isotope ratio mass spectrometry. *Analytical Chemistry* **2012**, *84*, 7656–7663.

(12) Zhang, L.; Kujawinski, D. M.; Jochmann, M. A.; Schmidt, T. C. High-temperature reversed-phase liquid chromatography coupled to isotope ratio mass spectrometry. *Rapid Communications in Mass Spectrometry* **2011**, *25*, 2971–2980.

(13) Godin, J.-P.; Hopfgartner, G.; Fay, L. Temperature-programmed high-performance liquid chromatography coupled to isotope ratio mass spectrometry. *Analytical chemistry* **2008**, *80*, 7144–7152.

(14) Kujawinski, D. M.; Wolbert, J. B.; Zhang, L.; Jochmann, M. A.; Widory, D.; Baran, N.; Schmidt, T. C. Carbon isotope ratio measurements of glyphosate and AMPA by liquid chromatography coupled to isotope ratio mass spectrometry. *Analytical and Bioanalytical Chemistry* **2013**, *405*, 2869–2878.

(15) Nowack, B. Environmental chemistry of phosphonates. *Water Research* **2003**, *37*, 2533–2546.

(16) Jarvie, H. P.; Neal, C.; Withers, P. J. Sewage-effluent phosphorus: a greater risk to river eutrophication than agricultural phosphorus? *Science of the Total Environment* **2006**, *360*, 246–253.

(17) Wu, L. H.; Luo, Y. M.; Christie, P.; Wong, M. H. Effects of EDTA and low molecular weight organic acids on soil solution properties of a heavy metal polluted soil. *Chemosphere* **2003**, *50*, 819–822.

(18) Nowack, B. Aminopolyphosphonate removal during wastewater treatment. *Water Research* **2002**, *36*, 4636–4642.

(19) Rott, E.; Steinmetz, H.; Metzger, J. W. Organophosphonates: A review on environmental relevance, biodegradability and removal in wastewater treatment plants. *Science of the Total Environment* **2018**, *615*, 1176–1191.

(20) Nowack, B.; Stone, A. T. Degradation of Nitrilotris(methylenephosphonic Acid) and Related (Amino)Phosphonate Chelating Agents in the Presence of Manganese and Molecular Oxygen. *Environmental Science & Technology* **2000**, *34*, 4759–4765.

(21) Lesueur, C.; Pfeffer, M.; Fuerhacker, M. Photodegradation of phosphonates in water. *Chemosphere* **2005**, *59*, 685–691.

(22) Martinez, R. J.; Farrell, J. Understanding Nitrilotris(methylenephosphonic acid) reactions with ferric hydroxide. *Chemosphere* **2017**, *175*, 490–496.

(23) Dolan, J. W. Peak tailing and resolution. *LC-GC The Magazine of Separation Science* **2002**, *20*, 430–437.

(24) Elsner, M. Stable isotope fractionation to investigate natural transformation mechanisms of organic contaminants: principles, prospects and limitations. *Journal of Environmental Monitoring* **2010**, *12*, 2005–2031.

(25) Nowack, B.; Stone, A. T. Homogeneous and heterogeneous oxidation of nitrilotrismethylenephosphonic acid (NTMP) in the presence of manganese (II, III) and molecular oxygen. *The Journal of Physical Chemistry B* **2002**, *106*, 6227–6233.

(26) Jochmann, M. A.; Blessing, M.; Haderlein, S. B.; Schmidt, T. C. A new approach to determine method detection limits for compound-specific isotope analysis of volatile organic compounds. *Rapid Communications in Mass Spectrometry* **2006**, *20*, 3639–3648.

(27) Wei, X.; Gilevska, T.; Wetzig, F.; Dorer, C.; Richnow, H. H.; Vogt, C. Characterization of phenol and cresol biodegradation by compound-specific stable isotope analysis. *Environmental Pollution* **2016**, *210*, 166–173.

(28) Gilevska, T.; Gehre, M.; Richnow, H. H. Performance of the wet oxidation unit of the HPLC isotope ratio mass spectrometry system for halogenated compounds. *Analytical Chemistry* **2014**, *86*, 7252–7257.

(29) Hettmann, E.; Brand, W. A.; Gleixner, G. Improved isotope ratio measurement performance in liquid chromatography/isotope ratio mass spectrometry by removing excess oxygen. *Rapid Communications in Mass Spectrometry* **2007**, *21*, 4135–4141.

(30) Alberic, P. Liquid chromatography/mass spectrometry stable isotope analysis of dissolved organic carbon in stream and soil waters. *Rapid Communications in Mass Spectrometry* **2011**, *25*, 3012–3018.

(31) Köster, D.; Sanchez Villalobos, I. M.; Jochmann, M. A.; Brand, W. A.; Schmidt, T. C. New Concepts for the Determination of Oxidation Efficiencies in Liquid Chromatography-Isotope Ratio Mass Spectrometry. *Analytical Chemistry* **2019**, *91*, 5067–5073.

(32) Scheibe, A.; Krantz, L.; Gleixner, G. Simultaneous determination of the quantity and isotopic signature of dissolved organic matter from soil water using high-performance liquid chromatography/isotope ratio mass spectrometry. *Rapid Communications in Mass Spectrometry* **2012**, *26*, 173–180.

(33) Klinger, J.; Sacher, F.; Brauch, H.-J.; Maier, D.; Worch, E. Behaviour of phosphonic acids during drinking water treatment. *Vom Wasser* **1998**, *91*, 15–28.

(34) Nowack, B.; Stone, A. T. Adsorption of Phosphonates onto the Goethite-Water Interface. *Journal of Colloid and Interface Science* **1999**, *214*, 20–30.

(35) Nowack, B.; Stone, A. T. The Influence of Metal Ions on the Adsorption of Phosphonates onto Goethite. *Environmental Science & Technology* **1999**, *33*, 3627–3633.

(36) Schmidt, T. C.; Jochmann, M. A. Origin and fate of organic compounds in water: characterization by compound-specific stable isotope analysis. *Annual Review of Analytical Chemistry* **2012**, *5*, 133–155.

(37) Kuhn, R.; Tóth, E.; Geppert, H.; Fischer, T.; Liebsch, S.; Martienssen, M. Identification of the Complete Photodegradation Pathway of Ethylenediaminetetra(methylenephosphonic acid) in Aqueous Solution. *CLEAN - Soil, Air, Water* **2017**, *45*.

(38) Kuhn, R.; Jensch, R.; Bryant, I. M.; Fischer, T.; Liebsch, S.; Martienssen, M. The influence of selected bivalent metal ions on the photolysis of diethylenetriamine penta(methylenephosphonic acid). *Chemosphere* **2018**, *210*, 726–733.

(39) Schmidt, C. K.; Raue, B.; Brauch, H.-J.; Sacher, F. Trace-level analysis of phosphonates in environmental waters by ion chromatography and inductively coupled plasma mass spectrometry. *International Journal of Environmental Analytical Chemistry* **2013**, *94*, 385–398.

(40) Wang, S.; Sun, S.; Shan, C.; Pan, B. Analysis of trace phosphonates in authentic water samples by pre-methylation and LC-Orbitrap MS/MS. *Water Research* **2019**, *161*, 78–88.

(41) Torrento, C.; Bakkour, R.; Glauser, G.; Melsbach, A.; Ponsin, V.; Hofstetter, T. B.; Elsner, M.; Hunkeler, D. Solid-phase extraction method for stable isotope analysis of pesticides from large volume environmental water samples. *Analyst* **2019**, *144*, 2898–2908.

3 Two pathways compete in the Mn(II)–catalyzed oxidation of aminotrismethylene phosphonate (ATMP)

Philipp R. Martin, Daniel Buchner, Maik A. Jochmann, Martin Elsner, Stefan B. Haderlein

Author	Author position	Scientific ideas	Data generation*	Analysis & interpretation	Paper writing
P. Martin	1	50 %	70 %	40 %	40 %
D. Buchner	2	30 %	0 %	30 %	30 %
M. Jochmann	3	10 %	0 %	10 %	10 %
M. Elsner	4	0 %	0 %	10 %	10 %
S. Haderlein	5	10 %	0 %	10 %	10 %

Title of the paper:
Two pathways compete in the Mn(II)–catalyzed oxidation of aminotrismethylene phosphonate (ATMP)

Status in the publication process:
submitted for publication to *Environmental Science & Technology*

* Experiments were conducted with the help of Stephanie Graaf (see acknowledgments)

Published after revision:
Martin, P. R., Buchner, D., Jochmann, M. A., Elsner, M. & Haderlein, S. B.
Environmental Science & Technology **Article ASAP**.
DOI: 10.1021/acs.est.1c06407

3.1 Abstract

Mn(II)–catalyzed oxidation by molecular oxygen is considered a relevant transformation process for the environmental fate of aminopolyphosphonate chelating agents such as aminotrismethylene phosphonate (ATMP). However, the role of potential Mn(III)–intermediates for the underlying transformation mechanisms remains imperfectly understood. We applied kinetic studies, compound–specific stable carbon isotope analysis and equilibrium speciation modelling to investigate the role of Mn(II)–ATMP speciation on underlying reaction mechanisms. Surprisingly, both (i) Mn(II)ATMP–normalized transformation rate constants of ATMP and (ii) observed carbon isotope enrichment factors (ε–values) inversely correlated with the fraction of ATMP complexed with Mn(II). These findings provide evidence of two parallel ATMP transformation pathways exhibiting distinctly different reaction kinetics and carbon isotope fractionation: (i) slow oxidation of ATMP present in Mn(III)ATMP–complexes ($\varepsilon \approx -10\,‰$) and (ii) fast oxidation of free ATMP by these catalytic Mn(III)ATMP–species ($\varepsilon \approx -1\,‰$). This slow self–decomposition, but elevated activity of catalytic Mn(III)ATMP for oxidation of free solutes (here: uncomplexed ATMP) implies that Mn(III)ATMP likely acts as oxidant also for other reductants in aqueous environments. In comparison, our results indicate that their self–decomposition is comparatively slow implying a diminished share of Mn(II)–catalyzed oxidation to overall ATMP transformation in the environment.

3.2 Introduction

Persistent and mobile organic contaminants have the potential to threaten surface and groundwater bodies and thus drinking water resources.[1–3] A compound class of rising concern are polyphosphonate chelating agents.[4] Due to their ability to form strong complexes with di– and trivalent cations, they are increasingly used to replace polycarboxylates (e.g., ethylenediaminetetraacetate, EDTA) and polyphosphates in various applications, for instance as bleaching stabilizers in household and industrial cleaners, or as scale inhibitors in cooling water cycles and membrane filtration.[5,6] Hence, polyphosphonates are released into the environment via industrial as well as domestic wastewater. Although knowledge on the environmental occurrence of polyphosphonates is limited due to the lack of analytical methods for routine analysis, available studies indicate that polyphosphonates occur in many wastewater–receiving surface waters.[7–9] Thus, further research on polyphosphonate transformation processes is needed (i) to get a more comprehensive understanding of their environmental fate and (ii) to develop strategies to reduce the overall load of polyphosphonates in receiving surface waters. While bio–transformation under environmentally relevant conditions has not been reported yet, various abiotic transformation pathways such as direct photolysis of Fe(III)–phosphonate complexes and ozonation are known.[10–12] Mn(II)–catalyzed oxidation by molecular oxygen is considered a relevant pathway for the removal of aminopolyphosphonates (i.e., polyphosphonates containing at least one tertiary amine group), based on the widespread presence of manganese in the environment and the strong tendency of aminopolyphosphonates to form

complexes.[5] Nowack and Stone presented a transformation scheme for aminotrismethylene phosphonate (ATMP) and proposed a three step transformation mechanism comprising (i) formation of a Mn(II)ATMP complex, (ii) oxidation of the complex by molecular oxygen to yield Mn(III)ATMP and finally (iii) breakdown of ATMP via C–P bond cleavage initiated by an inner–sphere electron transfer leading to the back–reduction of Mn(III) to Mn(II).[13–15] However, further insights in the transformation process in terms of rate–limiting steps within the multi-step reaction as well as the role of Mn(III)–intermediates are needed to assess the relevance of Mn(II)–catalyzed oxidation in environmental systems. The speciation of Mn(II)–ATMP appears to be a key factor controlling the Mn(II)–catalyzed oxidation of ATMP as the formation of the Mn(II)ATMP complex is rate–limiting for ATMP breakdown.[13] Furthermore, the fraction of ATMP complexed with Mn potentially influences the underlying transformation mechanisms, as shown for Mn(III)EDTA. This complex is not only subject to self–decomposition via an inner–sphere electron transfer leading to EDTA breakdown, but is also capable of oxidizing free, un–complexed EDTA.[16,17] The latter pathway is in accordance with the characteristics of Mn(III)–complexes as potent oxidation agents.[18–20]

Besides kinetic studies, compound–specific stable isotope analysis (CSIA) of light elements (e.g., $^{13}C/^{12}C$) is a powerful approach to characterize transformation mechanisms of organic pollutants (for an extensive review on CSIA we refer to Elsner, 2010).[21] Carbon CSIA for polar and thus water–soluble compounds, can be achieved by coupling liquid chromatography with isotope ratio mass spectrometry (LC–IRMS), as demonstrated in our recent work for three widely used polyphosphonate–chelating agents including ATMP.[22–24] CSIA allows to determine kinetic isotope effects associated with transformation reactions, i.e., the difference in reaction rate constants for molecules possessing either a light or heavy stable isotope of a certain element at the reactive site (for carbon: $KIE_C = {}^{12}k/{}^{13}k$).[25] Consequently, heavy isotopes are discriminated against so that they progressively accumulate in the remaining substrate and the KIE leads to a gradual shift of the isotopic composition in the substrate over the course of its transformation. The extent of the intrinsic kinetic isotope effect and the enrichment of heavy isotopes over time is governed by the corresponding transition state structure.[21,26] This allows in selected cases to distinguish different reaction mechanisms by carbon CSIA, provided that (i) these mechanisms are characterized by distinct intrinsic kinetic isotope effects (i.e., transition states) and (ii) the full extent of the intrinsic isotope effect of the mechanisms is observed.[21,27,28] However, CSIA allows only the indirect determination of the KIE, by measuring the observable isotope fractionation, reflected in the carbon isotope enrichment factor (ε_C). Therefore, CSIA may also provide information on rate–determining steps within a reaction cascade governed by a known mechanism.[21] In multistep reactions the intrinsic isotope fractionation can be diminished (i.e., masked) by preceding non/ small–fractionating but rate–determining steps. In such cases, the observable ε_C would be very small. Vice versa, a distinct observed carbon KIE indicates that cleavage of a carbon bond is the rate–determining step within a multistep reaction.

The aim of our study was to obtain a comprehensive mechanistic understanding of Mn(II)–catalyzed ATMP oxidation. Thus, we applied a combination of kinetic studies, as well as compound–specific carbon isotope analysis and equilibrium speciation modelling in carefully designed laboratory batch experiments to elucidate (i) rate–limiting steps and (ii) the role of Mn(III)ATMP–intermediates. To this end, we controlled the fraction of ATMP complexed with Mn(II) by varying the initial Mn(II):ATMP ratio and the pH–value. The overarching goal was to better understand mechanisms of Mn(II)–catalyzed oxidation of aminopolyphosphonates under environmentally relevant conditions in order to enable a more profound assessment of the environmental fate of these compounds.

3.3 Materials and methods

Transformation batch experiments

Experimental setup: Transformation experiments were conducted in duplicates (and one Mn–free control) at $22 \pm 2\,^{\circ}C$ under constant rapid stirring (approx. 750 rpm) in open clear glass bottles exposed to air. The experiments were started by adding a $MnCl_2$ ($\geqslant$ 99 %, Merck Millipore, Darmstadt, Germany) stock solution ($\leqslant$ 2 vol%) to a pH–adjusted (buffered) ATMP ($\geqslant$ 97 % (T), Sigma Aldrich, Steinheim, Germany) solution. 20 mM MES buffer (PUFFERAN® $\geqslant$ 99 %, Carl Roth, Karlsruhe, Germany) was used for the experiments at pH 6.8 ± 0.1. Alternatively, 20 mM $NaNO_3$ ($\geqslant$ 99 %, Carl Roth, Karlsruhe, Germany) was used as background electrolyte for the unbuffered experiments. Ultra–pure water for all solutions was obtained from a Barnstead™GenPure™system (Thermo Fisher Scientific, Germany) and pH was adjusted with NaOH (1 M, Merck Millipore).

Sampling: For each time point, 5 mL of sample were withdrawn and added to a 10 mL vial containing 100 ± 2 mg of cation exchange resin (DOWEX®50 W X 8, 100–200 mesh, H^+–form, Carl Roth, Karlsruhe, Germany). In order to remove Mn from the sample and transfer ATMP into its free, un–complexed form, the vials were shaken 15 min overhead. Afterwards, the samples were filtered through a 0.45 µm syringe filter (regenerated celluloses, Sartorius, Göttingen, Germany) and 3 mL of the samples were distributed equally into three HPLC vials containing 50 µL of a 50 mM EDTA ($\geqslant$ 99 %, Sigma–Aldrich, Steinheim, Germany) solution, in order to complex remaining Mn in solution.[13] Afterwards, samples were stored at $-20\,^{\circ}C$ if not analyzed at the same day. The samples were stable with respect to concentration, as well as isotopic composition.

Concentration analysis of ATMP

For the quantification of remaining ATMP in solution, an UltiMate3000 HPLC–system (Thermo Fisher Scientific, Germering, Germany) equipped with an IC NI–424 anion chromatography column (4.6 mm $\times$ 100 mm, Shodex, Munich, Germany), held at $40\,^{\circ}C$ was connected to a refraction index detector (RI–101, Shodex, Munich, Germany), held at $35\,^{\circ}C$. A sample volume

of 50 µL was injected and 4 mM sulfuric acid (prepared from 95 % to 97 % H_2SO_4, EMSURE®, Merck Millipore, Darmstadt, Germany) at a flow rate of 500 µL min^{-1} was used as eluent. External standards were used for quantification ($R^2 \geqslant 0.99$). The limit of quantification was 10 mg L^{-1}.

Quantification of ortho–phosphate

Ortho–phosphate was quantified spectroscopically by the molybdenum blue method according to Murphy and Riley.[29] Briefly, samples were diluted 1:10 with ultra–pure water in a 1 cm cuvette in order to obtain absorbance values within the calibration range. After mixing the sample with the reagent solution and a reaction time of 30 min, the absorbance was measured at 710 nm (photolab®6600 UV–Vis, WTW, Weilheim, Germany).

Compound–specific isotope analysis

Stable carbon isotope ratios in the residual ATMP fraction were analyzed by means of LC–IRMS, as described elsewhere.[24] Separation of ATMP from its transformation products was conducted on the UltiMate3000 HPLC–system as described earlier, except for a reduced flow rate of 500 µL min^{-1}. Analysis of carbon isotope ratios was conducted on a Delta V Plus IRMS, which was hyphenated to the HPLC via a LC Isolink interface (both Thermo Fisher Scientific, Bremen, Germany). The eluent stream was mixed within a mixing–tee with 1.5 M phosphoric acid (prepared from 85 % H_3PO_4, EMSURE®, Merck Millipore, Darmstadt, Germany) and 30 g L^{-1} sodium persulfate (for analysis EMSURE®, Merck Millipore, Darmstadt, Germany), which were delivered at flow rates of 50 µL min^{-1} and 75 µL min^{-1}, respectively. The δ^{13}C–values of ATMP were obtained using a concentration–adjusted ATMP reference standard (measured by EA–IRMS as described elsewhere[30] with $\delta^{13}C_{EA\text{–}value} = -44.5 \pm 0.1$ ‰ (n = 3) in VPDB scale) bracketing six samples by duplicate standards. Samples were diluted with ultra–pure water to the same concentration before analysis. The uncertainty of the measurements was $\leqslant 0.5$ ‰ (n = 2–3).

Calculations

Carbon isotope enrichment factor: For the calculation of carbon isotope enrichment factors (ε_C), the data was evaluated applying the linearized Rayleigh distillation equation, without forcing through the origin, as proposed by Scott, et al.:[31]

$$\ln\left(\frac{R(t)}{R(0)}\right) = \ln\left(\frac{\delta^{13}C(t)+1}{\delta^{13}C(t)+1}\right) = \varepsilon_C \times \ln\left(\frac{c(t)}{c(0)}\right) \tag{3.1}$$

with the isotopic ratio R ($= {}^{13}C/{}^{12}C$), the isotopic signature normalized to an international reference standard δ^{13}C and the concentration c at the beginning of the experiment (0) and at time point t.

Equilibrium speciation: Calculations of the equilibrium speciation of ATMP in the presence of Mn(II) were conducted in the PhreeqC software package (version 3.4.0.12927).[32] The wateq4f–database was used for all calculations, which was supplemented with the acidity constants for ATMP and the equilibrium constants for the bimolecular Mn(II)ATMP–complexes taken from Lacour, et al.[33] and Popov, et al.,[34] respectively. The temperature was set to 22 °C for all calculations and 20 mM $NaNO_3$ was added as background electrolyte.

3.4 Results and discussion

Effect of the initial Mn(II) to ATMP ratio and pH on the reaction kinetics

If the formation of a Mn(II)–complex was the first step in the reaction sequence leading to oxidative breakdown of ATMP via complex decomposition – as suggested by Nowack and Stone[13] – the rate constant of ATMP disappearance should be higher when more ATMP is present in its complexed reactive form, f_{compl}. To investigate this hypothesis, the influence of the Mn(II)–complexed ATMP fraction on the transformation kinetics and carbon isotope fractionation was investigated in experiments with varying initial Mn(II) concentrations and a fixed initial ATMP concentration at a pH of 6.8 ± 0.1, resulting in initial Mn(II):ATMP ratios (Mn(II):ATMP(0)) of 1:100 to 1:1 and initial Mn(II)–complexed ATMP fractions ($f_{\mathrm{compl}}(0)$) of 0.01 to 0.82 (calculated based on equilibrium assumptions). In accordance with findings of Nowack and Stone,[13] ATMP was degraded at all four initial Mn(II):ATMP ratios, revealing the catalytic role of Mn(II) in the system (see **Figure 3.1(a)**). Transformation of ATMP via C–P bond cleavage was confirmed by the detection of ortho–phosphate as transformation product, resulting in a closed phosphorus mass balance for all experiments (i.e., ATMP + o–PO_4^{3-} $\geqslant$ 0.85 mM, see **Figure B.1**).

Figure 3.1(a), however, also shows that ATMP transformation profiles followed a complex behavior, whereby different transformation profiles for the two (i) low (1:100 and 1:10) and (ii) high (1:2 and 1:1) initial Mn(II):ATMP ratios respectively could be distinguished. For the two lower Mn(II):ATMP ratios, an initial phase with slow transformation was followed by an increasing transformation rate until a constant rate was reached, resulting in a linear decrease in concentration at later time points. For the higher initial Mn(II):ATMP ratios, however, a short lag phase and a rapid initial decrease in ATMP concentration was followed by a third regime, in which the transformation rate slowed down distinctly. As a result, the overall transformation of ATMP was slowest for the highest initial Mn(II):ATMP ratio (corresponding to $f_{\mathrm{compl}}(0) = 0.82$), for which no complete transformation within the experimental run time of 40 h was reached. A limitation of oxygen as cause for the significant decrease in the reaction rate can be excluded, as the concentration of dissolved oxygen (0.12 mM to 0.28 mM) had no influence on the ATMP transformation kinetics (see **Figure B.2(a)**). The pronounced decrease in the reaction rate was supported by monitoring the transformation of ATMP with varying starting concentrations (1 mM to 5 mM) in the presence of 1 mM Mn(II) (see **Figure B.3** for transformation profiles). Irrespective of the initial ATMP concentration, the transformation

rate decreased substantially at a remaining ATMP concentration of around 0.2 mM to 0.3 mM. Consistent with these observations, transformation of 2 mM ATMP in the presence of 2 mM Mn(II) already leveled off at an ATMP concentration of around 0.7 mM. Surprisingly, reaction rates therefore seemed to become smaller rather than greater when all ATMP was trapped in Mn–complexes and no free ATMP was left in solution.

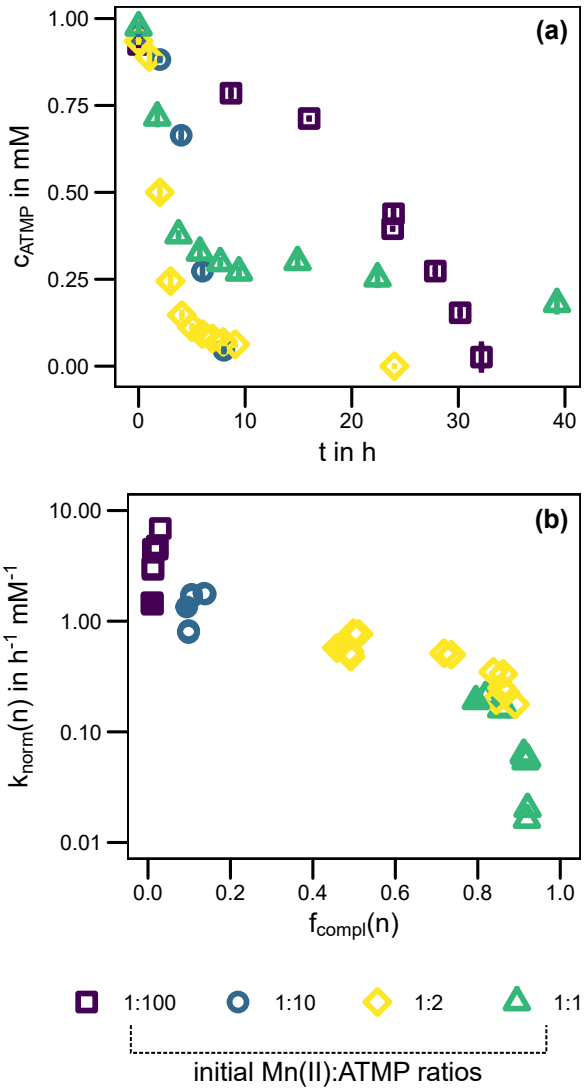

Figure 3.1: (**a**) Temporal transformation profiles of ATMP for varying Mn(II):ATMP(0) (corresponding to Mn(II) concentrations of 0.01 mM to 1 mM) at pH 6.8 ± 0.1. Shown are the average concentrations of duplicate batch experiments. Error bars representing one standard deviation. (**b**) Stepwise calculated initial (0^{th} order) transformation rate constants (obtained from linear regressions of three consecutive data points) normalized to the concentration of Mn(II)ATMP at the beginning of the segment ($k_{norm}(n)$) vs. the complexed ATMP fraction at the beginning of the segment ($f_{compl}(n)$). Filled symbols show the initial transformation rates at t_0.

However, evaluation of the data in **Figure 3.1(a)** is complicated by the fact that our systematic variation of the Mn(II):ATMP ratio in the different experiments influenced not only f_{compl}, but also the concentration of putative reactive Mn–ATMP species. Therefore, a different approach to evaluate the data was applied, where initial (pseudo 0^{th} order) rate constants were determined

stepwise for a time interval n, comprising three consecutive data points (see **Figure B.4**). These rate constants were then normalized to the concentration of Mn(II)ATMP–complexes at the beginning of the interval (Mn(II)ATMP(n), calculated based on equilibrium assumption, see appendix B) resulting in normalized initial transformation rate constants (k_{norm}). **Figure 3.1(b)** shows k_{norm} as function of the complexed fraction of ATMP ($f_{\mathrm{compl}}(n)$). The obtained k_{norm}–values decreased with increasing complexed ATMP fraction (f_{compl} between 0.01 and 0.92) with values between $7\,\mathrm{h^{-1}mM^{-1}}$ (Mn:ATMP(0) = 1:100) and $0.2\,\mathrm{h^{-1}mM^{-1}}$ (Mn:ATMP(0) = 1:1). This consistent picture of **Figure 3.1(b)** has two implications. (i) It indicates that Mn–ATMP complexes indeed act as active/catalytic species, else normalization of rates to Mn(II)ATMP would not have the observed leveraging effect on the y–axis. (ii) At the same time, it indicates that the Mn–ATMP complexes themselves decompose very slowly, otherwise reaction rates would not decrease by orders of magnitude when all ATMP is caught up in complexes.

These observations were further strengthened by results from experiments conducted at a different pH of 3.6 ± 0.1 (see **Figure B.5(a)** for transformation profiles). As the fraction of complexed ATMP decreases with decreasing pH value in a given system, the normalized initial transformation rate constant for Mn(II):ATMP(0) = 1:1 ($f_{\mathrm{compl}}(0) = 0.05$) at pH 3.6 was approximately ten times higher in comparison to pH 6.8 ($6.5\,\mathrm{h^{-1}mM^{-1}}$ vs. $0.6\,\mathrm{h^{-1}mM^{-1}}$) and comparable to the value for Mn(II):ATMP(0) = 1:100 ($f_{\mathrm{compl}}(0) = 0.01$) at pH 6.8. The observation of faster transformation at lower pH is consistent with observations from Nowack and Stone, who also reported faster transformation of 0.85 mM ATMP in the presence of an equimolar concentration of Mn(II) at pH 3.4 in comparison to pH 7.1.[14] Combining the observation that reaction rate constants decreased by orders of magnitude when all ATMP was caught up in complexes, and the fact that limitation in the oxygen supply can be ruled out as possible reason calls for a second, faster reaction mechanism involving free ATMP in solution. To confirm its existence by independent evidence, carbon CSIA was used as a complementary tool, to probe whether such competing transformation pathways are associated with different kinetic isotope effects.

Effect of the initial Mn to ATMP ratio and pH on the observed carbon isotope fractionation

Carbon CSIA revealed a significant enrichment ($> 0.5\,‰$) in ^{13}C for all four investigated Mn(II):ATMP ratios at pH 6.8 and therefore a normal kinetic isotope effect.[21] Fits of the data sets according to the Rayleigh distillation equation are shown in **Figure 3.2** ($R^2 \geqslant 0.97$). The obtained carbon isotope enrichment factors (ε_C, including their 95 % confidence interval, CI) ranged from $-0.8 \pm 0.1\,‰$ (Mn(II):ATMP(0) = 1:100, $f_{\mathrm{compl}}(0) = 0.01$) to $-9.4 \pm 0.6\,‰$(Mn(II):ATMP(0) = 1:1, $f_{\mathrm{compl}}(0) = 0.82$). The ε_C–values for Mn(II):ATMP(0)–values of 1:10 ($\varepsilon_C = -2.0 \pm 0.2\,‰$) and 1:2 ($\varepsilon_C = -7.2 \pm 0.9\,‰$) fell between these values. In accordance with the transformation profiles, the observed ε_C–values were independent of the concentration of dissolved oxygen in the investigated range (see **Figure B.2(c)**). Hence, the observed magnitude of carbon isotope fractionation at pH 6.8 increased with the applied Mn(II) concentration and therefore with the fraction of ATMP complexed with Mn(II) at the beginning of

the experiments.

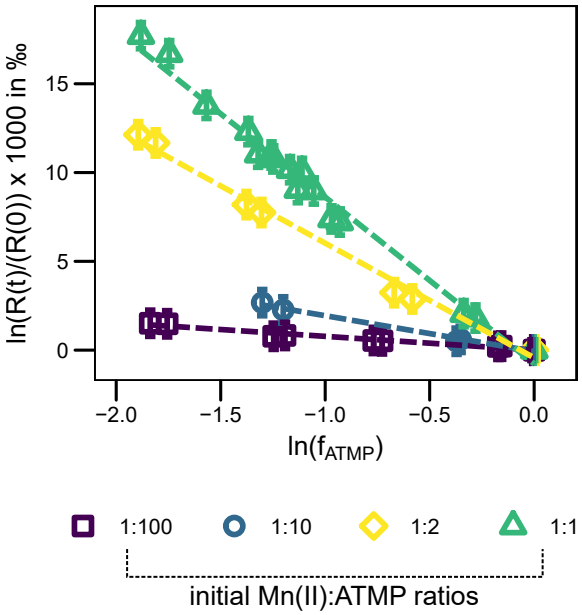

Figure 3.2: Double–logarithmic Rayleigh plot showing carbon isotope fractionation of ATMP for varying Mn(II):ATMP(0) (corresponding to Mn(II) concentrations of 0.01 mM to 1 mM) at pH 6.8 ± 0.1, including the linear regressions according to the Rayleigh model. Error bars were calculated by means of Gaussian error propagation assuming an error of the $\delta^{13}C$ value of 0.5 ‰.

For experiments conducted at pH 3.6, ε_C–values ranged between -2.0 ± 0.2 ‰ and -4.0 ± 0.3 ‰. The low variation of the observed ε_C–values despite significant changes in the initial Mn:ATMP ratio can be explained by the narrower range of $f_{compl}(0)$ at this pH (0.01 to 0.09). The observed carbon isotope fractionation for Mn(II):ATMP(0) = 1:1 was significantly lower at pH 3.6 ($\varepsilon_C = -3.2 \pm 0.2$ ‰, see **Figure B.5(b)**) than at pH 6.8 ($\varepsilon_C = -9.4 \pm 0.6$ ‰) and therefore comparable with the isotope enrichment factor for Mn(II):ATMP(0) = 1:10 at pH 6.8 ($\varepsilon_C = -2.0 \pm 0.2$ ‰), for which a similar initial Mn(II)–complexed ATMP fraction of 0.1 was calculated. Hence, the significantly different carbon isotope enrichment factors strengthen the hypothesis of the presence two reaction mechanisms for different Mn(II)–complexed ATMP fractions, as both, the observed isotope fractionation, as well as the fraction of ATMP complexed with Mn(II) increases with (i) the Mn(II) concentration at a constant pH and (ii) with increasing pH values for a constant Mn(II):ATMP(0) (see **Figure B.6** for speciation calculations). This picture of distinct reaction mechanisms for varying Mn(II)–complexed fractions is also in accordance with that hypothesized for Mn(III)–EDTA systems.[16,17] To explore this relationship further, in the next section we evaluated this correlation quantitatively.

The Mn(II)–complexed ATMP fraction quantitatively correlates with observable carbon isotope fractionation

Table 3.1: Compilation of experiments with an initial ATMP concentration of 1 mM. Shown are the (initial) pH, the concentration of the applied buffer or background electrolyte, the concentration of Mn(II), the calculated fraction of ATMP complexed with Mn(II) at the beginning of the experiment ($f_{compl}(0)$), as well as the carbon isotope enrichment factor including its 95 % confidence interval (CI, obtained from linear fitting the experimental data according to the Rayleigh model).

pH_{t0}	3.6				6.8				7.2		
buffer/ electrol.	20 mM $NaNO_3$				20 mM MES				20 mM $NaNO_3$		
c(Mn(II)) (mM)	0.01	0.1	1	2	0.01	0.1	0.5	1	0.1	0.2	0.4
$f_{compl}(0)$ (ATMP)	6.0 $\times10^{-4}$	4.7 $\times10^{-3}$	0.05	0.09	0.01	0.1	0.51	0.82	0.09	0.2	0.4
ε_C (‰)	−2.0	−2.3	−3.2	−4.0	−0.8	−2.0	−7.2	−9.4	−2.5	−4.7	−5.3
±95 % CI	±0.3	±0.4	±0.2	±0.2	±0.1	±0.2	±0.9	±0.6	±0.7	±0.4	±0.4

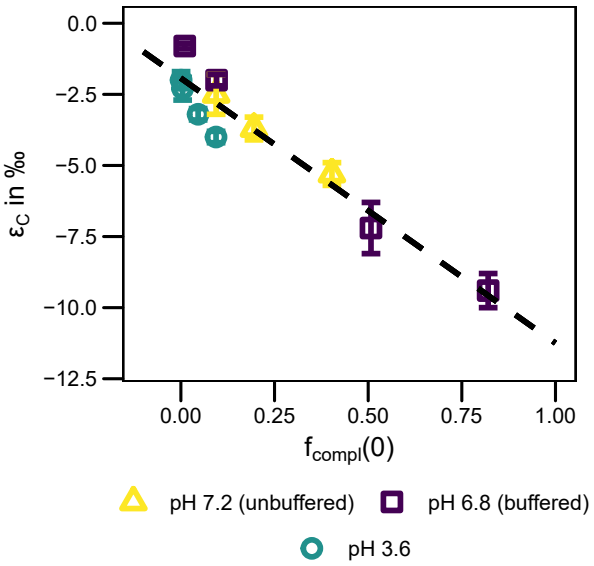

Figure 3.3: Carbon isotope enrichment factors (ε_C, including their 95 % CI) vs. the fraction of ATMP (1 mM starting concentration) complexed to Mn(II) at the beginning of the transformation experiments ($f_{compl}(0)$) assuming complexation equilibrium (see Table 3.1). The dashed line is a linear regression for all data points ($R^2 = 0.92$).

For a quantitative evaluation of the correlation of observed kinetic isotope fractionation with the fraction of ATMP initially complexed by Mn(II), we plotted the carbon isotope enrichment factor versus the corresponding $f_{compl}(0)$–value (see **Table 3.1**). Considering all experimental data sets (pH 3.6 (unbuffered, see **Figure B.5**)), pH 6.8 (buffered) and pH 7.2 (unbuffered, see **Figure B.7**)) resulted in an inverse linear correlation of ε_C–values and the initially complexed fraction ($R^2 = 0.92$, see **Figure 3.3**). The fact that all data sets could be described by the

same correlation implies that the applied buffer had no significant effect on carbon isotope fractionation. Hence, the magnitude of carbon isotope fractionation is primarily determined by the fraction of ATMP initially complexed with Mn(II). Observed carbon isotope fractionations ranged from $\varepsilon_C = -0.8 \pm 0.1$ ‰ for small complexed ATMP fractions ($f_{compl}(0) = 0.01$) to $\varepsilon_C = -9.4 \pm 0.6$ ‰ for high complexed fractions ($f_{compl}(0) = 0.82$).

However, these findings entail shifts in the extent of the isotope fractionation within single transformation events, as the Mn(II)–complexed fraction of ATMP is steadily shifted to higher values due to the increasing Mn(II):ATMP ratio over the course of the transformation experiment. Therefore, we conducted a stepwise evaluation of Rayleigh plots for experiments with significant changes of the complexed ATMP fraction over the course of the experiment ($\Delta f_{compl} \geqslant 0.13$, see **Figure B.8**). In accordance with the trend shown in **Figure 3.3**, ε_C–values decreased during transformation, resulting in curved rather than linear Rayleigh plots.

Overall, the dependency of the observable isotope fractionation on the Mn(II)–complexed ATMP fraction within individual transformation experiments as well as for experiments with differing $f_{compl}(0)$ followed the same trend, confirming that the fraction of ATMP complexed with Mn(II) is the predominant influence on the observed carbon isotope fraction during Mn(II)–catalyzed ATMP transformation. Therefore, the obtained pattern from the isotopic investigation supports the conclusions of two reaction mechanisms based on the normalized reaction rate constants. In experiments with significant changes within the Mn(II)–complexed ATMP fraction isotope analysis reveals gradual changes from one mechanism to the other.

The transformation by the one reaction mechanism and different degree of masking of the intrinsic kinetic isotope effect can be ruled out by the observed reaction kinetics. The cause for an increasing masking of the observable isotope effect for decreasing complexed ATMP fractions might be the inhibited formation of the initial Mn(II)ATMP complex, which is considered to be rate–determining for the investigated reaction.[13] As no carbon atoms are involved in the complex formation step, a minor carbon isotope effect associated with this step is expected.[35] Consequently, the shift to a minor carbon isotope effect could be caused by increasing masking of the C–P bond cleavage step by the non–fractionating initial complex formation step. However, if the formation of Mn(II)ATMP becomes rate–determining in the overall multistep reaction for low complexed ATMP fractions, a decreasing observed isotope effect would be linked to a decreasing apparent reaction rate, similar as shown for the hydrolysis of the herbicide isoproturon.[21,36] For Mn(II)–catalyzed oxidation of ATMP, however, the normalized reaction rate constant decreased rather than increased with the Mn(II)ATMP concentration, as shown in **Figure 3.1(b)**. On the other hand, the carbon isotope fractionation was significantly lower at 0.1 mM Mn(II) compared to 1 mM Mn(II). Hence, a masking of the C–P bond cleavage step by the formation of the Mn(II)ATMP–complex cannot explain the observed isotope fractionation pattern.

Mechanistic interpretation of observed reaction kinetics and kinetic isotope fractionation

The observed reaction kinetics revealed an inverse correlation of the reaction rate and the fraction of Mn(II)ATMP – the higher the complexed fraction of ATMP in the system the slower the reaction rate. The observed kinetic carbon isotope effects for Mn(II)–catalyzed oxidation of ATMP range from minor values (ε_C–values of around -1 ‰ for low fractions ($f_{\text{compl}} \approx 0.01$) of ATMP complexed with Mn(II)) to pronounced values (ε_C–values in the range of -10 ‰ for $f_{\text{compl}} \approx 0.82$). Both data sets suggest two different reaction mechanisms with different reaction rates and distinct intrinsic kinetic carbon isotope effects.

According to the proposed reaction scheme, Mn(II)–catalyzed oxidation of ATMP proceeds via C–P bond cleavage and therefore a pronounced carbon isotope effect is expected. As published data on the kinetic isotope effect associated with C–P bond cleavage are lacking, we estimated the observable carbon isotope enrichment factor from the semiclassical Streitwieser limit (i.e., the theoretically maximum intrinsic kinetic isotope effect based on vibrational energy differences)[26] using published vibrational frequencies for the C–P bond in various (amino–)phosphonates, (see appendix B for calculations). The estimated maximal possible ε_C–value was about -15 ‰. Considering that this value can only serve as a rough approximation and likely overestimates the intrinsic KIE, it can be assumed that the maximum experimentally determined enrichment factor of around -10 ‰ reflects the C-P bond cleavage step.[26]

So far, the proposed pathway for Mn(II)–catalyzed oxidation of ATMP accounts only for transformation of complexed ATMP via oxidation of the Mn(II)ATMP complex and subsequent complex decomposition due to inner–sphere electron transfer from the ATMP ligand to the Mn(III) central atom (see **Equation 3.2** to **3.4** and **Figure 3.4**, steps 1–4b).[14]

$$\mathrm{Mn^{2+} + H_2ATMP^{4-}} \rightleftharpoons \mathrm{Mn(II)H_2ATMP^{2-}} \tag{3.2}$$

$$\mathrm{Mn(II)H_2ATMP^{2-} + O_2} \longrightarrow \mathrm{Mn(III)H_2ATMP^{-} + {O_2}^{-\cdot}} \tag{3.3}$$

$$\mathrm{Mn(III)H_2ATMP^{-}} \longrightarrow \mathrm{Mn(II)H_2ATMP^{-\cdot}} \longrightarrow \ldots \tag{3.4}$$

While data on reactions involving Mn(III)–aminopolyphosphonate complexes is scarce, there are several studies on the reactivity of Mn(III) complexed with aminopolycarboxylates, such as ethylenediaminetetraacetate (EDTA) and trans–1,2–diaminocyclohexane–N,N,N',N'–tetraacetate (CDTA). Similar to Mn(III)ATMP, Mn(III)EDTA was shown to undergo complex decomposition via inner–sphere electron transfer.[16,17] In addition, Mn(III)EDTA and Mn(III)CDTA are capable of oxidizing a variety of organic compounds, including oxalate,[37] ascorbic acid[38] and dihydroxybenzenes,[39] which is in accordance with the known property of Mn(III)(–ligands) as strong oxidizing agent.[19,20,40–42] Notably, Mn(III)EDTA is also capable of oxidizing free, un–complexed EDTA when EDTA is provided in excess.[16,17] Applying these findings to the Mn–ATMP system presented here, the reaction between an intermediate Mn(III)ATMP–complex and a free ATMP molecule (**Equation 3.5** and **Figure 3.4**, steps 1–4a) can be considered as an

additional reaction mechanism:

$$Mn(III)H_2ATMP^- + H_2ATMP^{4-} \longrightarrow Mn(II)H_2ATMP^{2-} + Mn(II)H_2ATMP^{3-\cdot} \longrightarrow ... \quad (3.5)$$

While Mn(III)ATMP complex–decomposition (**Equation 3.4**) is expected to occur predominately at high fractions of ATMP complexed with Mn(II) (i.e., low concentration of free ATMP), oxidation of free ATMP by Mn(III)ATMP (**Equation 3.5**) should dominate at high fractions of free ATMP. Consequently, complex decomposition is associated with a pronounced kinetic isotope effect, representing the cleavage of the C–P bond (e.g. $\varepsilon_C = -9.4 \pm 0.6$ ‰ for an initially complexed ATMP fraction of 0.82). The oxidation of free ATMP, on the other hand, shows a minor kinetic isotope effect (e.g. $\varepsilon_C = -0.8 \pm 0.1$ ‰ for an initially complexed ATMP fraction of 0.01). Thus, it can be assumed that for oxidation of free ATMP not the C–P bond cleavage is rate–determining, but rather a preceding step within the overall multistep reaction.[21]

To decipher the difference between the two mechanisms in terms of rate–determining steps, the reversibility of the electron transfer for the respective mechanism must be considered. During complex decomposition (pathway b in **Figure 3.4(a)**), the Mn(III)ATMP–intermediate reacts to a N–centered radical via an intermolecular electron transfer (step 3b). In general Mn(III)–complexes have been reported to oxidize superoxide via an one–electron transfer.[43–45] In addition, the ATMP radical formed during complex decomposition is coordinated to a transition–metal central atom that increases the stability of N–centered radicals due to delocalization of the unpaired electron.[46,47] As a consequence, the back–reaction of the intermediate N–centered radical to the precursor Mn(II)ATMP complex (step –3b and –2) might become favorable over complex decomposition (step 4b). Hence, electron transfer in the complex decomposition pathway is partially reversible as it does not necessarily lead to C–P bond cleavage in the complexed ATMP. In such a scenario the C–P bond cleavage is the rate–determining step during complex decomposition, leading to the distinct observable isotope fractionation (pathway b in **Figure 3.4(b)**).

Oxidation of a free ATMP (pathway a in **Figure 3.4(a)**) however, entails the formation of a free, un–complexed N–centered radical via the one–electron transfer from the free ATMP to the Mn(III)ATMP–intermediate (step 3a). This free N–centered radical, in contrast to the complex decomposition pathway, is not coordinated to a Mn–center and therefore highly instable, leading to fast breakdown of the radical (step 4a). Thus, the electron transfer step, preceding C–P bond cleavage, is practically irreversible. As no carbon atom is involved in the electron transfer, negligible carbon isotope fractionation is expected for this step. Thus, the intrinsic KIE of C–P bond cleavage represents not the bottleneck in the overall reaction resulting in minor observable KIE (pathway a in **Figure 3.4(b)**).[21]

The assumption of a (partially) reversible electron transfer during complex decomposition resulting in slow transformation via this mechanism is further supported by the determined normalized reaction rates. As discussed in **Figure 3.1(b)**, the substantial decrease of the trans-

formation rate can be rationalized by the fact that the concentration of free ATMP drops over time to marginal values (around 0.01 mM based on equilibrium calculations, corresponding to un–complexed fractions of $\leqslant 0.1$), preventing transformation via the non–reversible (faster) oxidation of free ATMP. In contrast to this, free ATMP is the predominant species in the observed concentration range in the experiments with initial Mn(II):ATMP ratios of 1:100 and 1:10 (corresponding to $f_{\mathrm{compl}}(0) = 0.01$ and $f_{\mathrm{compl}}(0) = 0.1$, respectively). Thus, transformation via the (faster) oxidation of a free ATMP predominates over the complete course of the experiment preventing a pronounced decrease in the transformation rate. This conclusion is also in agreement with the Mn(III)EDTA system, where oxidation of free EDTA was shown to be significantly faster than complex decomposition.[16,17]

In conclusion, based on the correlation of normalized reaction rate constants, carbon CSIA and equilibrium speciation modelling we conclude that Mn(II)–catalyzed breakdown of ATMP proceeds not only via the previously described complex decomposition, but also via a much faster oxidation of a free ATMP by a Mn(III)ATMP intermediate. The distinctly different magnitudes of reaction rates of these two mechanisms arise from a (partially) reversible electron transfer during complex decomposition while the distinctly different magnitudes of carbon isotope fractionation arise from differing rate–limiting (i.e., carbon KIE determining) steps (see **Figure 3.4**). To further underpin this conclusion, monitoring the Mn(III)ATMP decomposition in the presence of varying excess concentrations of ATMP could be helpful. However, direct quantification of Mn(III)ATMP with UV–VIS spectroscopy failed due to the lack of specific spectroscopic features of the complexes (see **Figure B.10** for UV/Vis spectra).[14] Alternatively, δ^{15}N–CSIA would allow for 2D–CSIA and thus could help to further characterize the underlying mechanisms, as masking and varying reaction mechanisms could be clearly distinguished.[21] However, LC–IRMS systems for δ^{15}N–CSIA are not available yet.

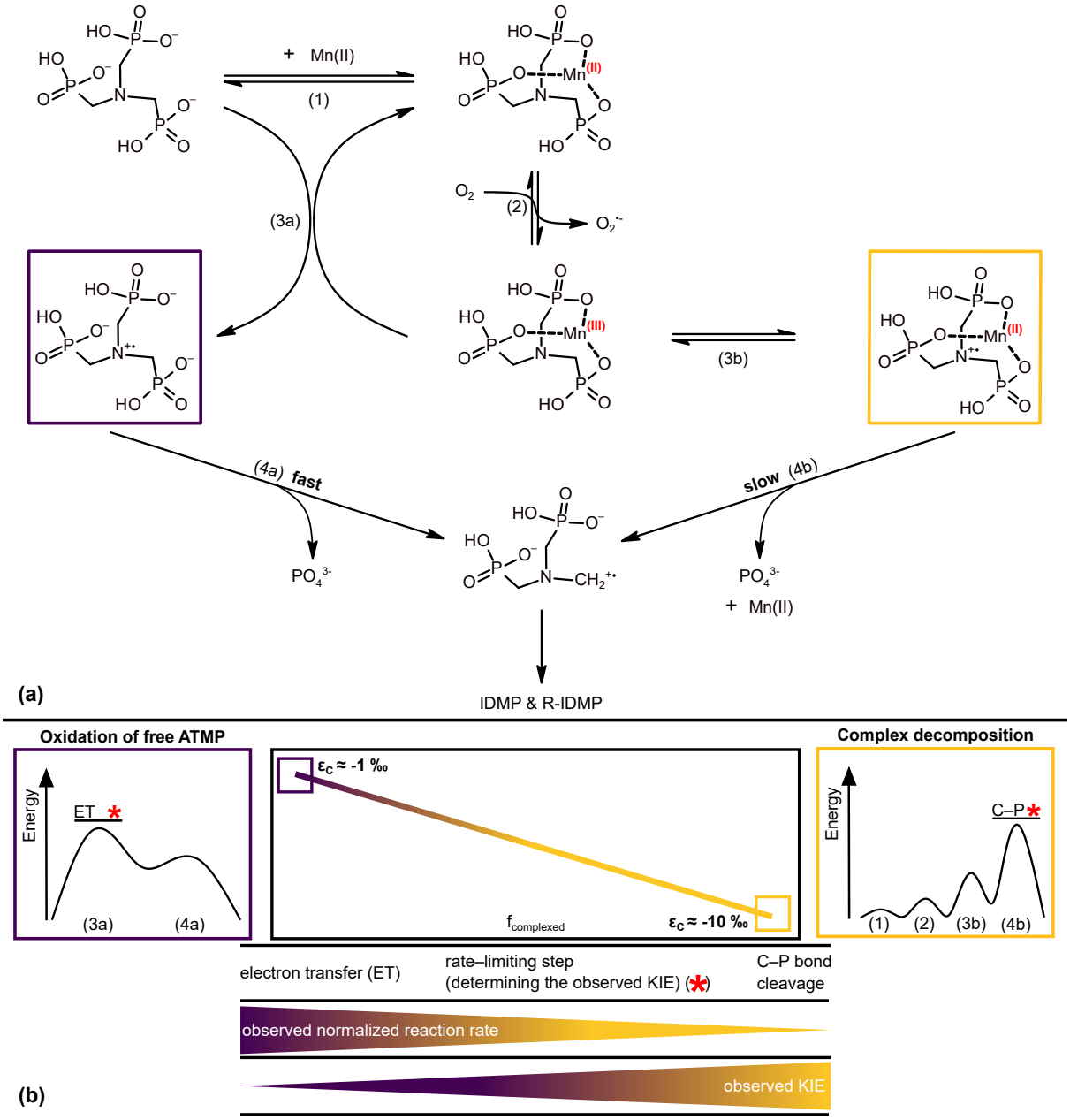

Figure 3.4: (**a**) Proposed reaction scheme for Mn(II)–catalyzed oxidation of ATMP via two distinct reaction mechanisms: oxidation of a free ATMP by a Mn(III)ATMP–intermediate (pathway a) and complex decomposition of Mn(III)ATMP (pathway b). (**b**) Simplified energy profiles with rate–limiting (i.e., kinetic carbon isotope effect determining) steps (marked by red asterisks), as well as the observed isotope enrichment factor and normalized reaction rate as a function of the relative contribution of the two mechanisms to the overall ATMP transformation.

Implications for the environmental fate of ATMP

Since dissolved manganese is present in most waste– and surface waters a substantial fraction of dissolved ATMP may be present as MnATMP–complexes as shown for EDTA.[48,49] Hence, Mn(II)–catalyzed transformation of ATMP is considered a relevant removal process for the non–sorbed ATMP fraction via ATMP breakdown by complex decomposition.[4,15] However, based on the results presented in this study, a reactive Mn(III)ATMP–intermediate complex has to be taken into account as demonstrated by our laboratory model systems containing Mn(II) and ATMP. In contrast to the model systems studied here, waste or surface waters contain oxidizable organics, such as partially reduced natural organic matter (NOM)[50] or small organic acids produced from the turnover of NOM[51] at concentrations likely higher than those of ATMP, which occurs at concentrations in the low $\mu g\,L^{-1}$–range in treated waste water.[8] Hence, it can be assumed that Mn(III)ATMP intermediates will be reacting rather with oxidizable NOM than with free ATMP molecules. In this case, the Mn(II)–ATMP complex may act as a catalyst for breakdown of other oxidizable species, while its own breakdown and, hence, breakdown of ATMP may be comparatively very slow. Consequently, possible side reactions of the Mn(III)ATMP intermediate with NOM may result in an overestimation of the share of Mn(II)–catalyzed oxidation to the overall transformation of aqueous ATMP, when only the Mn(III)ATMP complex decomposition pathway is considered. As a result, competing transformation processes, such as oxidation at manganese (hydr–)oxides[14] or photo–transformation of Fe(III)ATMP[10] might be of higher relevance. On the other hand, reactive Mn(III)ATMP are possibly acting as an effective oxidizing agent for natural and anthropogenic reductants, such as shown for Mn(III)–pyrophosphate.[19,40] Thus, further work on the reactivity of the Mn(III)ATMP intermediates towards different reducing agents, such as NOM model compounds is needed. Moreover, data on the behavior of Mn(III)–complexes of other widely used aminopolyphosphonate chelating agents are needed in order to gain a deeper understanding of the role of dissolved manganese for the environmental fate of this compound class.

References

(1) Bernhard, M.; Muller, J.; Knepper, T. P. Biodegradation of persistent polar pollutants in wastewater: comparison of an optimised lab-scale membrane bioreactor and activated sludge treatment. *Water Research* **2006**, *40*, 3419–3428.

(2) Blum, K. M.; Andersson, P. L.; Ahrens, L.; Wiberg, K.; Haglund, P. Persistence, mobility and bioavailability of emerging organic contaminants discharged from sewage treatment plants. *Science of the Total Environment* **2018**, *612*, 1532–1542.

(3) Schulze, S.; Zahn, D.; Montes, R.; Rodil, R.; Quintana, J. B.; Knepper, T. P.; Reemtsma, T.; Berger, U. Occurrence of emerging persistent and mobile organic contaminants in European water samples. *Water Research* **2019**, *153*, 80–90.

(4) Rott, E.; Steinmetz, H.; Metzger, J. W. Organophosphonates: A review on environmental relevance, biodegradability and removal in wastewater treatment plants. *Science of the Total Environment* **2018**, *615*, 1176–1191.

(5) Nowack, B. Environmental chemistry of phosphonates. *Water Research* **2003**, *37*, 2533–2546.

(6) Jaworska, J.; Van Genderen-Takken, H.; Hanstveit, A.; van de Plassche, E.; Feijtel, T. Environmental risk assessment of phosphonates, used in domestic laundry and cleaning agents in the Netherlands. *Chemosphere* **2002**, *47*, 655–665.

(7) Schmidt, C. K.; Raue, B.; Brauch, H.-J.; Sacher, F. Trace-level analysis of phosphonates in environmental waters by ion chromatography and inductively coupled plasma mass spectrometry. *International Journal of Environmental Analytical Chemistry* **2013**, *94*, 385–398.

(8) Armbruster, D.; Rott, E.; Minke, R.; Happel, O. Trace-level determination of phosphonates in liquid and solid phase of wastewater and environmental samples by IC-ESI-MS/MS. *Analytical and Bioanalytical Chemistry* **2020**, *412*, 4807–4825.

(9) Wang, S.; Sun, S.; Shan, C.; Pan, B. Analysis of trace phosphonates in authentic water samples by pre-methylation and LC-Orbitrap MS/MS. *Water Research* **2019**, *161*, 78–88.

(10) Lesueur, C.; Pfeffer, M.; Fuerhacker, M. Photodegradation of phosphonates in water. *Chemosphere* **2005**, *59*, 685–691.

(11) Klinger, J.; Sacher, F.; Brauch, H.-J.; Maier, D.; Worch, E. Behaviour of phosphonic acids during drinking water treatment. *Vom Wasser* **1998**, *91*, 15–28.

(12) Steber, J.; Wierich, P. Properties of aminotris (methylenephosphonate) affecting its environmental fate: Degradability, sludge adsorption, mobility in soils, and bioconcentration. *Chemosphere* **1987**, *16*, 1323–1337.

(13) Nowack, B.; Stone, A. T. Degradation of Nitrilotris(methylenephosphonic Acid) and Related (Amino)Phosphonate Chelating Agents in the Presence of Manganese and Molecular Oxygen. *Environmental Science & Technology* **2000**, *34*, 4759–4765.

(14) Nowack, B.; Stone, A. T. Homogeneous and heterogeneous oxidation of nitrilotrismethylenephosphonic acid (NTMP) in the presence of manganese (II, III) and molecular oxygen. *The Journal of Physical Chemistry B* **2002**, *106*, 6227–6233.

(15) Nowack, B.; Stone, A. T. Manganese-catalyzed degradation of phosphonic acids. *Environmental Chemistry Letters* **2003**, *1*, 24–31.

(16) Schroeder, K. A.; Hamm, R. E. Decomposition of the Ethylenediaminetetraacetate Complex of Manganese(III). *Inorganic Chemistry* **1964**, *3*, 391–395.

(17) Klewicki, J. K.; Morgan, J. J. Kinetic Behavior of Mn(III) Complexes of Pyrophosphate, EDTA, and Citrate. *Environmental Science & Technology* **1998**, *32*, 2916–2922.

(18) Hu, E.; Zhang, Y.; Wu, S.; Wu, J.; Liang, L.; He, F. Role of dissolved Mn(III) in transformation of organic contaminants: Non-oxidative versus oxidative mechanisms. *Water Research* **2017**, *111*, 234–243.

(19) Kostka, J. E.; Luther, G. W.; Nealson, K. H. Chemical and biological reduction of Mn (III)-pyrophosphate complexes: Potential importance of dissolved Mn (III) as an environmental oxidant. *Geochimica et Cosmochimica Acta* **1995**, *59*, 885–894.

(20) Li, H.; Santos, F.; Butler, K.; Herndon, E. A Critical Review on the Multiple Roles of Manganese in Stabilizing and Destabilizing Soil Organic Matter. *Environmental Science & Technology* **2021**, *55*, 12136–12152.

(21) Elsner, M. Stable isotope fractionation to investigate natural transformation mechanisms of organic contaminants: principles, prospects and limitations. *Journal of Environmental Monitoring* **2010**, *12*, 2005–2031.

(22) Elsner, M.; Imfeld, G. Compound-specific isotope analysis (CSIA) of micropollutants in the environment - current developments and future challenges. *Current Opinion in Biotechnology* **2016**, *41*, 60–72.

(23) Krummen, M.; Hilkert, A. W.; Juchelka, D.; Duhr, A.; Schlüter, H.-J.; Pesch, R. A new concept for isotope ratio monitoring liquid chromatography/mass spectrometry. *Rapid Communications in Mass Spectrometry* **2004**, *18*, 2260–2266.

(24) Martin, P. R.; Buchner, D.; Jochmann, M. A.; Haderlein, S. B. Stable carbon isotope analysis of polyphosphonate complexing agents by anion chromatography coupled to isotope ratio mass spectrometry: method development and application. *Analytical and Bioanalytical Chemistry* **2020**, *412*, 4827–4835.

(25) Schmidt, T. C.; Jochmann, M. A. Origin and fate of organic compounds in water: characterization by compound-specific stable isotope analysis. *Annual Review of Analytical Chemistry* **2012**, *5*, 133–155.

(26) Elsner, M.; Zwank, L.; Hunkeler, D.; Schwarzenbach, R. P. A new concept linking observable stable isotope fractionation to transformation pathways of organic pollutants. *Environmental Science & Technology* **2005**, *39*, 6896–6916.

(27) Hofstetter, T. B.; Spain, J. C.; Nishino, S. F.; Bolotin, J.; Schwarzenbach, R. P. Identifying competing aerobic nitrobenzene biodegradation pathways by compound-specific isotope analysis. *Environmental Science & Technology* **2008**, *42*, 4764–4770.

(28) VanStone, N. A.; Focht, R. M.; Mabury, S. A.; Lollar, B. S. Effect of iron type on kinetics and carbon isotopic enrichment of chlorinated ethylenes during abiotic reduction on Fe (0). *Groundwater* **2004**, *42*, 268–276.

(29) Murphy, J.; Riley, J. P. A modified single solution method for the determination of phosphate in natural waters. *Analytica Chimica Acta* **1962**, *27*, 31–36.

(30) Köster, D.; Wolbert, J. B.; Schulte, M. S.; Jochmann, M. A.; Schmidt, T. C. Origin of Xylitol in Chewing Gum: A Compound-Specific Isotope Technique for the Differentiation of Corn- and Wood-Based Xylitol by LC-IRMS. *Journal of Agricultural and Food Chemistry* **2018**, *66*, 2015–2020.

(31) Scott, K. M.; Lu, X.; Cavanaugh, C. M.; Liu, J. S. Optimal methods for estimating kinetic isotope effects from different forms of the Rayleigh distillation equation. *Geochimica et Cosmochimica Acta* **2004**, *68*, 433–442.

(32) Parkhurst, D.; Appelo, C., *Description of input and examples for PHREEQC version 3–A computer program for speciation, batch-reaction, one-dimensional transport, and inverse geochemical calculations*; Techniques and Methods, Vol. book 6; U.S. Geological Survey: 2013; Chapter A43.

(33) Lacour, S.; Deluchat, V.; Bollinger, J.-C.; Bernard, S. Complexation of trivalent cations (Al(III), Cr(III), Fe(III)) with two phosphonic acids in the pH range of fresh waters. *Talanta* **1998**, *46*, 999–1009.

(34) Popov, K.; Rönkkömäki, H.; Lajunen, L. H. J. Critical evaluation of stability constants of phosphonic acids (IUPAC Technical Report). *Pure and Applied Chemistry* **2001**, *73*, 1641–1677.

(35) Martinez, R. J.; Farrell, J. Understanding Nitrilotris(methylenephosphonic acid) reactions with ferric hydroxide. *Chemosphere* **2017**, *175*, 490–496.

(36) Penning, H.; Cramer, C. J.; Elsner, M. Rate-dependent carbon and nitrogen kinetic isotope fractionation in hydrolysis of isoproturon. *Environmental Science & Technology* **2008**, *42*, 7764–7771.

(37) Suwyn, M. A.; Hamm, R. E. Mechanism of oxidation oxalate with trans-1,2-diaminocyclohexanetetraacetatomanganate(III) in aqueous solution. *Inorganic Chemistry* **1967**, *6*, 142–145.

(38) Gangopadhyay, S.; Saha, S. K.; Ali, M.; Banerjee, P. Kinetics of electron transfer reactions of manganese (III) complexes oftrans-cyclohexane-1,2-diamine,-NNN'N'-tetraacetic acid and 2,2'-bipyridyl with ascorbic acid in aqueous acid media. *International Journal of Chemical Kinetics* **1991**, *23*, 105–112.

(39) Giraudi, G.; Mentasti, E. The Kinetics and mechanisms of oxidation of dihydroxybenzenes by ethylenediaminetetraacetatomanganate(III). *Transition Metal Chemistry* **1981**, *6*, 230–234.

(40) Bielski, B. H. Fast kinetic studies of dioxygen-derived species and their metal complexes. *Philosophical Transactions of the Royal Society B: Biological Sciences* **1985**, *311*, 473–482.

(41) Sun, B.; Guan, X.; Fang, J.; Tratnyek, P. G. Activation of Manganese Oxidants with Bisulfite for Enhanced Oxidation of Organic Contaminants: The Involvement of Mn(III). *Environmental Science & Technology* **2015**, *49*, 12414–12421.

(42) Davies, G. Some aspects of the chemistry of manganese(III) in aqueous solution. *Coordination Chemistry Reviews* **1969**, *4*, 199–224.

(43) Faulkner, K. M.; Liochev, S. I.; Fridovich, I. Stable Mn(III) porphyrins mimic superoxide dismutase in vitro and substitute for it in vivo. *Journal of Biological Chemistry* **1994**, *269*, 23471–23476.

(44) Iranzo, O. Manganese complexes displaying superoxide dismutase activity: a balance between different factors. *Bioorganic Chemistry* **2011**, *39*, 73–87.

(45) Spasojevic, I.; Batinic-Haberle, I. Manganese(III) complexes with porphyrins and related compounds as catalytic scavengers of superoxide. *Inorganica Chimica Acta* **2001**, *317*, 230–242.

(46) Büttner, T.; Geier, J.; Frison, G.; Harmer, J.; Calle, C.; Schweiger, A.; Schönberg, H.; Grützmacher, H. A stable aminyl radical metal complex. *Science* **2005**, *307*, 235–238.

(47) Suarez, A. I. O.; Lyaskovskyy, V.; Reek, J. N.; van der Vlugt, J. I.; de Bruin, B. Complexes with Nitrogen-Centered Radical Ligands: Classification, Spectroscopic Features, Reactivity, and Catalytic Applications. *Angewandte Chemie International Edition* **2013**, *52*, 12510–12529.

(48) Howe, P.; Malcolm, H.; Dobson, S., *Manganese and its compounds: environmental aspects*; World Health Organization: 2004.

(49) Kari, F. G.; Giger, W. Speciation and fate of ethylenediaminetetraacetate (EDTA) in municipal wastewater treatment. *Water Research* **1996**, *30*, 122–134.

(50) Kappler, A.; Haderlein, S. B. Natural organic matter as reductant for chlorinated aliphatic pollutants. *Environmental Science & Technology* **2003**, *37*, 2714–2719.

(51) Dahlén, J.; Bertilsson, S.; Pettersson, C. Effects of UV-A irradiation on dissolved organic matter in humic surface waters. *Environment International* **1996**, *22*, 501–506.

4 Oxidation of iminodimethylene phosphonate (IDMP) at MnO_2 – transformation kinetics and stable carbon isotope fractionation

Philipp R. Martin, Daniel Buchner, Stefan B. Haderlein

Author	Author position	Scientific ideas	Data generation*	Analysis & interpretation	Paper writing
P. Martin	1	60 %	50 %	60 %	60 %
D. Buchner	2	30 %	0 %	30 %	30 %
S. Haderlein	3	10 %	0 %	10 %	10 %

Title of the paper:
Oxidation of iminodimethylene phosphonate (IDMP) at MnO_2 – transformation kinetics and stable carbon isotope fractionation

Status in the publication process:
Manuscript in preparation

* Experiments were conducted with the help of Swarada Badwe, Tamara Pruneddu & Larissa Werle (see acknowledgments)

4.1 Abstract

Aminopolyphosphonates are synthetic chelating agents increasingly used in various household and industrial applications leading to their emission into the environment. Oxidation at manganese oxides was proposed as a potentially relevant removal process for aminopolyphosphonates, but the underlying mechanisms are not fully deciphered yet. In this study, we systematically investigated the oxidation of iminodimethylene phosphonate (IDMP) at MnO_2. IDMP is an environmentally relevant representative of aminophosphonates as it is (i) the major transformation product of aminopolyphosphonates and (ii) a precursor of aminomethyl phosphonate (AMPA), a major transformation product of the herbicide glyphosate. A combination of kinetic modeling and compound–specific carbon isotope analysis (carbon CSIA) was applied to investigate the influence of environmentally relevant parameters including MnO_2 mineralogy and pH on the IDMP transformation rate and the associated kinetic carbon isotope fractionation. IDMP was oxidized at both investigated manganese oxides via C−P bond cleavage, indicated by the formation of ortho–phosphate. First–order reaction kinetics in combination with moderate isotope enrichment factors of -3.8 ± 0.4 ‰ to -8.4 ± 0.5 ‰ suggested electron transfer as rate–limiting step rather than adsorption. A more pronounced kinetic isotope fractionation at low pH and high Mn(III)–content indicated that electron transfer was facilitated under these conditions. Our results provide first insights into the underlying reaction mechanisms, the rate–limiting steps and highlight the role of manganese oxides as potential oxidants of amino–(poly–)phosphonates and therefore contribute to a more profound understanding of their fate in the environment.

4.2 Introduction

Aminopolyphosphonates (APPs) are strong synthetic chelating agents possessing three or more phosphonate ($R-PO_3^{2-}$) moieties and at least one amine functional group. During the last decades, they were increasingly used in industrial and household applications, mainly as anti–scaling agents and bleach stabilizers.[1,2] Due to potential environmental threats arising from their increasing discharge in surface waters, such as eutrophication and heavy metal remobilization, aminopolyphosphonates represent a substance class of rising concern.[1] The strong affinity of APPs to form complexes with di– and trivalent cations (e.g., Fe(III) or Ca(II)) affects their fate in the environment and in wastewater treatment plants (WWTP).[3] One major pathway for their removal from the aqueous phase is proposed to be adsorption onto mineral surfaces, such as iron (oxyhydr–)oxides and clays associated with WWTP sewage sludge and river sediments.[4–6] However, sorption to such minerals does not lead to a net elimination of APPs from the environment – in contrast to the interaction of APPs with manganese oxide minerals. Manganese oxides comprise a group of around 30 (mixed) Mn(III)/Mn(IV) (hydr–) oxides that are widespread in various environmental compartments including soils and sediments. They typically form tunnel or layer structures and are characterized by a low crystallinity and consequently high surface area.[7,8] Owing to the high redox potentials of the Mn(IV)/Mn(II)

and Mn(III)/Mn(II) redox couples and their high specific surface area, Mn oxides are among the most potent environmental oxidants.[9,10] As a result, they are capable of oxidizing a variety of inorganic (e.g., heavy metals) and organic contaminants.[10,11] APPs are prone to transformation by manganese oxides, while nitrogen–free representatives are resilient to oxidation.[12–14] These observations highlight the role of the amine functional group for electron transfer. Investigated reactions between manganese oxides and amino–(poly–)phosphonates include the oxidation of aminotrismethylene phosphonate (ATMP), the broad–spectrum herbicide glyphosate (N–(phosphonomethyl) glycine), and aminomethylene phosphonate (AMPA) – a transformation product of glyphosate, as well as of APPs.[15–17] The oxidation of aminophosphonates at manganese oxides is a textbook example for the reaction mechanism described for the transformation of organic compounds. Such a three–step reaction comprises (i) the formation of an inner– or outer–sphere surface precursor complex, (ii) an one–electron transfer from the reactant to a Mn(IV) or Mn(III) surface site leading to the formation of a reactant intermediate radical and (iii) the breakdown of the radical by a second one–electron transfer, either once again from a mineral surface site, or from dissolved species such as O_2.[10] Hence, the reaction results in reductive dissolution of the mineral with the formation of dissolved Mn(II).[18] In the case of aminophosphonate oxidation, the electron is likely transferred from the amine–N to the mineral surface.[19] For symmetric aminophosphonates, subsequent intermolecular electron transfer results in C−P bond cleavage, as shown for ATMP. Major transformation products of ATMP were ortho–phosphate and the diphosphonate iminodimethylene phosphonate (IDMP).[12] Although the transformation of IDMP at manganese oxides was not investigated so far, IDMP might get further oxidized to AMPA after cleavage of another C−P bond, as shown for Fe–catalyzed photolysis.[20,21] Hence, the transformation of aminopolyphosphonates might be considered a source for AMPA in the environment, which is more persistent than its precursors and is under debate due to its potential (eco–)toxicological risks.[17,22] Moreover, ortho–phosphate resulting from C−P bond cleavage may contribute to surface water eutrophication.[1] Consequently, the oxidation of aminopolyphosphonates at manganese oxide surfaces is of high environmental relevance. In order to get a better understanding of this so far poorly investigated process, studies on the driving factors, such as pH and manganese oxide mineralogy, are essential.

Compound–specific stable carbon isotope analysis (carbon CSIA) represents a promising tool to gain insights into underlying reaction processes, particularly as an addition to the evaluation of kinetic data. CSIA allows to quantify the kinetic isotope effect (KIE) associated with transformation reactions, i.e., the small difference in bond cleavage rate constants for molecules possessing either a light or heavy stable isotope of a certain element at the reactive site (for carbon: $KIE_C = {}^{12}k/{}^{13}k$).[23,24] The kinetic isotope effect leads to a gradual change in the isotopic composition of the residual reactant pool over the course of its transformation. As ^{13}C–containing bonds typically react slightly slower than their ^{12}C counter parts, the reactant molecules containing ^{13}C generally are enriched. This shift can be quantified by CSIA allowing to calculate the isotope enrichment factor (for carbon: ε_C), which represents an integrated value over the isotope effects associated with each step in the multistep reaction. Hence, the

magnitude of the measured ε_C–value depends (i) on the corresponding transition state structure of the respective reaction, and subsequently on its underlying reaction mechanism.[25] Moreover, the ε_C–value can vary (ii) in systems with a given reaction mechanism because the observable isotope fractionation is primarily determined by the slowest, i.e., rate–limiting step within the multistep reaction.[23] Consequently, when the reaction is not rate–limited by the bond cleavage, but rather by a preceding, non or weak fractionating step (e.g., adsorption), the intrinsic KIE of bond cleavage is diminished ("masked"), leading to a lower observable kinetic isotope fractionation.[23] Hence, CSIA can provide information on the rate–limiting step within a multistep reaction of known reaction mechanism.[23] Recent studies presented carbon CSIA methods for the aminophosphonates ATMP, glyphosate and AMPA using LC–IRMS .[26–28] Mogusu et al. applied carbon CSIA for a preliminary investigation of the carbon isotope fractionation associated with oxidation of glyphosate at manganese oxide.[28] However, the effect of environmentally relevant parameters, such as pH on the observed kinetic isotope fractionation was not considered.

With the presented study we aimed to provide deeper insights into the oxidation of amino–(poly–)phosphonates at manganese oxide surfaces. To this end, we investigated the transformation of IDMP, which is – unlike aminopolyphosphonates (e.g., ATMP)– not subjected to homogeneous Mn(II)–catalyzed oxidation in the aqueous phase. Hence, IDMP can be regarded as a model compound to study exclusively the heterogeneous reaction of the aminophosphonate at the mineral surface. The influence of manganese oxide mineralogy and pH on the reaction in terms of (i) transformation kinetics and (ii) possible rate–limiting steps was investigated quantitatively in laboratory batch experiments. Therefore, we combined kinetic modeling and compound–specific carbon isotope analysis. The results presented contribute to a more comprehensive understanding of the role of manganese oxides as environmentally relevant oxidants for IDMP and aminophosphonates in general and consequently their environmental behavior.

4.3 Materials and methods

Transformation batch experiments

Experimental setup: Transformation experiments were conducted in duplicates (and one MnO_2–free control) at $22 \pm 2\,^{\circ}C$ under constant rapid stirring (approx. 750 rpm) in open clear glass bottles exposed to air. The experiments were started by adding MnO_2 particles ((i) self–synthesized as described in appendix C or (ii) manganese(IV) oxide, $\geqslant$ 98 %, Carl Roth, Karlsruhe, Germany) to a pH–adjusted, buffered IDMP ($\geqslant$ 97 % (T), Sigma Aldrich, Steinheim, Germany) solution. 20 mM sodium formate (prepared from formic acid, Optima™, Fisher Chemical, Schwerte, Germany), 20 mM MES and 20 mM Tris (or 20 mM HEPES) (all PUFFERAN®$\geqslant$ 99 %, Carl Roth) were used for the experiments at pH 3.0 ± 0.1, 6.0 ± 0.1 and 8.0 ± 0.1, respectively. Ultra–pure water for all solutions was obtained from a Barnstead™GenPure™system (Thermo Fisher Scientific, Germany) and the pH was adjusted with 1 M NaOH or 1 M HCl (EMSURE,

Merck).

Sampling: : For each time point, 5 mL of sample was withdrawn and distributed equally into four 1.5 mL centrifugation tubes. After centrifugation at 20 000 rcf for 15 min, the supernatant was filtered through a 0.22 µm syringe filter (PES, BGB Analytik, Boeckten, Switzerland) and stored at −20 °C if not analyzed at the same day. The samples were stable with respect to concentration, as well as isotopic composition.

Concentration analysis of IDMP

Quantification of remaining IDMP in solution was conducted on an 883 Basic IC Plus equipped with a Metrosep A Supp 4 anion chromatography column (250 mm × 4 mm) and an electrical conductivity detector (Metrohm Germany, Filderstadt, Germany). A sample volume of 20 µL was injected and 5 mM Na_2CO_3 / 1 mM $NaHCO_3$ (both EMSURE®, Merck Millipore, Darmstadt, Germany) at a flow rate of 1 mL min^{-1} was used as eluent. External standards in the range of 1 mg L^{-1} and 20 mg L^{-1} were used for quantification ($R^2 \geqslant 0.99$). Prior to analysis, samples were diluted 1:10 with ultrapure water. For the experiments at pH 6 and 8, dissolved Mn had to be removed from the sample to transfer IDMP into its free, un–complexed form. To this end, 2.5 mL of diluted sample was added to a 5 mL centrifugation tube containing 50 ± 2 mg of cation exchange resin in its Na^+ form (prepared from DOWEX®50 W X 8, 100–200 mesh, H^+ form (Carl Roth) by washing with 1 M NaOH and ultrapure water afterwards), which was shaken for 15 min. Afterwards, the samples were centrifuged for 10 min at 10 000 rcf and the supernatant was analyzed.

Quantification of ortho–phosphate

Ortho–phosphate was quantified spectroscopically by the molybdenum blue method according to Murphy and Riley.[29] Briefly, samples were diluted 1:10 with ultra–pure water in a 1 cm cuvette in order to obtain absorbance values within the calibration range. After mixing the sample with the reagent solution and a reaction time of 30 min, the absorbance was measured at 710 nm (UV5Bio, Mettler Toledo, Greifensee, Switzerland).

Quantification of dissolved manganese

Dissolved manganese in the centrifuged and filtered samples was analyzed by a 4200 MP–AES, equipped with a SPS 3 autosampler, a cyclonic spray chamber and an easy–fit torch (Agilent Technologies, Santa Clara, United States). The selected wavelength was 403.076 nm. The read time and gas nebulizer gas flow were set to 5 s and 0.85 L min^{-1}, respectively. Samples were diluted prior to analysis with 2 % (v/v) HNO_3. External standards in the range between 0.25 mg L^{-1} and 5.00 mg L^{-1} were used for quantification ($R^2 \geqslant 0.99$). Between every analysis, the system was rinsed with 0.1 % (v/v) HNO_3.

Compound–specific carbon isotope analysis

Stable carbon isotope ratios in the residual IDMP fraction were analyzed by means of LC–IRMS, as described elsewhere.[26] Separation of IDMP from its transformation products and the matrix was conducted on the UltiMate3000 HPLC–system (Thermo Fisher Scientific, Germering, Germany), equipped with an IC NI–424 anion chromatography column (100 mm × 4.6 mm, Shodex, Munich, Germany), held at 40 °C. A sample volume of 50 µL was injected and 2.5 mM NaH_2PO_4 (EMSURE®, Merck Millipore, Darmstadt, Germany), adjusted to pH 2.6 with H_3PO_4 (85 %, EMSURE®, Merck Millipore, Darmstadt, Germany) at a flow rate of 500 µL min^{-1} was used as eluent. Analysis of carbon isotope ratios was conducted on a Delta V Plus IRMS, which was hyphenated to the HPLC via a LC Isolink interface (both Thermo Fisher Scientific, Bremen, Germany). The eluent stream was mixed within a mixing–tee with 1.5 M phosphoric acid and 30 g L^{-1} sodium persulfate (for analysis EMSURE®, Merck Millipore, Darmstadt, Germany), which were delivered at flow rates of 50 µL min^{-1} and 75 µL min^{-1}, respectively. The δ^{13}C–values of IDMP were obtained using concentration adjusted IDMP reference standard (measured by EA–IRMS as described elsewhere[30] with $\delta^{13}C_{EA-value} = -35.2 \pm 0.2$ ‰ (n = 3) in VPDB scale) bracketing six samples by duplicate standards. Samples were diluted with ultra–pure water to the same concentration before analysis. The uncertainty of the measurements was $\leqslant$ 0.5 ‰ (n = 2–3).

Calculations

Carbon isotope enrichment factor: For the calculation of carbon isotope enrichment factors (ε_C), the data was evaluated applying the linearized Rayleigh distillation equation, without forcing through the origin, as proposed by Scott, et al.:[31]

$$\ln\left(\frac{R(t)}{R(0)}\right) = \ln\left(\frac{\delta^{13}C(t)+1}{\delta^{13}C(t)+1}\right) = \varepsilon_C \times \ln\left(\frac{c(t)}{c(0)}\right) \tag{4.1}$$

with the isotopic ratio R ($= {}^{13}C/{}^{12}C$), the isotopic signature normalized to an international reference standard δ^{13}C and the concentration c at the beginning of the experiment (0) and at time point t.

Fitting of kinetic data: Transformation kinetics were fitted by the two models proposed by Zhang et al. (2008).[32] Model PF (precursor formation, **Equation 4.2**) can be applied in the case that formation of the precursor complex (i.e., adsorption) is the rate determining step:

$$-\frac{dc(t)}{dt} = k_{PF} \times (c_{rss} - (c(0) - c(t))) \times c(t) \tag{4.2}$$

With the concentration of IDMP c at time point t and at the beginning of the experiment in mM, the pseudo 2nd order rate constant k_{PF} in mM^{-1}h^{-1} and the concentration of reactive surface sites c_{rss} in mM.

Model ET (electron transfer, **Equation 4.3**) holds in the case that electron transfer between IDMP and surface–bond Mn(IV/III) after formation of the precursor complex is rate limiting:

$$-\frac{dc(t)}{dt} = k_{ET} \times (c_{rss} - (c(0) - c(t))) \tag{4.3}$$

With the pseudo 1st order rate constant k_{ET} in h^{-1}.

The experimental data was fitted to the two models using the ReKinSim model framework by Gharasoo et al. (2017).[33] The 95 % confidence interval (CI) of the fitted rate constant was calculated by multiplying the standard error obtained by fitting with the Student's t–value for n_{exp}.

4.4 Results and discussion

To investigate (i) the potential of manganese oxides as oxidants for IDMP and thereon (ii) the underlying processes, batch experiments with varying MnO_2 mineralogy and concentration, as well as the suspension pH were conducted and discussed with respect to reaction kinetics and observed isotope enrichment factors (see **Table 4.1**).

Table 4.1: Compilation of experiments on the oxidation of IDMP at MnO_2 under varying conditions. Shown are the varied parameters pH, buffer (20 mM, adjusted with NaOH and HCl), concentration of MnO_2 (commercial or self–synthesized), extent of transformation and the phosphorus mass balance (MB_P) at the end of the experiment, as well as the first order rate constant according to Model ET (k_{ET}, including 95 % confidence interval) and the carbon isotope enrichment factor (fits excluding T_0, including 95 % confidence interval). All experiments were conducted with an initial IDMP concentration of 1 mM at 22 ± 2 °C.

pH	3	6			8		
Buffer	formate	MES			Tris		HEPES
Manganese dioxide ($g\,L^{-1}$)	1.7 com.	1.7 synth.	1.7 com.	3.4 com.	1.7 synth.	1.7 com.	1.7 com.
Transformation (%)	100	81	73	75	80	67	55
MB_P (%)	77	86	87	64	53	84	108
$k_{ET} \pm 95\,\%$ CI (h^{-1})	0.31 $\pm$0.06	0.32 $\pm$0.03	(3 ± 2) $\times 10^{-3}$	0.4 $\pm$0.1	(7 ± 1) $\times 10^{-3}$	(2.1 ± 0.4) $\times 10^{-3}$	0.16 $\pm$0.03
$\varepsilon_C \pm 95\,\%$ CI (‰)	-7.7 $\pm$0.8	-4.2 $\pm$0.6	-5.2 $\pm$0.4	-3.8 $\pm$0.4	-4.0 $\pm$0.6	-5.9 $\pm$0.7	-8.4 $\pm$0.5

Effect of MnO_2 mineralogy on transformation kinetics

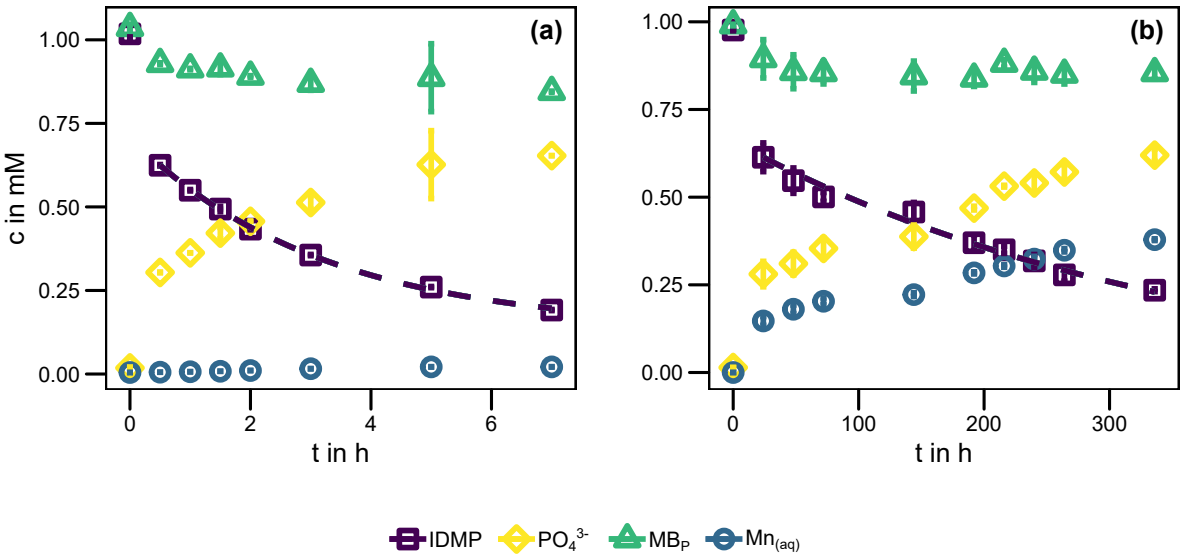

Figure 4.1: Temporal profile of IDMP (including the fit according to Model ET), ortho–phosphate, the phosphorus mass balance ($MB_P = [IDMP] + [PO_4^{3-}]$) and dissolved manganese in the presence of $1.7\,g\,L^{-1}$ (a) self–synthesized and (b) commercial MnO_2 at pH 6.0 ± 0.1 (20 mM MES). Shown are the average concentrations of duplicate batch experiments. Error bars represent one standard deviation for the measured concentrations and the error was calculated via Gaussian error propagation for the MB_P, respectively.

Experiments conducted at pH 6.0 showed that IDMP was transformed in the presence of both, the commercial MnO_2 ($MnO_{2/com}$), as well as self–synthesized MnO_2 ($MnO_{2/synth}$, see **Figure 4.1**). About 70 % to 80 % of IDMP was removed from the aqueous phase within around 340 h and 7 h for $MnO_{2/com}$ and $MnO_{2/synth}$, respectively. Ortho–phosphate was detected in both experiments as transformation product, indicating IDMP transformation via C−P bond cleavage. This is in line with findings for the reaction of manganese oxides with glyphosate, AMPA and ATMP.[13,14,19,34] The phosphorus mass balance in aqueous solution ($MB_P = [IDMP] + [PO_4^{3-}]$) exceeded 86 %. A loss of about 10 % was observed between the beginning of the experiment and the first sampling time point, with stable values afterwards. This observation indicates fast initial sorption of IDMP, which is in accordance with sorption timescales of minutes to hours described in literature for the sorption of (poly–)phosphonic acids on iron and manganese oxides.[5,19,34,35] Hence, IDMP loss from the aqueous phase at the beginning of the experiment is caused by the superimposition of both (i) sorption and (ii) transformation. Therefore, the first sampling point (t_0) was disregarded in quantitative evaluation of the kinetic data according to Model PF (precursor complex formation is the rate–limiting step) and Model ET (electron transfer is the rate–limiting step). For $MnO_{2/com}$, Model PF yielded unrealistically high parameter uncertainties (relative errors around 1×10^3 %) and therefore, this model could not be applied to describe the data (see **Table C.1** for model fit comparison). Fitting the data according to Model ET on the other side resulted in considerably smaller relative uncertainties

in the order of 1×10^1 %. Hence, the transformation of IDMP followed a first–order kinetic, implying that electron transfer is rate–limiting in the multistep process.[32] For $MnO_{2/synth}$, both models gave comparable fits, with Model ET resulting in smaller parameter uncertainties. As both data sets could be described better by Model ET, the first order transformation rate constants (k_{ET}) were compared. The fitted IDMP transformation rate constant was around two orders of magnitude higher for $MnO_{2/synth}$ ($k_{ET} = 0.32 \pm 0.03\,h^{-1}$) than for $MnO_{2/com}$ ($k_{ET} = 0.003 \pm 0.002\,h^{-1}$) (**Table 4.1**). The significantly faster transformation at $MnO_{2/synth}$ is likely attributed to the differences in the mineral properties. While both minerals shared an amorphous nature (based on XRD spectra, see **Figure C.1**), further characterization of the particles showed distinct differences with respect to their mineralogical properties (see appendix C). Foremost the significantly higher specific surface area (SSA) of $MnO_{2/synth}$ ($326 \pm 1\,m^2\,g^{-1}$ vs. $64.5 \pm 0.2\,m^2\,g^{-1}$), as well as the higher Mn(III)–content (5 % vs 1 %) likely contributed to its higher reactivity.

For $MnO_{2/com}$ the ratio of dissolved manganese to degraded IDMP was 0.5 at the end of the experiment (340 h, **Figure 4.1(b)**). Hence, one Mn(IV) surface site is able to oxidize two IDMP. This is in accordance with the mechanisms proposed for the oxidation of ATMP at Mn(III)OOH in the presence of oxygen.[12] For earlier time points, the ratio was slightly smaller (0.4), which supports the hypothesis of IDMP removal from the aqueous phase by sorption at the beginning of the experiment, as the sorption process did not stimulate dissolution of MnO_2. While it can be assumed that the same mechanism holds for $MnO_{2/synth}$, only a negligible concentration of dissolved manganese (< 0.02 mM) was detected in this setup (**Figure 4.1(a)**). This can probably be explained by the higher SSA for $MnO_{2/synth}$ in combination with its low pH_{pzc} of 2.3 ± 0.1 (95 % CI), leading to strong resorption of the reduced Mn(II) onto the mineral surface.[12,36,37] In the presence of $MnO_{2/com}$, resorption is less favorable due to the lower SSA and higher pH_{pzc} of 5.6 ± 0.1.

Doubling the concentration of $MnO_{2/com}$ ($3.4\,g\,L^{-1}$) resulted in faster transformation of IDMP (see **Figure C.3**). In agreement with the results discussed earlier, the data could be fitted according to Model ET, yielding a two–orders of magnitude higher reaction rate constant ($k_{ET} = 0.4 \pm 0.1\,h^{-1}$) in comparison to half the $MnO_{2/com}$ concentration. The ratio of dissolved Mn to degraded IDMP was 0.1 and thus significantly lower than for $1.7\,g\,L^{-1}$ $MnO_{2/com}$, likely due to more available surface sites and thus a higher extend of IDMP and Mn(II) sorption. The lower concentration of dissolved Mn is also consistent with the higher reaction rate constant observed for the higher MnO_2 concentration. Sorption of Mn(II) was shown to lead to structural changes in birnessite–type manganese oxides induced by the formation of Mn(III).[38] The proposed mechanism comprises (i) sorption of Mn(II) to vacant sites on the mineral surface and subsequent (ii) comproportionation of Mn(II) and surrounding Mn(IV).[39–41] The formation of weakly stabilized Mn(III) via the reduction of MnO_2 by bisulfite has shown to increase the reaction rate constant for the oxidation of methyl blue at MnO_2 by three orders of magnitude.[42] As also O–donor ligands such as phosphonates and phosphate were shown to stabilize Mn(III) in solution, a similar kind of Mn(III)–stabilization mechanism by complexation with IDMP or

its transformation products (e.g., phosphate) is conceivable in the IDMP–MnO_2 system.[18,43] Hence, the more pronounced resorption of Mn(II) and subsequent formation of reactive Mn(III) can explain the much faster reaction for a doubled $MnO_{2/com}$ concentration.

Effect of pH and Mn(III)–content on the transformation kinetics

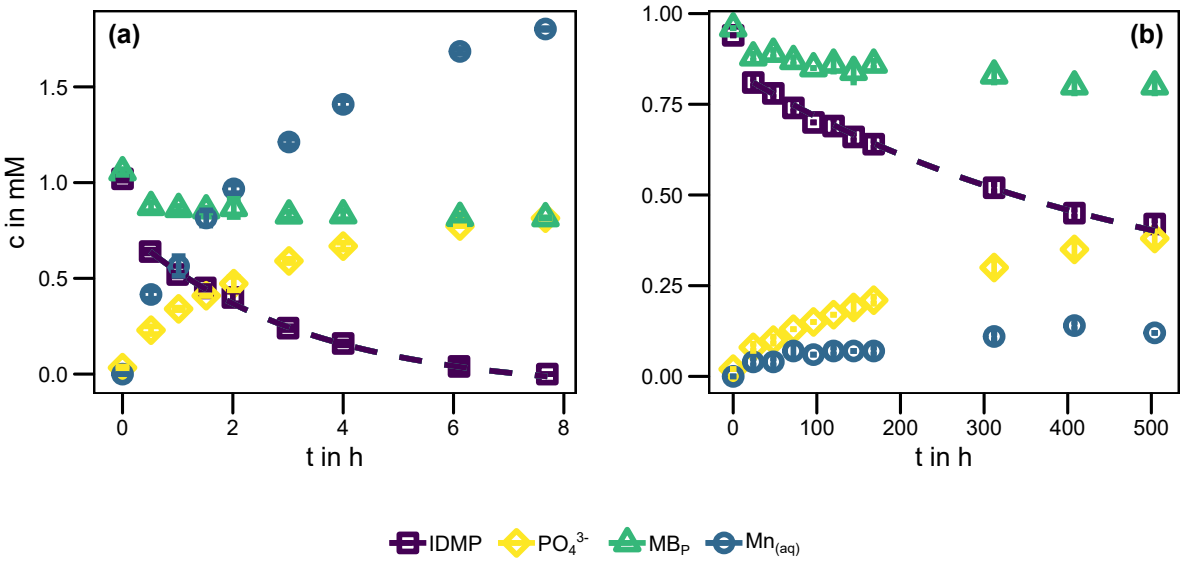

Figure 4.2: Temporal profile of IDMP (including the fit according to Model ET), ortho–phosphate, the phosphorus mass balance ($MB_P = [IDMP] + [PO_4^{3-}]$) and dissolved manganese in the presence of 1.7 g L^{-1} commercial MnO_2 at (a) pH 3.0 ± 0.2 (20 mM formate) and (b) pH 8.0 ± 0.1 (20 mM Tris) (for data at pH 6, please see Figure 4.1(b)). Shown are average concentrations of duplicate batch experiments. Error bars represent one standard deviation for the measured concentrations and the error was calculated via Gaussian error propagation for the MB_P, respectively.

Experiments conducted at pH 3 and 8 revealed a faster transformation of IDMP at MnO_2 with decreasing pH (see **Figure 4.2** for experiments with $MnO_{2/com}$ and **Figure C.4** for experiment at pH 8 with $MnO_{2/synth}$). The experiment at pH 3 could be fitted according to Model ET, while Model PF gave high parameter uncertainties (see **Table C.1**). This is in line with the hypothesis of strong sorption of IDMP at pH 3 due to electrostatic attraction facilitated by the positive surface charge of the mineral. The data for pH 8 could be described by both models. However, Model ET again yielded smaller uncertainties, similar to the results for pH 6 (see **Table C.1**). By applying Model ET, rate constants of $0.31 \pm 0.06\,h^{-1}$ and $(2.1 \pm 0.4) \times 10^{-3}\,h^{-1}$ for pH 3 and pH 8, respectively, were obtained. IDMP transformation at $MnO_{2/synth}$ and pH 8 could also be described by Model ET and the obtained reaction rate constant was about three times higher ($(7 \pm 1) \times 10^{-3}\,h^{-1}$) than for $MnO_{2/com}$. Hence, the difference in the transformation kinetics of the experiments conducted at pH 8 was significantly smaller than at pH 6 (k_{ET}–values differed by the factor of 100). The inverse relation of reaction rate and pH is in accordance with various studies on the oxidation of anionic organics by manganese dioxide minerals, such as substituted phenols or small organic acids (including phosphonoformic acid).[9,18,44] Four

factors were proposed to account for the inverse relation of reaction rate and pH, namely (i) stronger sorption of anions to MnO_2 at lower pH, (ii) increasing redox potential of MnO_2 with decreasing pH, (iii) faster electron transfer at lower pH and (iv) higher surface charge density MnO_2 at low pH. Among these factors, the redox potential is assumed to be the most dominant one.[10]

Dissolution of $MnO_{2/com}$ at pH 3 was significantly more pronounced compared to pH 6 with $Mn_{(aq)}$:$IDMP_{degraded}$–ratios increasing from 1.1 at early time points to 1.8 at the end of the experiment. This observation indicates accelerated reductive dissolution of the mineral, potentially due to side reactions between the manganese dioxide and formate, as shown for other small organic acids.[18] Consequently, dissolved manganese concentrations for the experiment at pH 3 are inconclusive, calling for the use of a different buffer system for future experiments. At pH 8, the $Mn_{(aq)}$:$IDMP_{degraded}$–ratio was smaller than 0.5 during the entire course of the experiment. Moreover, only in this experiment the ratio decreased over time from 0.3 to 0.2. This observation can be rationalized by strong (re–)adsorption of Mn(II) to the mineral surface, which is reasonable considering the negative net charge of $MnO_{2/com}$ at pH 8 ($pH_{pzc}(MnO_{2/com})$ = 5.5).

To evaluate the effect of the Mn(III)–content of MnO_2 minerals on the reaction rates, an experiment with Mn(III)–enriched $MnO_{2/com}$ was conducted at pH 8. To this end, HEPES rather than Tris buffer was used as HEPES can partially reduce $Mn(IV)O_2$, leading to an enrichment of Mn(III) surface sites (see appendix C for characterization).[45] Following this approach, the Mn(III)–content of $MnO_{2/com}$ was increased from 1 % to 9 %. Transformation of IDMP at the Mn(III)–enriched mineral was significantly faster, with an increase of k_{ET} by a factor of 80 (see **Figure C.5** for temporal profile). Although k_{ET} was used to compare the experiments, fitting the data according to Model PF gave almost identical parameter values and parameter uncertainties like Model ET for this experiment. The faster transformation at the Mn(III)–enriched MnO_2 is in accordance with published studies showing the promoting effect of Mn(III) surface sites on the transformation rate of organic compounds, such as phenol and bisphenol A at Mn(III)/Mn(IV) mixed oxides.[46,47]

In conclusion, oxidative transformation of IDMP at MnO_2 was observed in all experiments. The kinetic models implied that electron transfer within the Mn(IV)–IDMP precursor complex was rate–determining. However, formation of the precursor–complex (i.e., sorption) as the slowest step within the multistep reaction could not be ruled out in some experiments based on this approach. To get deeper insights into the underlying processes of IDMP oxidation at MnO_2, carbon CSIA was applied as a complementary tool.

Effect of MnO_2 mineralogy and pH on the observed kinetic carbon isotope fractionation

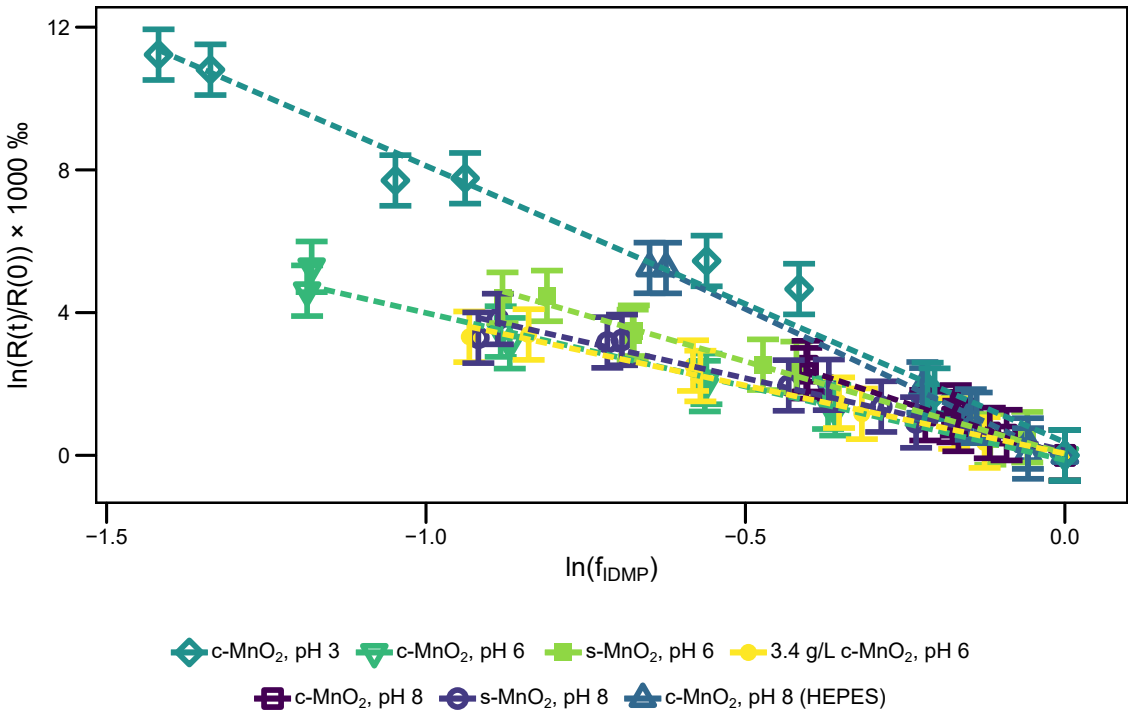

Figure 4.3: Double–logarithmic Rayleigh plot showing carbon isotope fractionation of IDMP for varying experimental conditions: Applied mineral, mineral loading ($1.7\,g\,L^{-1}$ if not stated otherwise), pH and buffer (formate (pH 3), MES (pH 6) and Tris (pH 8) if not stated otherwise). Additionally, shown are the linear regressions according to the Rayleigh model normalized to the first data point after t_0 (i.e., excluding t_0). Error bars were calculated by means of Gaussian error propagation assuming an error of the $\delta^{13}C$–value of 0.5 ‰.

To quantify the kinetic carbon isotope fractionation associated with IDMP oxidation, all data sets were fitted according to the Rayleigh model ($R^2 \geqslant 0.96$, **Figure C.6**). Linear fitting resulted in negative y–intercepts for most of the experiments. The extent of the negative shift was seemingly correlated with the extent of sorption in the experiments, i.e., increasing with (i) the MnO_2 concentration at constant pH, (ii) decreasing pH at a constant MnO_2 concentration, and (iii) SSA of the mineral at constant pH. In accordance with this hypothesis, lower (more negative) y–intercepts were observed for (i) $3.4\,g\,L^{-1}$ $MnO_{2/com}$ at pH 6 and (ii) $1.7\,g\,L^{-1}$ $MnO_{2/com}$ at pH 3 in comparison to $1.7\,g\,L^{-1}$ $MnO_{2/com}$ at pH 6 and pH 8. This observation is indicative of a shift in the slope of the linear regression, i.e., a less pronounced isotope enrichment factor at early in comparison to later time points. The findings suggest that the observed isotope fractionation at early time points is caused by a superimposition of a fractionating process (i.e., the transformation of IDMP) and a non/weaker fractionating process, likely sorption. Consequently, the observed isotope fractionation patterns support the hypothesis of superimposed sorption and oxidation at the beginning of the experiment, as proposed based on the modeled kinetics and the measured dissolved manganese concentrations. To avoid misinterpretation based on varying extent of IDMP sorption in the different experiments, the Rayleigh plots were

normalized to t_1 or t_2, depending on the experiment in accordance with the normalization applied on the kinetic data and double–logarithmic Rayleigh plots with a constant slope were obtained, resulting in a consistent origin of all linear fits (see **Figure 4.3**).

The sorption–corrected Rayleigh plots revealed that the oxidation of IDMP at MnO_2 is associated with a normal kinetic isotope effect resulting in a significant enrichment (> 1 ‰) in ^{13}C during all experiments. The obtained ε_C–values ranged between -3.8 ± 0.4 ‰ (95 % CI) and -8.4 ± 0.5 ‰ (see **Table 4.1**). For all experiments at pH 6, similar enrichment factors were obtained (-4.2 ± 0.6 ‰ for $MnO_{2/synth}$, -5.2 ± 0.4 ‰ for $MnO_{2/com}$ and -3.8 ± 0.4 ‰ for a doubled concentration of $MnO_{2/com}$). This observation implied that the carbon isotope fractionation does not depend on the (i) reaction rates and (ii) sorption capacities of the system, as these two parameters differed significantly between the setups at pH 6.

Increasing the pH from 6 to 8 had no effect on the kinetic isotope fractionation for neither of both minerals. Deviations between the ε_C–values were 0.2 ‰ and 0.7 ‰ for $MnO_{2/synth}$ and $MnO_{2/com}$, respectively and thus smaller/ equal to the corresponding confidence intervals. However, decreasing the pH from 6 to 3 led to a small but significant increase in the observed isotope fractionation ($\varepsilon_C = -7.7 \pm 0.8$ ‰) associated with the oxidation at $MnO_{2/com}$.
Oxidation of IDMP at the Mn(III)–rich $MnO_{2/com}$ at pH 8 was associated with the highest isotope fractionation observed in this study, with an ε_C–value of -8.4 ± 0.5 ‰ and thus around 3 ‰ lower than for the oxidation at the non–modified $MnO_{2/com}$.

Summarizing, for most of the experiments, comparable ε_C–values were obtained (-3.8 ± 0.4 ‰ to -5.9 ± 0.7 ‰), implying that (i) reaction kinetics, as well as (ii) sorption had no significant effect on the observed kinetic carbon isotope fractionation. However, oxidation of IDMP (i) at pH 3 and (ii) at pH 8 and Mn(III)–rich $MnO_{2/com}$ were associated with a (slightly) higher isotope fractionation (ε_C of -7.7 ± 0.8 ‰ and -8.4 ± 0.6 ‰, respectively).

Implications of the observed kinetic carbon isotope fractionation on the proposed reaction scheme

Oxidation of organics at manganese oxides is proposed to be a three step reaction comprising formation of a reactant–MnO_2 precursor complex (adsorption of the reactant), electron transfer within the precursor, and finally break down of the reactant by bond cleavage.[10] In the case of IDMP oxidation to its (stable) transformation products (TPs) at a Mn(IV) surface site (=Mn(IV)), the reaction can be described by **Equations 4.4** to **4.7**:

$$=\mathrm{Mn(IV)} + \mathrm{IDMP} \rightleftharpoons [=\mathrm{Mn(IV)}, \mathrm{IDMP}] \tag{4.4}$$

$$[=\mathrm{Mn(IV)}, \mathrm{IDMP}] \rightleftharpoons [=\mathrm{Mn(III)}, \mathrm{IDMP^{\bullet}}] \tag{4.5}$$

$$[=\mathrm{Mn(III)}, \mathrm{IDMP^{\bullet}}] \longrightarrow [=\mathrm{Mn(III)}, \mathrm{TP}] \tag{4.6}$$

$$[=\mathrm{Mn(III)}, \mathrm{TP}] \rightleftharpoons =\mathrm{Mn(III)} + \mathrm{TP} \tag{4.7}$$

Within the multistep reaction, IDMP breakdown via C−P bond cleavage (**Equation 4.6**) is the only step for which a pronounced kinetic carbon isotope effect is expected due to the involvement of a carbon atom. In order to estimate the maximum observable kinetic carbon isotope effect, the semiclassical Streitwieser limit for C−P bond cleavage was calculated based on vibrational frequencies from the literature for different (amino–)phosphonates.[25] This approach resulted in an $\varepsilon_{C,max}$–value of around -25 ‰ (for calculations see appendix C). Hence, based on the observed isotope enrichment factors of -3.8 ± 0.4 ‰ to -8.4 ± 0.5 ‰ for IDMP oxidation at MnO_2 (see **Table 4.1**), it can be concluded that the intrinsic kinetic isotope fractionation of the bond cleavage step was (partially) masked by preceding, non/ weak fractionating steps, i.e., either by the formation of the precursor complex or by electron transfer (**Equation 4.4** and **4.5**). As in neither of these steps carbon atoms are involved, a negligible kinetic carbon isotope effect can be expected.[23] This hypothesis is in accordance with studies proposing fast break down after electron transfer and thus a rate–limitation by either adsorption or electron transfer during oxidation of organics at MnO_2.[32]

Based on the observed kinetic carbon isotope fractionation, rate–limitation by sorption can be excluded. In this case, the observed kinetic carbon isotope fractionation should increase with higher MnO_2 surface area at a given pH, as the driving force and thus rate constant for sorption is increasing. However, the obtained isotope enrichment factor was independent of the $MnO_{2/com}$ concentration at pH 6 (see **Table 4.1**). A similar behavior was reported for the oxidation of substituted anilines at MnO_2.[48] The subsequent electron transfer within the precursor complex likely takes place between the secondary amine–N to the Mn(IV/III) surface site, leading to the formation of a N–centered radical, as proposed for the oxidation of ATMP, AMPA and glyphosate at manganese oxides and for Mn(II)–catalyzed oxidation of ATMP by dissolved oxygen.[12–14,49] The critical role of the amine functional group was supported by observations that N–free phosphonates were not degraded at manganese oxide and by Mn(II)–catalyzed oxidation.[34,49] Due to the facts that (i) sorption was ruled out as rate–limiting step and (ii) a carbon KIE associated with the one–electron oxidation of the amine–N and manganese oxide surface can be excluded, the electron transfer step was proposed as (partially) rate–limiting within the multistep reaction. Subsequently, the N–centered radical formed via electron transfer (rapidly) breaks down to a methylene radical via C−P bond cleavage. Oxidation of the methylene radical likely involves dissolved oxygen species based on the observed concentrations of dissolved Mn(II), which is in accordance with the oxidation of ATMP at Mn(III)OOH in the presence of oxygen.[12] Stable transformation products (besides ortho–phosphate) are presumably AMPA and N–phosphonomethylene carbamate, in analogy to the proposed mechanisms for ATMP and glyphosate.[12–14]

Summarizing, the insights obtained by the observed kinetic isotope fractionation are in accordance with the kinetics, suggesting (partial) rate–limitation of the electron transfer within the multistep reaction. The more pronounced ε_C–values for low pH–value and increased Mn(III)–content indicate – in line with dara from literature – faster electron transfer in these setups.

Conclusion and environmental implications

The presented study provides the first detailed investigation on the oxidation of amino–(poly–)phosphonic acids on Mn(III)/Mn(IV) mixed oxides. It was shown that IDMP is transformed at MnO_2 under varying environmental conditions (pH, MnO_2 mineralogy, Mn(III)–content in the system) with the transformation kinetics following the behavior described in literature for anionic organic model compounds. These results emphasize the so far barely investigated role of manganese oxides in the environmental fate of amino–(poly–)phosphonic acids. Kinetic and isotope data suggested that electron transfer is rate–limiting within the multistep reaction under conditions investigated in this study. Despite a comparable isotope fractionation observed in most experiments (-3.8 ± 0.4 ‰ to -5.9 ± 0.7 ‰), (i) a low pH-value of 3 and (ii) an elevated Mn(III)–content (9 % vs. 1 %) facilitated electron transfer, resulting in a more pronounced kinetic isotope fractionation (-7.7 ± 0.8 ‰ and -8.4 ± 0.5 ‰). Consequently, while qualitative evidence of MnO_2–driven IDMP oxidation is possible under the investigated conditions due to the significant enrichment of ^{13}C in all experimental setups, the observed variations of the ε_C–values hamper an unequivocal identification of the reaction pathway. The system is even more complex for aminopolyphosphonates, as they can additionally be transformed via homogeneous Mn(II)–catalyzed oxidation, leading to an autocatalytic behavior under oxic conditions as soon as the manganese oxide is reductively dissolved upon aminipolyphosphonate oxidation.[12,49] As the homogeneous Mn(II)–catalyzed oxidation of ATMP also shows kinetic isotope fractionation that varies with the Mn–ATMP speciation (see chapter 3), a superimposition of the two processes may result in an ambiguous isotope fractionation pattern, preventing mechanistic interpretations solely based on carbon CSIA.

The results of this study call for more research on the kinetic isotope effects associated with the homogeneous and heterogeneous Mn–driven oxidation of amino–(poly–)phosphonates in order to get a better understanding of the individual processes: (i) Studying the oxidation of small aminophosphonates, e.g., AMPA at manganese oxides with varying properties (e.g., Mn(III)–content and mineralogy) under varying conditions (oxygen level, pH) on the one hand can give more insights on the underlying processes of the reaction at the mineral surface. (ii) Transformation of aminopolyphosphonates (e.g., ATMP) at MnO_2 on the other hand can provide a deeper understanding of the autocatalytic Mn–cycle and the relative importance of the homogeneous and heterogeneous oxidation pathways. Moreover, complementary methods such as transformation product identification via high resolution mass spectrometry and 2–D isotope analysis ($\delta^{15}N/\delta^{13}C$) have a great potential to provide deeper insights into the underlying reaction mechanisms of IDMP/ aminophosphonate oxidation.[50,51] However, LC–IRMS systems are only available for carbon CSIA so far. Thus, the development of a derivatization protocol for IDMP would be needed in order to allow nitrogen CSIA of IDMP by GC–IRMS as shown for glyphosate.[28]

References

(1) Rott, E.; Steinmetz, H.; Metzger, J. W. Organophosphonates: A review on environmental relevance, biodegradability and removal in wastewater treatment plants. *Science of the Total Environment* **2018**, *615*, 1176–1191.

(2) Jaworska, J.; Van Genderen-Takken, H.; Hanstveit, A.; van de Plassche, E.; Feijtel, T. Environmental risk assessment of phosphonates, used in domestic laundry and cleaning agents in the Netherlands. *Chemosphere* **2002**, *47*, 655–665.

(3) Nowack, B. Environmental chemistry of phosphonates. *Water Research* **2003**, *37*, 2533–2546.

(4) Nowack, B. Aminopolyphosphonate removal during wastewater treatment. *Water Research* **2002**, *36*, 4636–4642.

(5) Nowack, B.; Stone, A. T. Adsorption of Phosphonates onto the Goethite-Water Interface. *Journal of Colloid and Interface Science* **1999**, *214*, 20–30.

(6) Fischer, K. Sorption of chelating agents (HEDP and NTA) onto mineral phases and sediments in aquatic model systems: Part I: Sorption onto clay minerals. *Chemosphere* **1991**, *22*, 15–27.

(7) Post, J. E. Manganese oxide minerals: Crystal structures and economic and environmental significance. *Proceedings of the National Academy of Sciences* **1999**, *96*, 3447–3454.

(8) Tebo, B. M.; Bargar, J. R.; Clement, B. G.; Dick, G. J.; Murray, K. J.; Parker, D.; Verity, R.; Webb, S. M. Biogenic manganese oxides: properties and mechanisms of formation. *Annual Review of Earth and Planetary Sciences* **2004**, *32*, 287–328.

(9) Stone, A. T. Reductive dissolution of manganese (III/IV) oxides by substituted phenols. *Environmental Science & Technology* **1987**, *21*, 979–988.

(10) Remucal, C. K.; Ginder-Vogel, M. A critical review of the reactivity of manganese oxides with organic contaminants. *Environmental Science: Processes and Impacts* **2014**, *16*, 1247–66.

(11) Islam, M. A.; Morton, D. W.; Johnson, B. B.; Mainali, B.; Angove, M. J. Manganese oxides and their application to metal ion and contaminant removal from wastewater. *Journal of Water Process Engineering* **2018**, *26*, 264–280.

(12) Nowack, B.; Stone, A. T. Homogeneous and heterogeneous oxidation of nitrilotrismethylenephosphonic acid (NTMP) in the presence of manganese (II, III) and molecular oxygen. *The Journal of Physical Chemistry B* **2002**, *106*, 6227–6233.

(13) Barrett, K. A.; McBride, M. B. Oxidative degradation of glyphosate and aminomethylphosphonate by manganese oxide. *Environmental Science & Technology* **2005**, *39*, 9223–9228.

(14) Jaisi, D. P.; Li, H.; Wallace, A. F.; Paudel, P.; Sun, M.; Balakrishna, A.; Lerch, R. N. Mechanisms of Bond Cleavage during Manganese Oxide and UV Degradation of Glyphosate: Results from Phosphate Oxygen Isotopes and Molecular Simulations. *Journal of Agricultural and Food Chemistry* **2016**, *64*, 8474–8482.

(15) Borggaard, O. K.; Gimsing, A. L. Fate of glyphosate in soil and the possibility of leaching to ground and surface waters: a review. *Pest Management Science* **2008**, *64*, 441–456.

(16) Botta, F.; Lavison, G.; Couturier, G.; Alliot, F.; Moreau-Guigon, E.; Fauchon, N.; Guery, B.; Chevreuil, M.; Blanchoud, H. Transfer of glyphosate and its degradate AMPA to surface waters through urban sewerage systems. *Chemosphere* **2009**, *77*, 133–139.

(17) Grandcoin, A.; Piel, S.; Baures, E. AminoMethylPhosphonic acid (AMPA) in natural waters: Its sources, behavior and environmental fate. *Water Research* **2017**, *117*, 187–197.

(18) Wang, Y.; Stone, A. T. Reaction of MnIII, IV (hydr) oxides with oxalic acid, glyoxylic acid, phosphonoformic acid, and structurally-related organic compounds. *Geochimica et Cosmochimica Acta* **2006**, *70*, 4477–4490.

(19) Nowack, B.; Stone, A. T. Manganese-catalyzed degradation of phosphonic acids. *Environmental Chemistry Letters* **2003**, *1*, 24–31.

(20) Lesueur, C.; Pfeffer, M.; Fuerhacker, M. Photodegradation of phosphonates in water. *Chemosphere* **2005**, *59*, 685–691.

(21) Kuhn, R.; Jensch, R.; Bryant, I. M.; Fischer, T.; Liebsch, S.; Martienssen, M. The influence of selected bivalent metal ions on the photolysis of diethylenetriamine penta(methylenephosphonic acid). *Chemosphere* **2018**, *210*, 726–733.

(22) Bai, S. H.; Ogbourne, S. M. Glyphosate: environmental contamination, toxicity and potential risks to human health via food contamination. *Environmental Science and Pollution Research* **2016**, *23*, 18988–19001.

(23) Elsner, M. Stable isotope fractionation to investigate natural transformation mechanisms of organic contaminants: principles, prospects and limitations. *Journal of Environmental Monitoring* **2010**, *12*, 2005–2031.

(24) Schmidt, T. C.; Zwank, L.; Elsner, M.; Berg, M.; Meckenstock, R. U.; Haderlein, S. B. Compound-specific stable isotope analysis of organic contaminants in natural environments: a critical review of the state of the art, prospects, and future challenges. *Analytical and Bioanalytical Chemistry* **2004**, *378*, 283–300.

(25) Elsner, M.; Zwank, L.; Hunkeler, D.; Schwarzenbach, R. P. A new concept linking observable stable isotope fractionation to transformation pathways of organic pollutants. *Environmental Science & Technology* **2005**, *39*, 6896–6916.

(26) Martin, P. R.; Buchner, D.; Jochmann, M. A.; Haderlein, S. B. Stable carbon isotope analysis of polyphosphonate complexing agents by anion chromatography coupled to isotope ratio mass spectrometry: method development and application. *Analytical and Bioanalytical Chemistry* **2020**, *412*, 4827–4835.

(27) Kujawinski, D. M.; Wolbert, J. B.; Zhang, L.; Jochmann, M. A.; Widory, D.; Baran, N.; Schmidt, T. C. Carbon isotope ratio measurements of glyphosate and AMPA by liquid chromatography coupled to isotope ratio mass spectrometry. *Analytical and Bioanalytical Chemistry* **2013**, *405*, 2869–2878.

(28) Mogusu, E. O.; Wolbert, J. B.; Kujawinski, D. M.; Jochmann, M. A.; Elsner, M. Dual element ((15)N/(14)N, (13)C/(12)C) isotope analysis of glyphosate and AMPA by derivatization-gas chromatography isotope ratio mass spectrometry (GC/IRMS) combined with LC/IRMS. *Analytical and Bioanalytical Chemistry* **2015**, *407*, 5249–5260.

(29) Murphy, J.; Riley, J. P. A modified single solution method for the determination of phosphate in natural waters. *Analytica Chimica Acta* **1962**, *27*, 31–36.

(30) Köster, D.; Wolbert, J. B.; Schulte, M. S.; Jochmann, M. A.; Schmidt, T. C. Origin of Xylitol in Chewing Gum: A Compound-Specific Isotope Technique for the Differentiation of Corn- and Wood-Based Xylitol by LC-IRMS. *Journal of Agricultural and Food Chemistry* **2018**, *66*, 2015–2020.

(31) Scott, K. M.; Lu, X.; Cavanaugh, C. M.; Liu, J. S. Optimal methods for estimating kinetic isotope effects from different forms of the Rayleigh distillation equation. *Geochimica et Cosmochimica Acta* **2004**, *68*, 433–442.

(32) Zhang, H.; Chen, W.-R.; Huang, C.-H. Kinetic modeling of oxidation of antibacterial agents by manganese oxide. *Environmental Science & Technology* **2008**, *42*, 5548–5554.

(33) Gharasoo, M.; Thullner, M.; Elsner, M. Introduction of a new platform for parameter estimation of kinetically complex environmental systems. *Environmental Modelling and Software* **2017**, *98*, 12–20.

(34) Li, H.; Wallace, A. F.; Sun, M.; Reardon, P.; Jaisi, D. P. Degradation of glyphosate by Mn-oxide may bypass sarcosine and form glycine directly after C–N bond cleavage. *Environmental Science & Technology* **2018**, *52*, 1109–1117.

(35) Orcelli, T.; di Mauro, E.; Urbano, A.; Valezi, D. F.; da Costa, A. C.; Zaia, C. T. B.; Zaia, D. A. Study of interaction between glyphosate and goethite using several methodologies: an environmental perspective. *Water, Air, & Soil Pollution* **2018**, *229*, 1–18.

(36) Klausen, J.; Haderlein, S. B.; Schwarzenbach, R. P. Oxidation of substituted anilines by aqueous MnO2: Effect of co-solutes on initial and quasi-steady-state kinetics. *Environmental Science & Technology* **1997**, *31*, 2642–2649.

(37) Morgan, J. J.; Stumm, W. Colloid-chemical properties of manganese dioxide. *Journal of Colloid Science* **1964**, *19*, 347–359.

(38) Elzinga, E. J. Reductive Transformation of Birnessite by Aqueous Mn(II). *Environmental Science & Technology* **2011**, *45*, 6366–6372.

(39) Lefkowitz, J. P.; Rouff, A. A.; Elzinga, E. J. Influence of pH on the reductive transformation of birnessite by aqueous Mn (II). *Environmental Science & Technology* **2013**, *47*, 10364–10371.

(40) Zhao, H.; Zhu, M.; Li, W.; Elzinga, E. J.; Villalobos, M.; Liu, F.; Zhang, J.; Feng, X.; Sparks, D. L. Redox reactions between Mn (II) and hexagonal birnessite change its layer symmetry. *Environmental Science & Technology* **2016**, *50*, 1750–1758.

(41) Liu, J.; Zhang, Y.; Gu, Q.; Sheng, A.; Zhang, B. Tunable Mn Oxidation State and Redox Potential of Birnessite Coexisting with Aqueous Mn (II) in Mildly Acidic Environments. *Minerals* **2020**, *10*, 690.

(42) Sun, B.; Guan, X.; Fang, J.; Tratnyek, P. G. Activation of Manganese Oxidants with Bisulfite for Enhanced Oxidation of Organic Contaminants: The Involvement of Mn(III). *Environmental Science & Technology* **2015**, *49*, 12414–12421.

(43) Jiang, J.; Pang, S.-Y.; Ma, J. Role of ligands in permanganate oxidation of organics. *Environmental Science & Technology* **2010**, *44*, 4270–4275.

(44) Zhang, H.; Huang, C.-H. Oxidative transformation of triclosan and chlorophene by manganese oxides. *Environmental Science & Technology* **2003**, *37*, 2421–2430.

(45) Simanova, A. A.; Kwon, K. D.; Bone, S. E.; Bargar, J. R.; Refson, K.; Sposito, G.; Pena, J. Probing the sorption reactivity of the edge surfaces in birnessite nanoparticles using nickel(II). *Geochimica et Cosmochimica Acta* **2015**, *164*, 191–204.

(46) Nico, P. S.; Zasoski, R. J. Mn (III) center availability as a rate controlling factor in the oxidation of phenol and sulfide on δ-MnO_2. *Environmental Science & Technology* **2001**, *35*, 3338–3343.

(47) Huang, J.; Zhong, S.; Dai, Y.; Liu, C.-C.; Zhang, H. Effect of MnO2 phase structure on the oxidative reactivity toward bisphenol A degradation. *Environmental Science & Technology* **2018**, *52*, 11309–11318.

(48) Skarpeli-Liati, M.; Jiskra, M.; Turgeon, A.; Garr, A. N.; Arnold, W. A.; Cramer, C. J.; Schwarzenbach, R. P.; Hofstetter, T. B. Using nitrogen isotope fractionation to assess the oxidation of substituted anilines by manganese oxide. *Environmental Science & Technology* **2011**, *45*, 5596–5604.

(49) Nowack, B.; Stone, A. T. Degradation of Nitrilotris(methylenephosphonic Acid) and Related (Amino)Phosphonate Chelating Agents in the Presence of Manganese and Molecular Oxygen. *Environmental Science & Technology* **2000**, *34*, 4759–4765.

(50) Elsner, M.; Imfeld, G. Compound-specific isotope analysis (CSIA) of micropollutants in the environment - current developments and future challenges. *Current Opinion in Biotechnology* **2016**, *41*, 60–72.

(51) Willach, S.; Lutze, H. V.; Eckey, K.; Loppenberg, K.; Luling, M.; Wolbert, J. B.; Kujawinski, D. M.; Jochmann, M. A.; Karst, U.; Schmidt, T. C. Direct Photolysis of Sulfamethoxazole Using Various Irradiation Sources and Wavelength Ranges-Insights from Degradation Product Analysis and Compound-Specific Stable Isotope Analysis. *Environmental Science & Technology* **2018**, *52*, 1225–1233.

5 General conclusions and outlook

5.1 Conclusions

(Amino–)polyphosphonate chelating agents ((A)PPs) are ionic chemicals increasingly used in industrial and household applications. However, their fate in technical and environmental systems is not fully understood yet, partially due to a lack of suitable analytical methods.[1,2] Processes considered to be relevant for the environmental fate of APPs include the homogeneous and heterogeneous oxidation in the presence of manganese and dissolved oxygen. The elucidation of these reaction pathways solely by product analysis, however, is hampered by the fact that most transformation products are unspecific.[3,4] Compound–specific carbon isotope analysis (carbon CSIA) is a promising tool to narrow this knowledge gap by providing insights into transformation processes solely based on the isotopic signature of the parent compound.[5] Therefore, the presented work aimed to establish stable carbon isotope analysis as a tool to study the environmental fate of APPs and to apply this method in laboratory batch experiments to further elucidate the pathways and mechanisms of Mn–driven oxidation of APPs in the presence of oxygen.

The major outcomes of the presented thesis are:

(**i**) the successful development of an analytical framework for carbon CSIA of three widely used (A)PPs by LC–IRMS,
(**ii**) the proof of concept for the differentiation between equilibrium sorption and degradation of APPs by means of carbon CSIA and

new mechanistic insights into (**iii**) homogeneous and (**iv**) heterogeneous Mn–driven oxidation of APPs.

A brief synopsis of how the major goals of this work were achieved follows.

(**i**) The widely used PPs HEDP, ATMP and EDTMP could be separated successfully on an anion–exchange column under acidic conditions using a diluted sulfuric acid eluent. The method was also suitable to separate ATMP and its transformation products from laboratory batch experiments. The acidic separation conditions were beneficial to keep the CO_2 background in the IRMS low. In addition, the acidic pH prevented adverse effects of cations on the chromatographic separation due to complexation of the PPs as described for methods applying alkaline eluents.[6] Optimization of the oxidation conditions within the LC–IRMS interface showed that low persulfate concentrations (factor three to six lower compared to values described in literature) were sufficient to mineralize the PPs quantitatively to CO_2 which increased filament lifetime and consequently minimized instrument downtime. Thus, the developed method successfully improved the throughput of the LC–IRMS by optimization of the oxidation conditions.

(**ii**) The presented work provides for the first time data on the carbon isotope effect associated with the equilibrium sorption onto goethite, as well as Mn(II)–catalyzed oxidation of ATMP. Under the investigated conditions sorption of ATMP did not lead to a detectable carbon isotope effect whereas oxidation led to a significant kinetic isotope fractionation. These results imply

that carbon CSIA is a suitable tool to assign ATMP removal from the aqueous phase to either sorption or transformation. Hence, CSIA has great potential as a complementary tool to concentration analysis to distinguish different removal processes and thus to improve a process–based assessment of the fate of ATMP (and likely other (A)PPs) in wastewater treatment plants as well as receiving surface waters.

(iii) By combining the data from carbon CSIA and concentration analysis with equilibrium speciation modeling, the mechanisms contributing to Mn(II)–catalyzed oxidation of ATMP by molecular oxygen in homogeneous aqueous solution could be clarified and expanded. The experimental data confirmed that intermediate Mn(III)ATMP complexes play a central role in the reaction pathway. These Mn(III)–complexes of ATMP, however, are not only subjected to self–decomposition initiated by an intermolecular electron transfer, as proposed so far. Rather, they also act as catalytically active oxidants leading to the oxidation of free ATMP, which matches the reported well known property of Mn(III)–complexes as strong oxidants.[7,8] This second reaction pathway has major implications for the environmental fate of APPs. In natural systems, Mn(III)APP–intermediates likely react foremost with any reductants present at elevated concentrations, such as (complex) natural organic matter (NOM). As a consequence, APPs in the presence of dissolved manganese are (partially) trapped in catalytic complexes, resulting in a diminished potential of Mn(II)–catalyzed oxidation for APP transformation.

(iv) The heterogeneous Mn–driven oxidation of APPs at manganese dioxide was investigated using IDMP as a model compound, which is in contrast to ATMP resilient towards Mn(II)–catalyzed oxidation in homogeneous solution. Experiments with different manganese dioxides at varying pH showed first order transformation kinetics and moderate kinetic carbon isotope enrichment factors (around -5 ± 1 ‰) which were significantly smaller than the maximum theoretically observable enrichment factor for C$-$P bond cleavage (-25 ‰). Based on these findings, electron transfer within the precursor surface–complex was proposed as rate–limiting step rather than the sorption or bond cleavage. Under acidic conditions (pH 3) and at Mn(III)–enriched manganese dioxide, electron transfer was accelerated, leading to a more pronounced observed kinetic isotope fractionation of approximately -8.0 ± 0.5 ‰. Hence, the results obtained by carbon CSIA matched the modeled kinetic data with regard to the proposed underlying reaction mechanism. Furthermore, the distinct carbon isotope fractionation implied that carbon CSIA can be used to trace IDMP removal in environmental as well as technical systems via oxidation at MnO_2 – without the need for information on potential transformation products.

Overall, the presented work demonstrates that carbon CSIA is a promising, so far unexploited tool to study the environmental chemistry of aminopolyphosphonate chelating agents. The first data on sorption and transformation of ATMP and IDMP suggested that isotope analysis can be used to estimate the share of sorption and transformation on the removal of APPs from the aqueous phase. The role of Mn–driven oxidation for APP removal in technical and environmental systems proposed in the literature could be supported only partially. New insights

obtained by the presented work imply that APPs are not only transformed in the presence of manganese and oxygen, but also (partially) trapped in catalytic Mn(III)–complexes under certain conditions, diminishing the potential of Mn–driven oxidation for oxidative breakdown of APPs. Apart from these findings in homogeneous systems, also in heterogeneous systems (i.e., in the presence of manganese oxides), APPs possibly stabilize intermediate Mn(III)–species formed upon the reduction of the minerals. As a result, the complexation could hinder the disproportionation of the Mn(III), allowing the Mn(III)–APP complexes to act as potent oxidants. Similar effects were described for other complexing agents, such as pyrophosphate.[9] Hence, application of carbon CSIA succeeded in providing mechanistic insights into sorption and transformation processes of APPs under controlled laboratory conditions. Yet, prior to the application of carbon CSIA to study these processes *in–situ* in complex environmental or technical settings, more research is needed with respect to **(i)** the analytical limitations, **(ii)** the potential isotope fractionation associated with sorption, as well as the underlying reaction mechanisms of **(iii)** homogeneous and **(iv)** heterogeneous Mn–driven APP oxidation.

5.2 Outlook

Regarding **(i)** the analytics of APPs by LC–IRMS future work primarily should address the low sensitivity and selectivity with respect to matrix interference of the instrumentation. First, an optimization of the chromatographic performance is recommended, for instance by using more appropriate column dimensions (smaller diameter and/ or particle size). Moreover, a chromatographic system with a gradient option is likely a prerequisite for a baseline separation of APPs in high–matrix samples, such as environmental waters. But first and foremost, analysis of APPs at environmentally relevant concentrations requires the development of suitable enrichment techniques. The reason for this is the low inherent sensitivity of the IRMS, resulting in limits of precise isotope analysis which are about 10^3 – 10^4 times higher than the expected APP concentrations in the low $\mu g\,L^{-1}$–range.[10,11] These high anticipated enrichment factors entail also sample clean–up, as otherwise an overload of the system with matrix components is likely.[12] To this end, solid–phase extraction using molecular–imprinted polymers (MIP–SPE) is a promising approach, which can selectively enrich phosphonates, such as glyphosate and AMPA.[13,14] However, in case of non–quantitative sorption and/or desorption of the APPs on/ from the polymer, a throughout investigation of possible isotope fractionation associated with the phase transfer is needed, in order to guarantee true and precise measurements. Recent studies on large volume SPE showed that carbon CSIA of pesticides from environmental samples after a 2×10^5–fold enrichment is feasible.[15] Apart from the limitations of the LC–IRMS for carbon CSIA, a system for stable nitrogen isotope analysis ($\delta^{15}N$) would be of exceptional help to get further insights into the investigated processes. The combination of $\delta^{13}C$ and $\delta^{15}N$ would allow to separate masking processes from changes within the reactions mechanisms as masking by preceding rate–limiting steps (e.g., sorption) shows no element–specific isotope effect.[16] However, a commercial LC–IRMS interface for $\delta^{15}N$–CSIA is not yet available.

Further work on **(ii)** the differentiation between sorption and transformation should aim to narrow the knowledge gap on isotopic effects associated with sorption of APPs onto natural sorbents. Especially sorbents need to be studied, for which other sorption mechanisms than for goethite are conceivable (i.e., no metal (hydr–)oxides, but for instance activated carbon or clays). Moreover, information on potential isotope fractionation associated with slow sorption kinetics such as retarded intra–particle diffusion is needed in order to be able to assess the behavior of APPs in non–equilibrium systems, as recently discussed for chlorinated hydrocarbons.[17,18]

In order to get deeper insights into **(iii)** the homogeneous Mn(II)–catalyzed APP oxidation by dissolved oxygen, studies on the reactivity of the Mn(III)–intermediates towards model reductants (e.g., quinones, thiosulfate, NOM) are proposed. Thereby, a more comprehensive understanding on the relative importance of APP oxidation via complex self–decomposition versus trapping of APPs in catalytic Mn–complexes for the fate of APPs in the presence of dissolved manganese could be acquired. This information is a prerequisite to assess the significance of Mn(II)–catalyzed oxidation in natural or technical settings for the transformation of APPs in the aqueous phase. Furthermore, the influence of competing ligands on the oxidation of APPs in the presence of manganese and oxygen should be studied. Natural or synthetic chelating agents such as EDTA or pyrophosphate likely occur together with APPs in technical and environmental systems and might lead to either an attenuation or enhancement of APP transformation. On the one hand, they compete with APPs to form complexes with manganese and therefore inhibiting APP oxidation via self–decomposition of Mn(III)APP–intermediates. On the other hand, the presence of other chelating agents might lead to the formation of their corresponding Mn(III)–complexes – either by the oxidation of Mn(II)–complexes or the re–complexation of Mn(III) formed by the oxidation of Mn(II)–APP complexes.[19,20] In case they are more reactive than the Mn(III)APP–complexes, oxidation of APPs could be promoted.[7,8]

Future studies on **(iv)** heterogeneous oxidation at manganese oxides should investigate the variability of the observed ε_C–values and the underlying mechanisms. The results from this work indicated that the electron transfer rate primarily determines the observable isotope fractionation. However, the governing factors remain partially unclear so far. Thus, studying the effect of the MnO_2 mineralogy (e.g., Mn(III)–content and oxidation–potential) on the transformation of aminophosphonates, which are resilient towards homogeneous Mn(II)–catalyzed oxidation (such as IDMP and AMPA) and differ in their reduction potential might give further valuable insights. In line with this, the role of dissolved manganese and oxygen on the system with respect to Mn(III)–formation should be studied.

As the first results for the oxidation of IDMP at MnO_2 have shown, numerical modeling of the transformation kinetics has the potential to give further insights into the underlying mechanisms of Mn–driven oxidation of APPs. In future studies, more sophisticated models combining kinetics and isotope effects can be applied to better understand homogeneous and heterogeneous Mn–driven APP oxidation, as already successfully realized for other multistep transformation processes.[21–23] However, a prerequisite for this are more experimental data on (intermediate)

transformation products with respect to concentrations and isotopic composition.

As soon as a comprehensive understanding of the individual processes is obtained, the superimposed homogeneous and heterogeneous Mn–driven oxidation of APPs in the presence of manganese oxide can be studied. Applying the gained insights on the isolated processes, carbon CSIA (in combination with numerical modeling) might be feasible to estimate the relative share of homogeneous and heterogeneous oxidation on the transformation of APPs in complex systems containing manganese oxide as well as dissolved manganese. Ultimately, these findings would allow a more comprehensive assessment of the importance of Mn–driven oxidation for the environmental fate of APPs.

References

(1) Rott, E.; Steinmetz, H.; Metzger, J. W. Organophosphonates: A review on environmental relevance, biodegradability and removal in wastewater treatment plants. *Science of the Total Environment* **2018**, *615*, 1176–1191.

(2) Rott, E.; Happel, O.; Armbruster, D.; Minke, R. Behavior of PBTC, HEDP, and Aminophosphonates in the Process of Wastewater Treatment. *Water* **2020**, *12*, 53.

(3) Nowack, B. Environmental chemistry of phosphonates. *Water Research* **2003**, *37*, 2533–2546.

(4) Kuhn, R.; Jensch, R.; Bryant, I. M.; Fischer, T.; Liebsch, S.; Martienssen, M. The influence of selected bivalent metal ions on the photolysis of diethylenetriamine penta(methylenephosphonic acid). *Chemosphere* **2018**, *210*, 726–733.

(5) Elsner, M.; Zwank, L.; Hunkeler, D.; Schwarzenbach, R. P. A new concept linking observable stable isotope fractionation to transformation pathways of organic pollutants. *Environmental Science & Technology* **2005**, *39*, 6896–6916.

(6) Schmidt, C. K.; Raue, B.; Brauch, H.-J.; Sacher, F. Trace-level analysis of phosphonates in environmental waters by ion chromatography and inductively coupled plasma mass spectrometry. *International Journal of Environmental Analytical Chemistry* **2013**, *94*, 385–398.

(7) Kostka, J. E.; Luther, G. W.; Nealson, K. H. Chemical and biological reduction of Mn (III)-pyrophosphate complexes: Potential importance of dissolved Mn (III) as an environmental oxidant. *Geochimica et Cosmochimica Acta* **1995**, *59*, 885–894.

(8) Hu, E.; Zhang, Y.; Wu, S.; Wu, J.; Liang, L.; He, F. Role of dissolved Mn(III) in transformation of organic contaminants: Non-oxidative versus oxidative mechanisms. *Water Research* **2017**, *111*, 234–243.

(9) Sun, B.; Guan, X.; Fang, J.; Tratnyek, P. G. Activation of Manganese Oxidants with Bisulfite for Enhanced Oxidation of Organic Contaminants: The Involvement of Mn(III). *Environmental Science & Technology* **2015**, *49*, 12414–12421.

(10) Rott, E.; Happel, O.; Armbruster, D.; Minke, R. Influence of wastewater discharge on the occurrence of PBTC, HEDP, and aminophosphonates in sediment, suspended matter, and the aqueous phase of rivers. *Water* **2020**, *12*, 803.

(11) Wang, S.; Sun, S.; Shan, C.; Pan, B. Analysis of trace phosphonates in authentic water samples by pre-methylation and LC-Orbitrap MS/MS. *Water Research* **2019**, *161*, 78–88.

(12) Elsner, M.; Imfeld, G. Compound-specific isotope analysis (CSIA) of micropollutants in the environment - current developments and future challenges. *Current Opinion in Biotechnology* **2016**, *41*, 60–72.

(13) Puzio, K.; Claude, B.; Amalric, L.; Berho, C.; Grellet, E.; Bayoudh, S.; Nehmé, R.; Morin, P. Molecularly imprinted polymer dedicated to the extraction of glyphosate in natural waters. *Journal of Chromatography A* **2014**, *1361*, 1–8.

(14) Surapong, N.; Burakham, R. Magnetic Molecularly Imprinted Polymer for the Selective Enrichment of Glyphosate, Glufosinate, and Aminomethylphosphonic Acid Prior to High-Performance Liquid Chromatography. *ACS Omega* **2021**, 27007–27016.

(15) Torrento, C.; Bakkour, R.; Glauser, G.; Melsbach, A.; Ponsin, V.; Hofstetter, T. B.; Elsner, M.; Hunkeler, D. Solid-phase extraction method for stable isotope analysis of pesticides from large volume environmental water samples. *Analyst* **2019**, *144*, 2898–2908.

(16) Elsner, M. Stable isotope fractionation to investigate natural transformation mechanisms of organic contaminants: principles, prospects and limitations. *Journal of Environmental Monitoring* **2010**, *12*, 2005–2031.

(17) Wanner, P.; Parker, B. L.; Chapman, S. W.; Aravena, R.; Hunkeler, D. Does sorption influence isotope ratios of chlorinated hydrocarbons under field conditions? *Applied Geochemistry* **2017**, *84*, 348–359.

(18) Halloran, L. J.; Vakili, F.; Wanner, P.; Shouakar-Stash, O.; Hunkeler, D. Sorption-and diffusion-induced isotopic fractionation in chloroethenes. *Science of The Total Environment* **2021**, *788*, 147826.

(19) Madison, A. S.; Tebo, B. M.; Luther III, G. W. Simultaneous determination of soluble manganese (III), manganese (II) and total manganese in natural (pore) waters. *Talanta* **2011**, *84*, 374–381.

(20) Klewicki, J. K.; Morgan, J. J. Kinetic Behavior of Mn(III) Complexes of Pyrophosphate, EDTA, and Citrate. *Environmental Science & Technology* **1998**, *32*, 2916–2922.

(21) Jin, B.; Haderlein, S. B.; Rolle, M. Integrated carbon and chlorine isotope modeling: applications to chlorinated aliphatic hydrocarbons dechlorination. *Environmental science & technology* **2013**, *47*, 1443–1451.

(22) Gharasoo, M.; Thullner, M.; Elsner, M. Introduction of a new platform for parameter estimation of kinetically complex environmental systems. *Environmental Modelling and Software* **2017**, *98*, 12–20.

(23) Maggi, F.; Riley, W. J. Transient competitive complexation in biological kinetic isotope fractionation explains nonsteady isotopic effects: Theory and application to denitrification in soils. *Journal of Geophysical Research: Biogeosciences* **2009**, *114*.

A Supporting information to chapter 2

LC–IRMS chromatograms

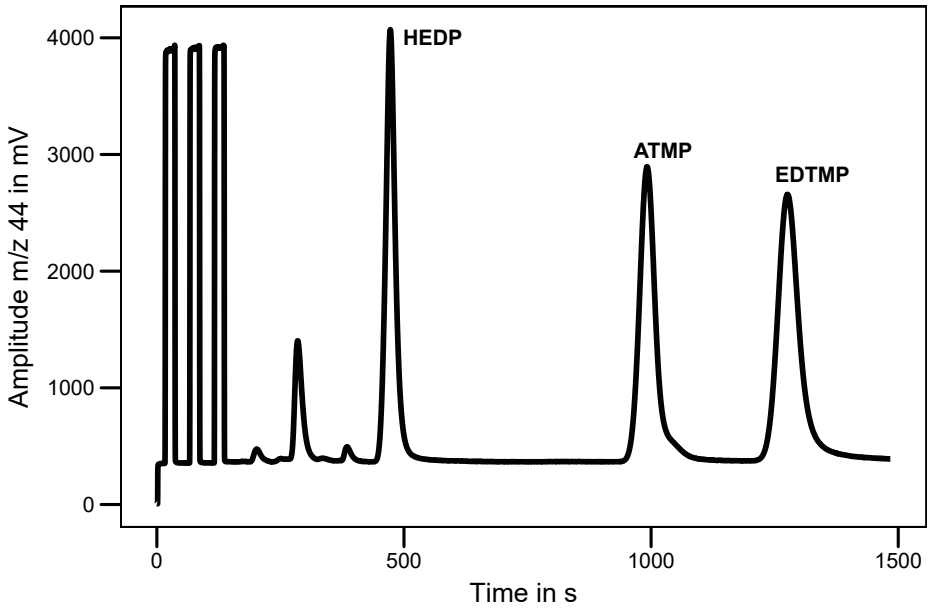

Figure A.1: Representative LC–IRMS chromatogram of the polyphosphonates HEDP, ATMP and EDTMP at concentrations of 50 mg L^{-1}. The first three peaks correspond to CO_2 reference gas pulses.

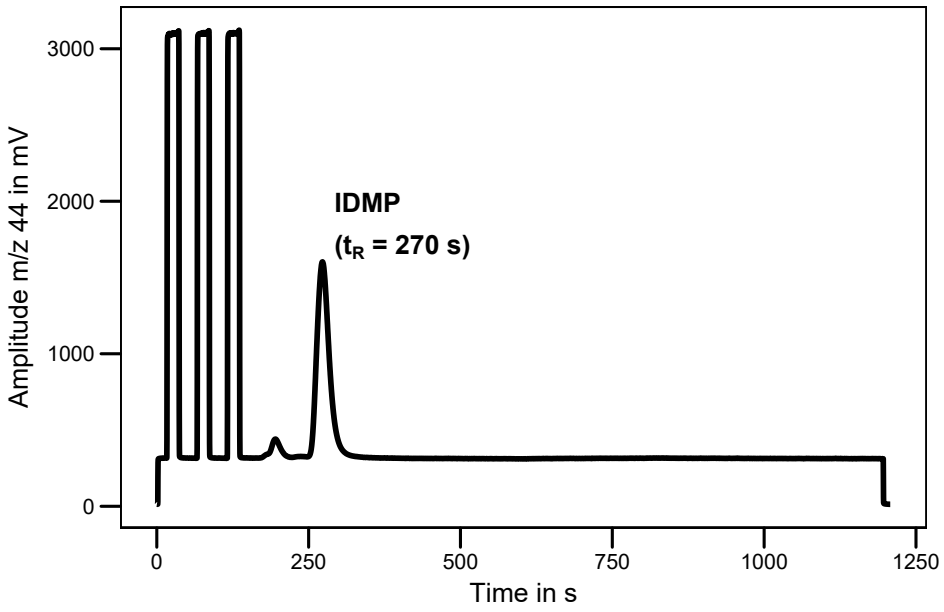

Figure A.2: Representative LC–IRMS chromatogram of IDMP at concentrations of 20 mg L^{-1}. The first three peaks correspond to CO_2 reference gas pulses.

Stepwise integration of ATMP in a sample from an ATMP degradation experiment and corresponding isotope ratio trace

The ATMP peak was integrated manually in approximately 50 mV steps using the skimmed background algorithm (see **Figure A.3**). The δ^{13}C–value of the automatically integrated peak (Peak Nr. 9) was −15.87 ‰ and the average δ^{13}C–value of all manually integrated peaks (Peak Nr. 11+ to 30+) was -15.82 ± 0.03 ‰ (n = 10).

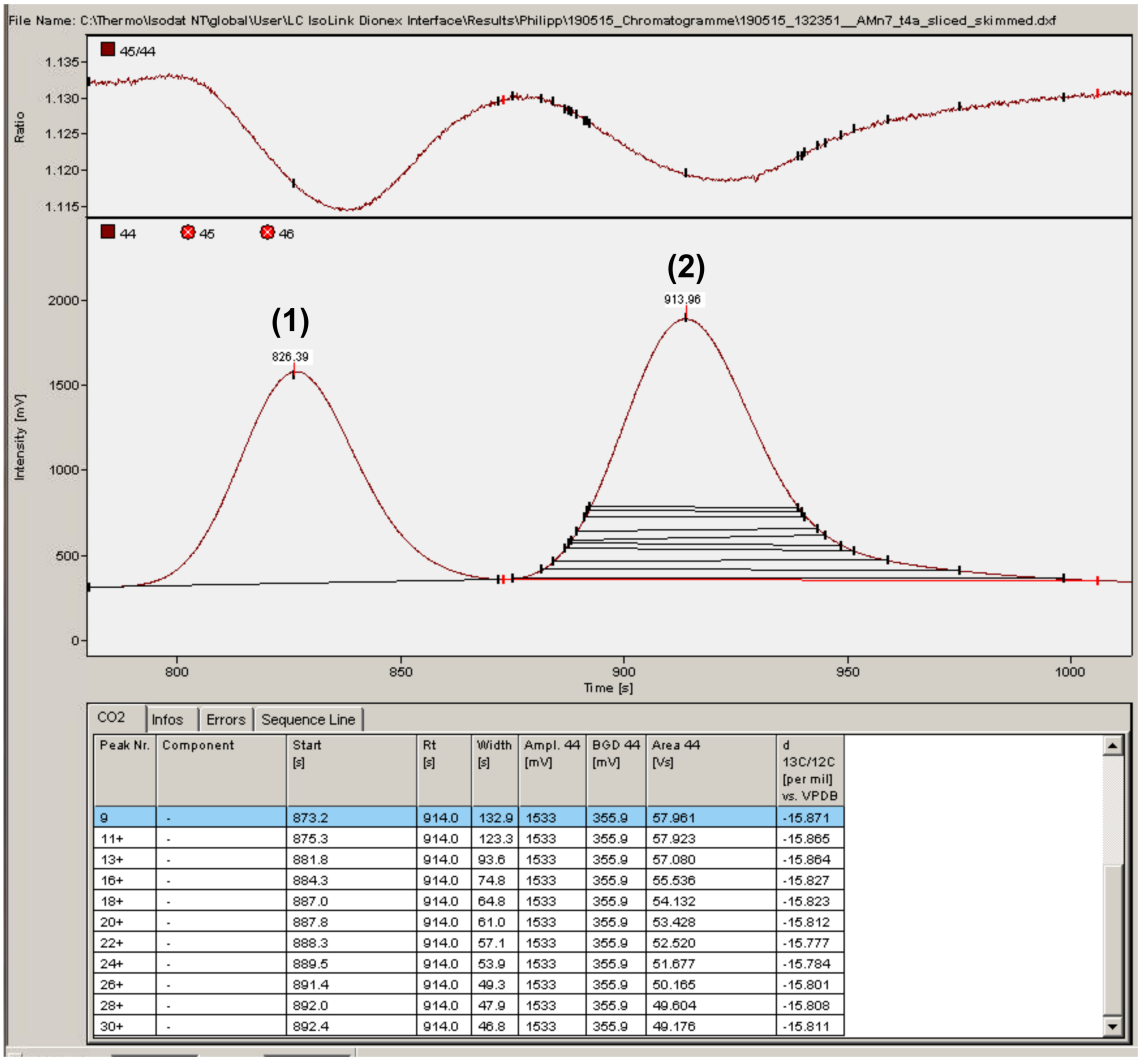

Peak Nr.	Component	Start [s]	Rt [s]	Width [s]	Ampl. 44 [mV]	BGD 44 [mV]	Area 44 [Vs]	d 13C/12C [per mil] vs. VPDB
9	-	873.2	914.0	132.9	1533	355.9	57.961	-15.871
11+	-	875.3	914.0	123.3	1533	355.9	57.923	-15.865
13+	-	881.8	914.0	93.6	1533	355.9	57.080	-15.864
16+	-	884.3	914.0	74.8	1533	355.9	55.536	-15.827
18+	-	887.0	914.0	64.8	1533	355.9	54.132	-15.823
20+	-	887.8	914.0	61.0	1533	355.9	53.428	-15.812
22+	-	888.3	914.0	57.1	1533	355.9	52.520	-15.777
24+	-	889.5	914.0	53.9	1533	355.9	51.677	-15.784
26+	-	891.4	914.0	49.3	1533	355.9	50.165	-15.801
28+	-	892.0	914.0	47.9	1533	355.9	49.604	-15.808
30+	-	892.4	914.0	46.8	1533	355.9	49.176	-15.811

Figure A.3: LC–IRMS chromatogram of ATMP (2) and one of its unknown degradation products (1) from an ATMP degradation experiment. The sample was diluted to an ATMP concentration of 50 mg L^{-1}. The upper panel shows the ratio of the m/z 45 and m/z 44 mass traces.

Oxidation temperature experiment with increased persulfate concentration

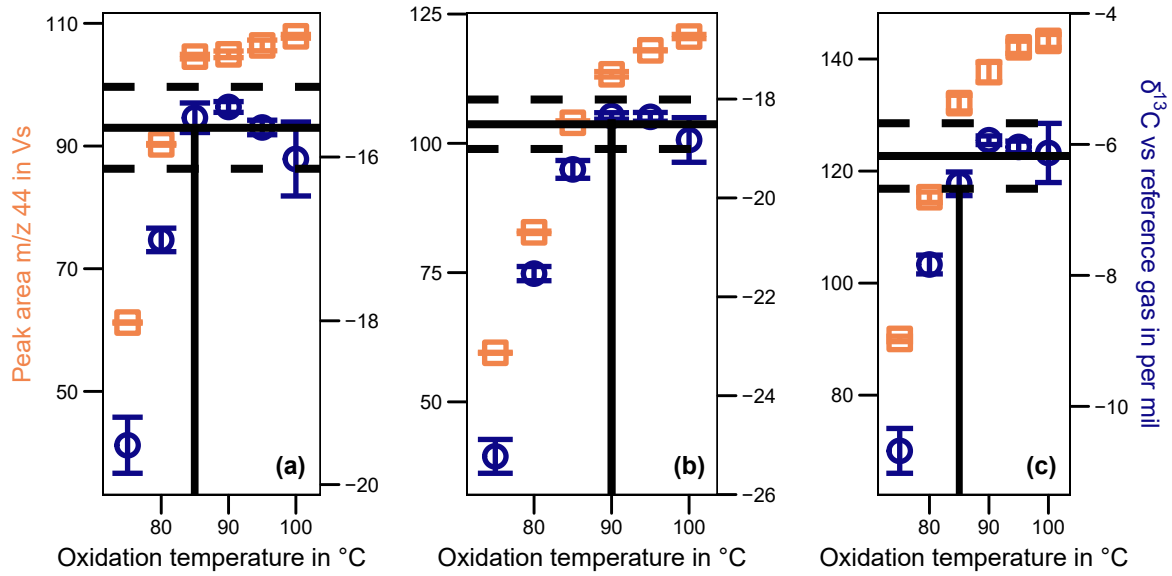

Figure A.4: Peak area (orange squares, left axis) and uncorrected isotopic signature (blue circles, right axis) of HEDP (a), ATMP (b) and EDTMP (c) (n = 3) over the oxidation temperature ($60\,g\,L^{-1}$ persulfate at $50\,\mu L\,min^{-1}$). The horizontal lines correspond to the mean isotopic signature (including a 0.5 ‰ error) for the range with stable isotopic signatures (marked by a vertical line).

Comparison of the IRMS sensitivities for oxalate and DIC in FIA mode

Oxalic acid (≥ 99.0 % (RT), Sigma–Aldrich, Steinheim, Germany) and potassium bicarbonate (for analysis, Merck, Darmstadt, Germany) were used for preparation of the aqueous standards. 50 µL of the standards were injected by an UltiMate3000 HPLC–system (Thermo Fisher Scientific, Germering, Germany). As eluent 4 mM sulfuric acid was used, delivered at a flow rate of $500\,\mu L\,min^{-1}$. Analysis of carbon isotope ratios was conducted on a Delta V Plus IRMS, which was hyphenated to the HPLC via a LC Isolink interface (both Thermo Fisher Scientific, Bremen, Germany). The eluent stream was mixed in a mixing-tee with 1.5 M phosphoric acid and $30\,g\,L^{-1}$ sodium persulfate, which were delivered at flow rates of $50\,\mu L\,min^{-1}$ and $75\,\mu L\,min^{-1}$, respectively. Organic carbon in the eluent stream was converted to CO_2 at 99.9 °C. After cooling the eluent stream down to room temperature, the CO_2 was transferred into the gas phase by a counter–stream of helium at a flow rate of $1.9\,mL\,min^{-1}$.

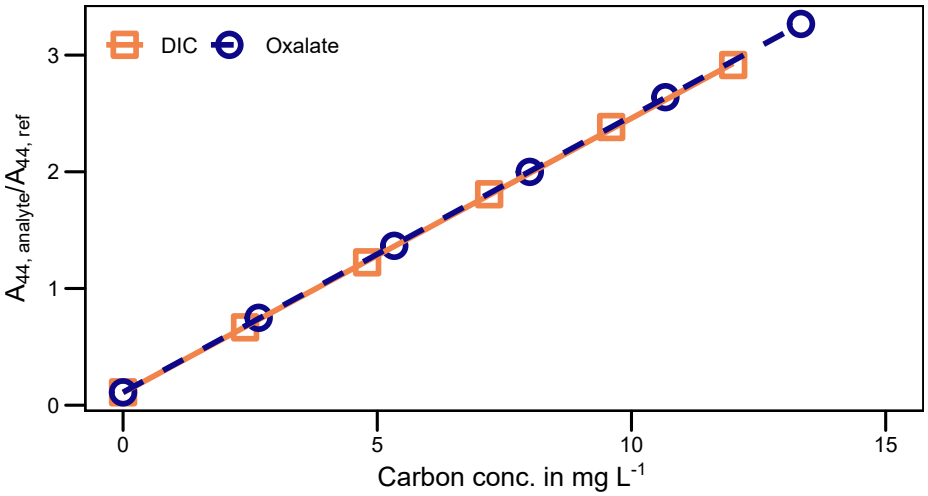

Figure A.5: Sensitivities for carbonate (DIC) and oxalate in FIA mode. The obtained peak areas were normalized to the average peak area of the reference gas pulses to account for varying ion source performance.

Sensitivities of oxalate and polyphosphonates at different persulfate concentrations

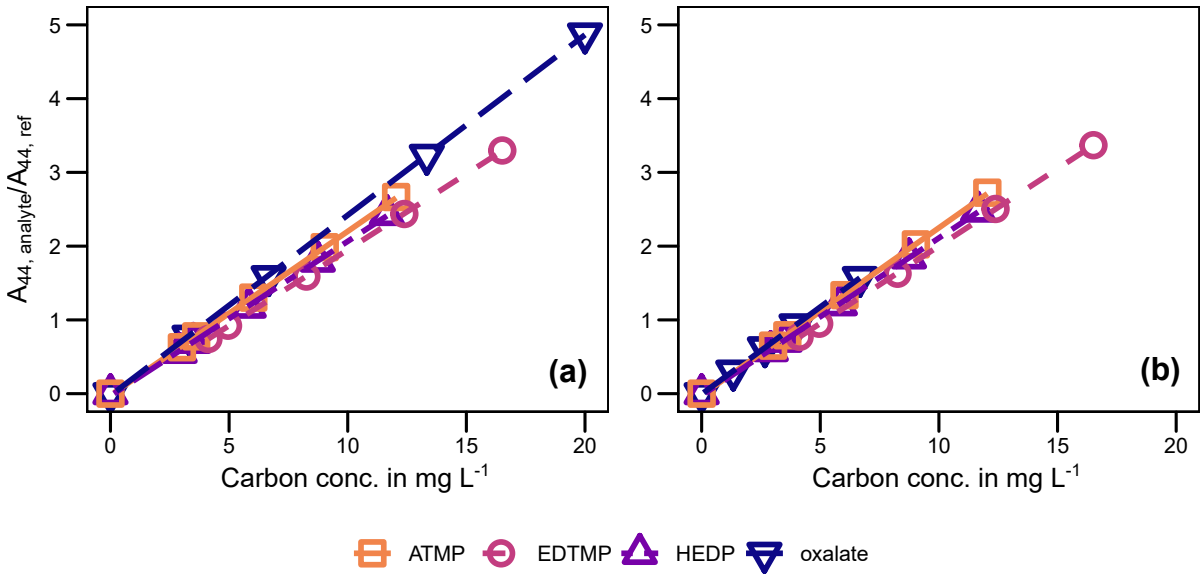

Figure A.6: Sensitivities for oxalate and polyphosphonates at persulfate concentrations 30 g L^{-1} (a) and 60 g L^{-1} (b). The obtained peak areas were normalized to the average peak area of the monitoring gas pulses to account for varying ion source performance.

Sorption isotherms and degradation profile

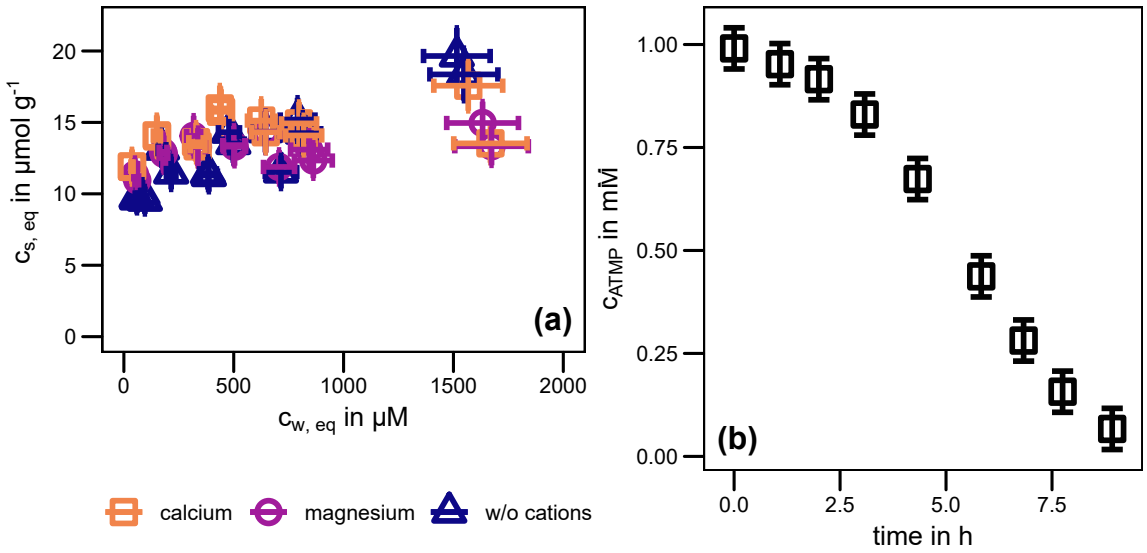

Figure A.7: (a) Sorption isotherms for the sorption of ATMP onto goethite in the absence and presence of calcium or magnesium. An error of 10 % was assumed for aqueous and sorbed ATMP concentration. (b) Degradation profile for manganese catalyzed degradation of ATMP by molecular oxygen. For the ATMP concentration an error of 5 % was assumed.

Calculation of carbon isotope enrichment factor for C−P bond cleavage according to the Streitwieser limit

The Streitwieser limit for C–P bond cleavage was calculated according to the following equation:[1]

$$KIE = \frac{1}{\exp\left(-100 \times \frac{hc\tilde{v}}{2kT}\left(1 - \sqrt{\frac{\mu_L}{\mu_H}}\right)\right)} \tag{A.1}$$

with the Planck constant $h = 6.626 \times 10^{-34}\,\mathrm{J\,s}$, the speed of light $c = 2.998 \times 10^{8}\,\mathrm{m\,s^{-1}}$, the Boltzmann's constant $k_B = 1.381 \times 10^{-23}\,\mathrm{J\,K^{-1}}$ and the absolute temperature T (298 K). μ_L and μ_H are the reduced masses of ^{12}C and ^{13}C in the C–P bond, respectively. For the vibrational wave number $\tilde{v}$ of the C–P bond a conservative value of 650 $\mathrm{cm^{-1}}$ was used, which is the lowest value found in the literature and hence yields the smallest isotope effect.[2]
With these assumptions, a Streitwieser limit of 1.045 was computed. This value was converted to an observable carbon isotope enrichment factor according to the equation below:[3]

$$\varepsilon_C = \left(\frac{1}{KIE} - 1\right) \times \frac{x}{n}\frac{1}{z} \tag{A.2}$$

With the number of carbon atoms $n = 3$, the number of carbon atoms in the reactive position x and the carbon atoms in intramolecular competition z. Due to the symmetric character of ATMP, $x = z = 3$ was assumed, yielding an enrichment factor of −14.4 ‰.

Reference

(1) Jochmann, M. A.; Schmidt, T. C., *Compound-specific stable isotope analysis*; Royal Society of Chemistry: 2015.

(2) Corbrjdge, D. Infra-red analysis of phosphorus compounds. *Journal of Applied Chemistry* **1956**, *6*, 456–465.

(3) Elsner, M. Stable isotope fractionation to investigate natural transformation mechanisms of organic contaminants: principles, prospects and limitations. *Journal of Environmental Monitoring* **2010**, *12*, 2005–2031.

B Supporting information to chapter 3

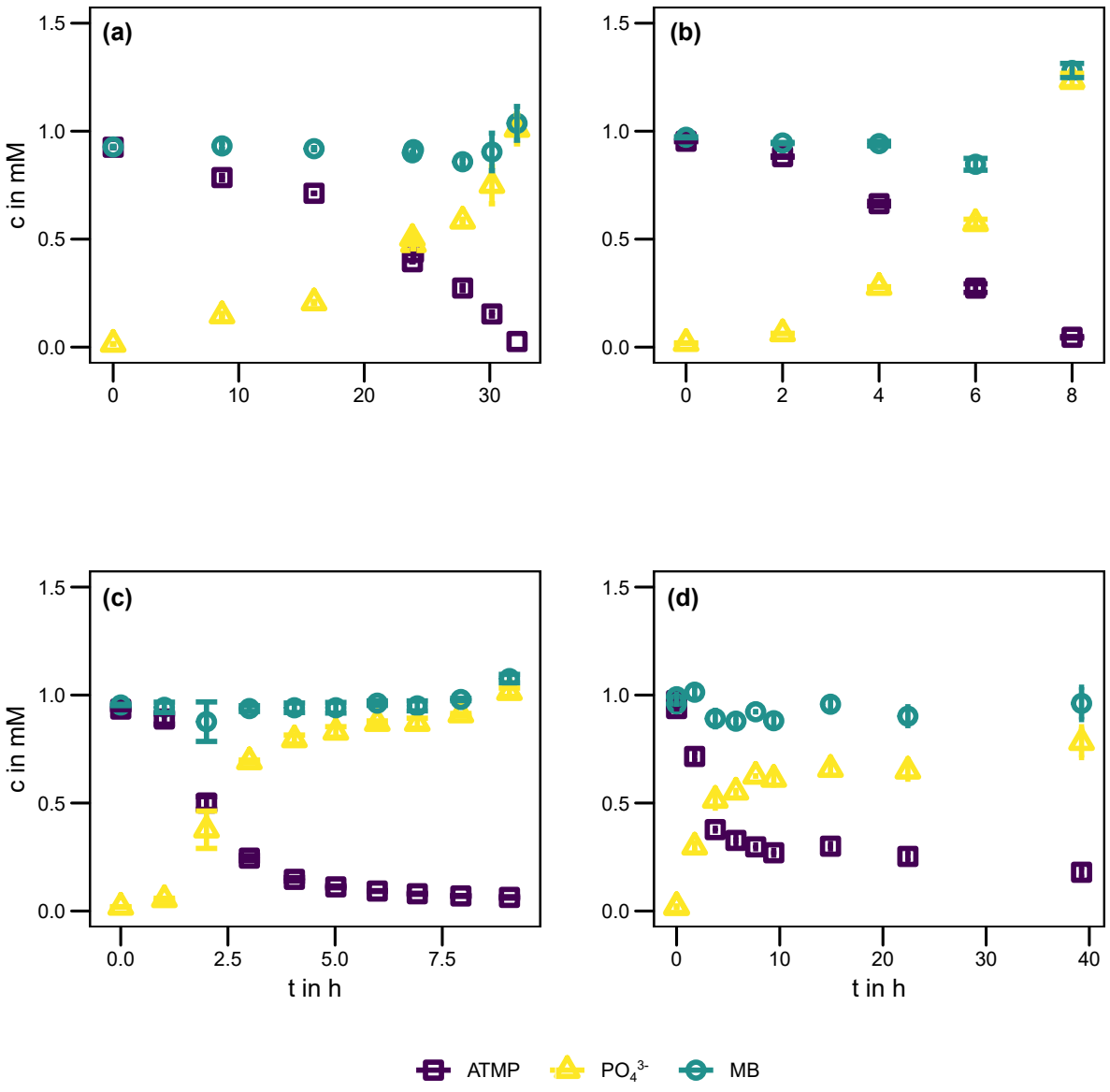

Figure B.1: Concentrations of ATMP, ortho–phosphate and the phosphorus mass balance (MB = ATMP + PO_4^{3-}) over time during transformation of ATMP (1 mM initial concentration) in the presence of molecular oxygen for initial Mn:ATMP ratios of (**a**) 1:100, (**b**) 1:10, (**c**) 1:2 and (**d**) 1:1 (corresponding to Mn(II) concentrations of 0.01 mM to 1 mM) at pH 6.8 ± 0.1. Shown are the average concentrations of duplicate batch experiments. Error bars for ATMP and PO_4^{3-} represent one standard deviation and the standard deviation of the mass balance was calculated using Gaussian error propagation.

Effect of the dissolved oxygen concentration on transformation kinetics and carbon isotope fractionation

Experimental setup and sampling were analogue to the experiments described in chapter 3. The experiments were conducted at pH 6.8 $\pm$ 0.1 (buffered with 20 mM MES) with an initial Mn:ATMP ratio of 1:1 (1 mM), as for this experiment the highest initial transformation rate was observed and thus the highest O_2 consumption was expected. In total three different setups were tested. Setup 1 (open) represented the setup described in chapter 3, i.e., open bottles and fast stirring (750 rpm). Setup 2 (saturated) was continuously purged with synthetic air (20.5 % O_2/ 79.5 % N_2, Westfalen, Münster, Germany) to ensure oxygen saturated conditions over the complete course of the experiment. Setup 3 (closed) represented oxygen limited conditions. To this end, the bottle was closed with a butyl rubber stopper before the addition of the $MnCl_2$ solution, resulting in an initial liquid:gas ratio of approximately 1.8 (75 mL:41 mL) and consequently an initial O_2:ATMP ratio of 5 (375 µmol:75 µmol). Sampling for setup 3 was conducted with 5 mL plastic syringes and the withdrawn sample volume was replaced by N_2 in order to ensure constant pressure conditions and oxygen limitation in the bottle.
Quantification of dissolved oxygen was quantified in the setups 1 and 2 *in–situ* with an OXY–4 ST (G3) oxygen meter, equipped with an oxygen dipping probe (PreSens, Regensburg, Germany). In setup 3, the quantification was conducted non–invasively from the outside of the bottles (which were equipped with oxygen sensor foils), using a fiber optic oxygen meter (Fibox3, PreSens, Regensburg, Germany).

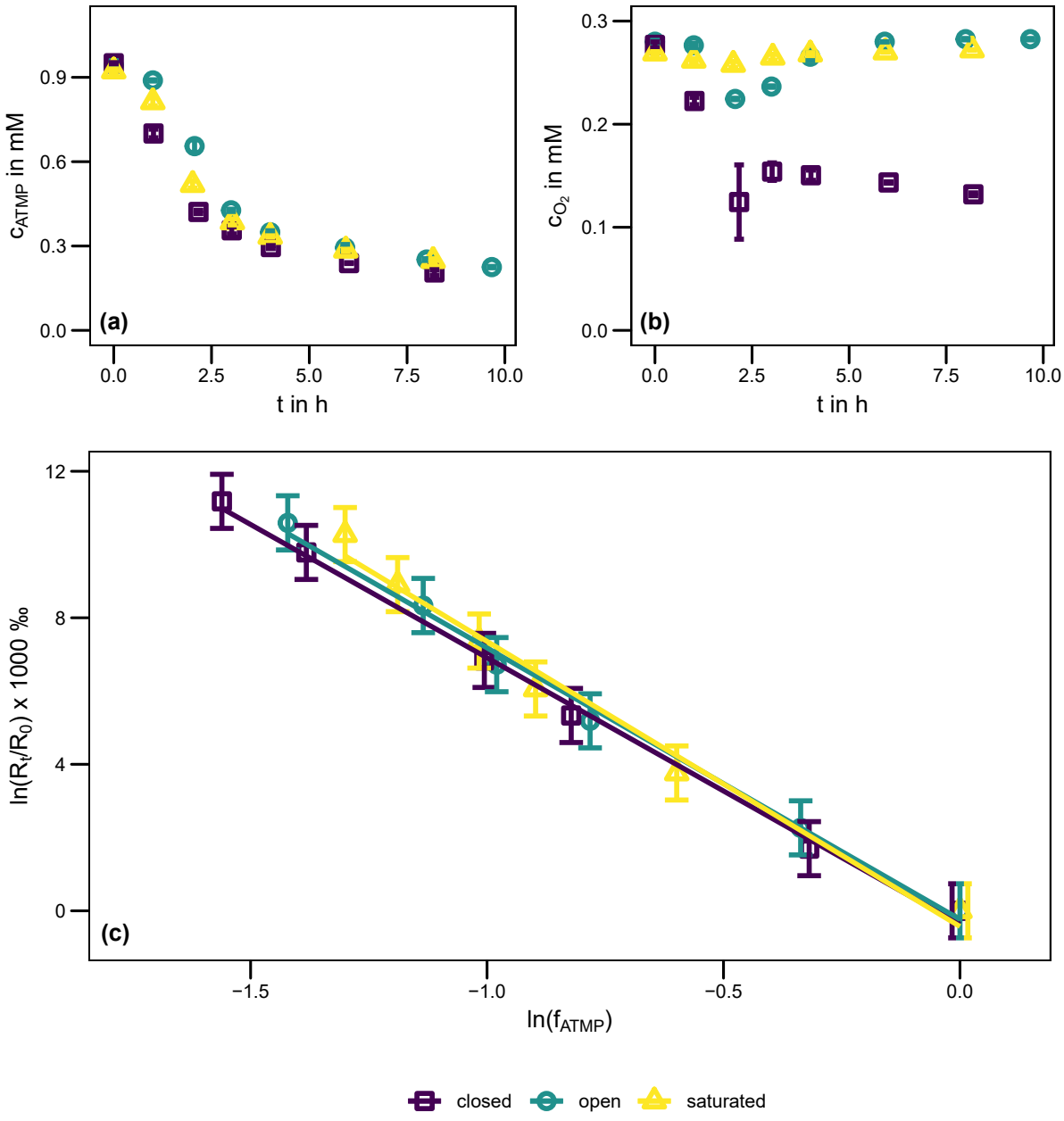

Figure B.2: Data of the experiments conducted at different dissolved oxygen levels and pH 6.8 ± 0.1 with an initial Mn:ATMP ratio of 1:1 (1 mM). Temporal profiles of (**a**) ATMP and (**b**) dissolved oxygen. Shown are the average concentrations of duplicate batch experiments. Error bars represent one standard deviation. (**c**) Double–logarithmic Rayleigh plot showing carbon isotope fractionation of ATMP. Error bars were calculated by means of Gaussian error propagation assuming an error of the δ^{13}C value of 0.5 ‰.

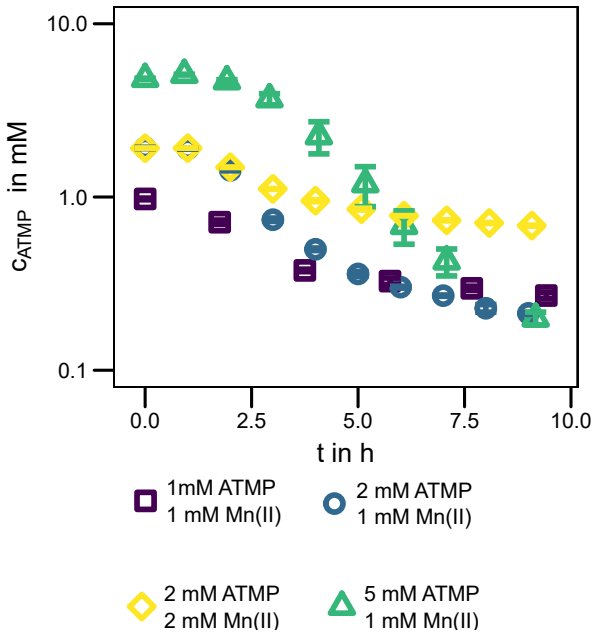

Figure B.3: Temporal transformation profiles of ATMP in the presence of molecular oxygen and varying amounts of Mn(II). Shown are the average concentrations of duplicate batch experiments. Error bars represent one standard deviation. For better visualization, the concentrations are plotted on a logarithmic scale.

Determination of stepwise Mn(II)ATMP–normalized transformation rate constants

In order to determine the influence of the Mn(II)ATMP concentration on the ATMP transformation rates, stepwise initial (0^{th} order) transformation rate constants were used. To this end, a linear regression for segments n in the $c(t)/c(0)$ vs. time plots was calculated from three consecutive data points (n to $n+2$) ($R^2 \geqslant 0.8$). Subsequently, the next slope was calculated for the data points $n+1$ to $n+3$. The graphical result is exemplarily shown for the experiment with an initial Mn:ATMP ratio of 1:2 in **Figure B.4**.
The resulting rates $k(n)$ where than normalized to the calculated concentration of Mn(II)ATMP complexes at the beginning of interval n, resulting in the normalized rate constant $k_{norm}(n)$.

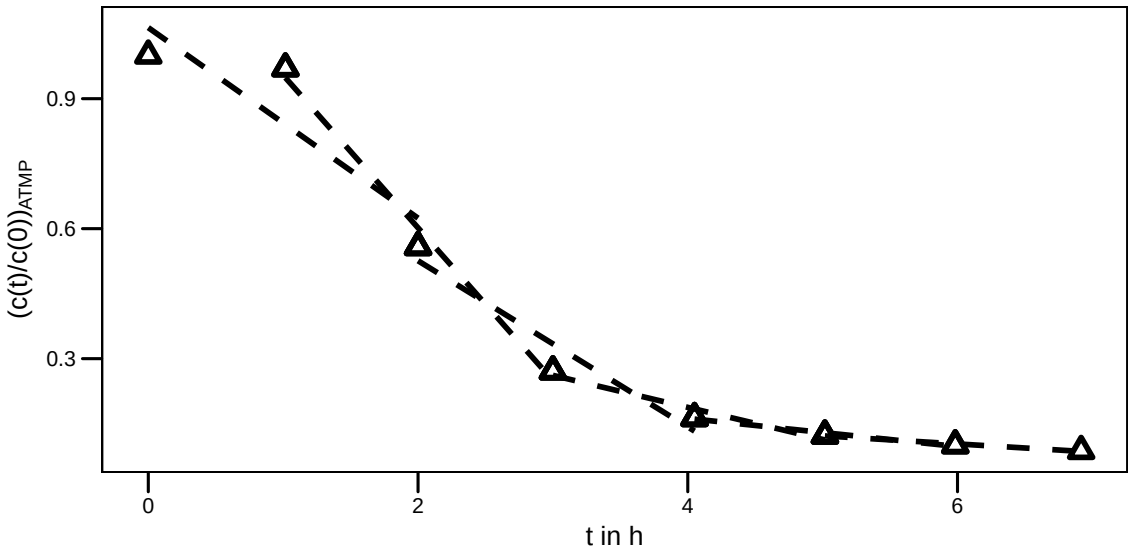

Figure B.4: Transformation of ATMP for an initial Mn(II):ATMP ratio of 1:2 (corresponding to Mn(II) concentration of 0.5 mM) at pH 6.8 ± 0.1. Shown are the average relative concentrations of duplicate batch experiments. Additionally shown are the stepwise linear regressions used for the calculation of initial (0^{th} order) rate constants.

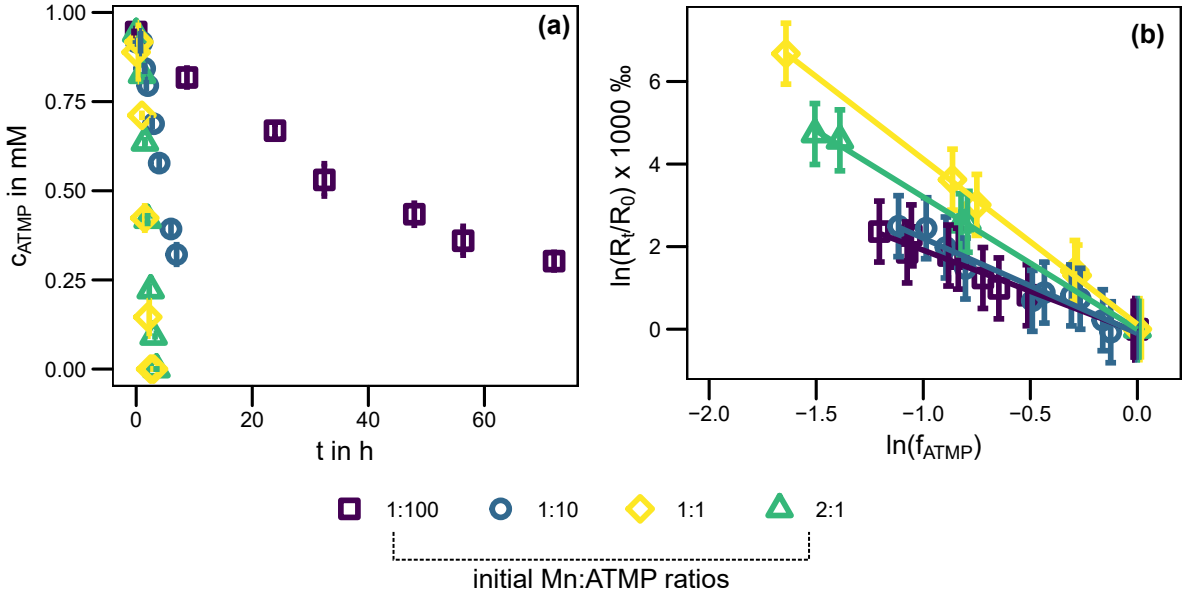

Figure B.5: Kinetics and isotope fractionation of ATMP in unbuffered experiments conducted at pH 3.6 ± 0.1. (**a**) Temporal transformation profiles of ATMP in the presence of molecular oxygen for different initial Mn:ATMP ratios (corresponding to Mn(II) concentrations of 0.01 mM to 2 mM). Shown are the average concentrations of duplicate batch experiments. Error bars represent one standard deviation. (**b**) Double–logarithmic Rayleigh plot showing carbon isotope fractionation of ATMP (1 mM initial concentration) during transformation in the presence of molecular oxygen for different initial Mn:ATMP ratios (corresponding to Mn(II) concentrations of 0.01 mM to 2 mM), including the linear regressions according to the Rayleigh model. Error bars were calculated by means of Gaussian error propagation assuming an error of the $\delta^{13}C$ value of 0.5 ‰.

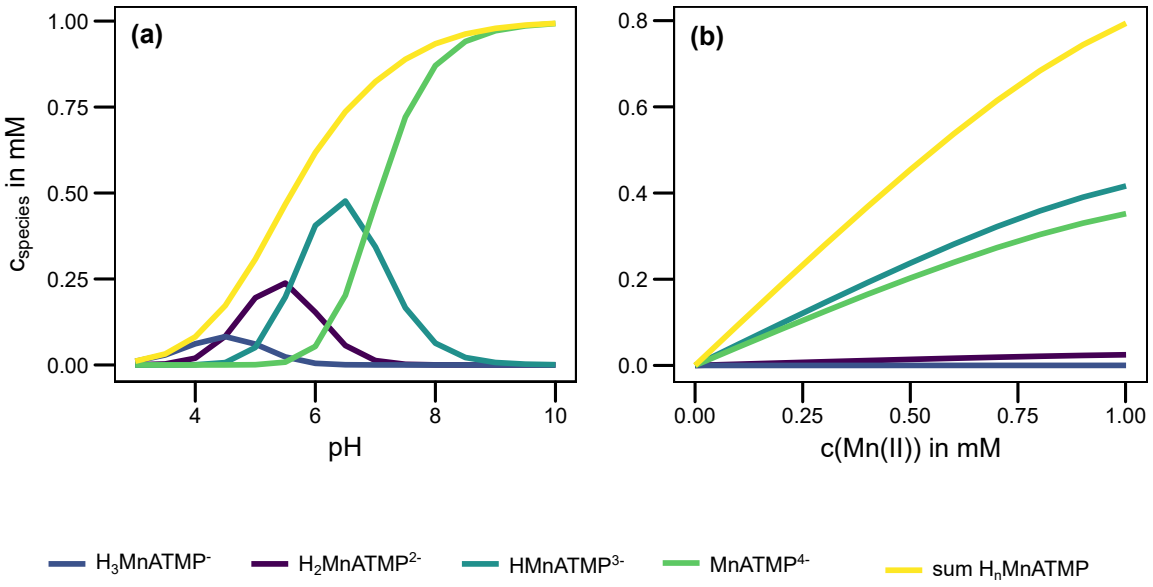

Figure B.6: Calculated concentrations of bimolecular Mn(II)ATMP complexes (ATMP concentration of 1 mM) (**a**) as function of pH in the presence of 1 mM $MnCl_2$ and (**b**) as function of Mn(II) concentration at pH 6.8. The temperature was set to 20 °C and 20 mM $NaNO_3$ was used as background electrolyte. Acidity constants for ATMP and equilibrium constants for Mn(II)ATMP complexes were taken from Lacour, et al.[1] and Popov, et al.,[2] respectively.

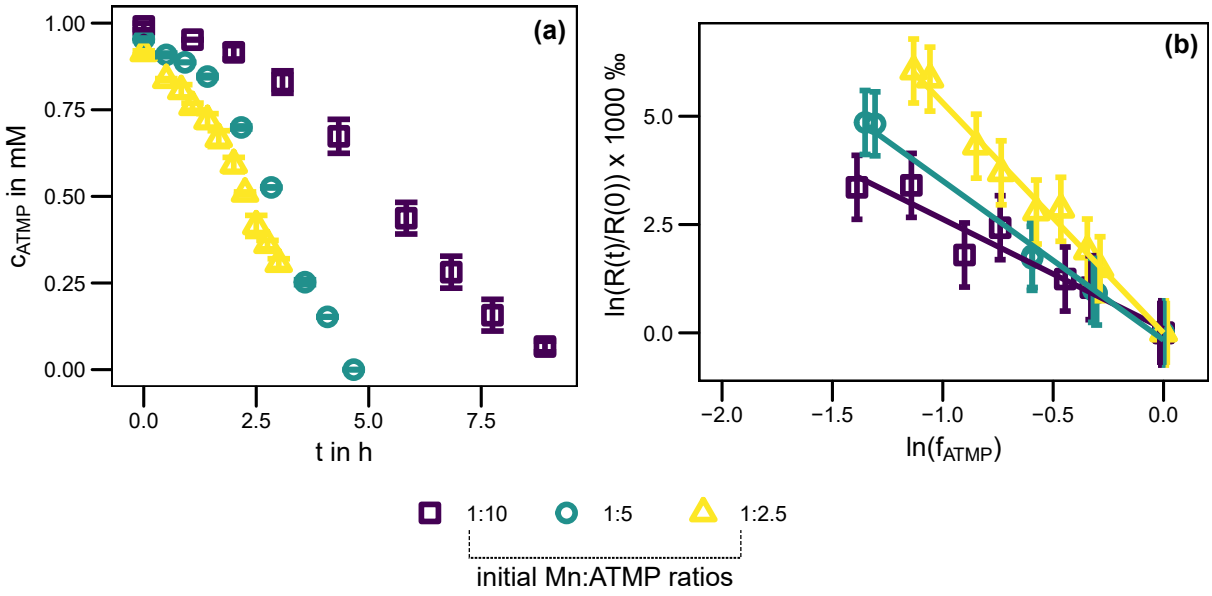

Figure B.7: Kinetics and isotope fractionation of ATMP in unbuffered experiments conducted at pH 7.2 ± 0.1. (**a**) Temporal transformation profiles of ATMP in the presence of molecular oxygen for different initial Mn:ATMP ratios (corresponding to Mn(II) concentrations of 0.1 mM to 0.4 mM). Shown are the average concentration of duplicate batch experiments. Error bars represent one standard deviation. (**b**) Double–logarithmic Rayleigh plot showing carbon isotope fractionation of ATMP (1 mM initial concentration) during transformation in the presence of molecular oxygen for different initial Mn:ATMP ratios (corresponding to Mn(II) concentrations of 0.1 mM to 0.4 mM), including the linear regressions according to the Rayleigh model. Error bars were calculated by means of Gaussian error propagation assuming an error of the $\delta^{13}C$ value of 0.5 ‰.

Calculation of stepwise enrichment factors

The double logarithmic Rayleigh plots for experiments conducted at pH 6.8 with Mn(II):ATMP(0) of 1:5, 1:2 and 1:1 were evaluated in detail, as for these initial Mn(II):ATMP ratios the range of complexed ATMP fractions varied considerably during the course of the experiments ($\Delta f_{\mathrm{compl}} \geqslant 0.13$ for the single experiments, see **Table B.1**). The detailed analysis of the double–logarithmic Rayleigh plots of these experiments showed curved rather than linear shapes even though the linear fits had R^2 values of $\geqslant 0.97$ (see **Figure B.8(a)**). This non–linear behavior is in line with distinctly negative y–intercepts of the linear regressions ($\leqslant -0.7$ ‰) for all four experiments and indicative for changes in the underlying isotope fractionation. In order to highlight this non–linear behavior, isotope enrichment factors were calculated stepwise following a procedure proposed by Mundle, et al. (2013).[3] To this end, three consecutive data points were fitted to the Rayleigh model, yielding the stepwise calculated enrichment factor $\varepsilon_{\mathrm{C}}(n)$ for the respective segment n (see **Table B.2**). In **Figure B.8(b)** the resulting $\varepsilon_{\mathrm{C}}(n)$–values against the Mn(II)–complexed ATMP fraction at the beginning of the segment n are shown. In all four experiments, the $\varepsilon_{\mathrm{C}}(n)$–value decreased with increasing complexed ATMP fraction. When plotting $\varepsilon_{\mathrm{C}}(n)$–values as function of the complexed ATMP fraction for the experiments with Mn(II):ATMP(0) = 1:5 and 1:2 almost identical slopes were obtained (-7 ± 2 ‰ to -10 ± 3 ‰, see **Table B.2**). In addition, the trends were in good agreement with the overall trend for all experiments with varying initial complexed ATMP fractions (-9 ± 2 ‰). The offset to more negative values for Mn(II):ATMP(0) = 1:5 can be attributed to the lower number of data points for this experiment, leading to an overestimation of the isotope fractionation, especially at early time points (see **Figure B.9** for comparison of point densities & calculations). The results of the experiment with Mn(II):ATMP(0) = 1:1 showed a steeper slope (-25 ± 15 ‰) and a weaker coefficient of determination, which can be rationalized by the less pronounced changes in the complexed fraction of ATMP of 0.13 during this experiment in comparison to the other experiments ($\Delta f_{\mathrm{compl}} \geqslant 0.40$).

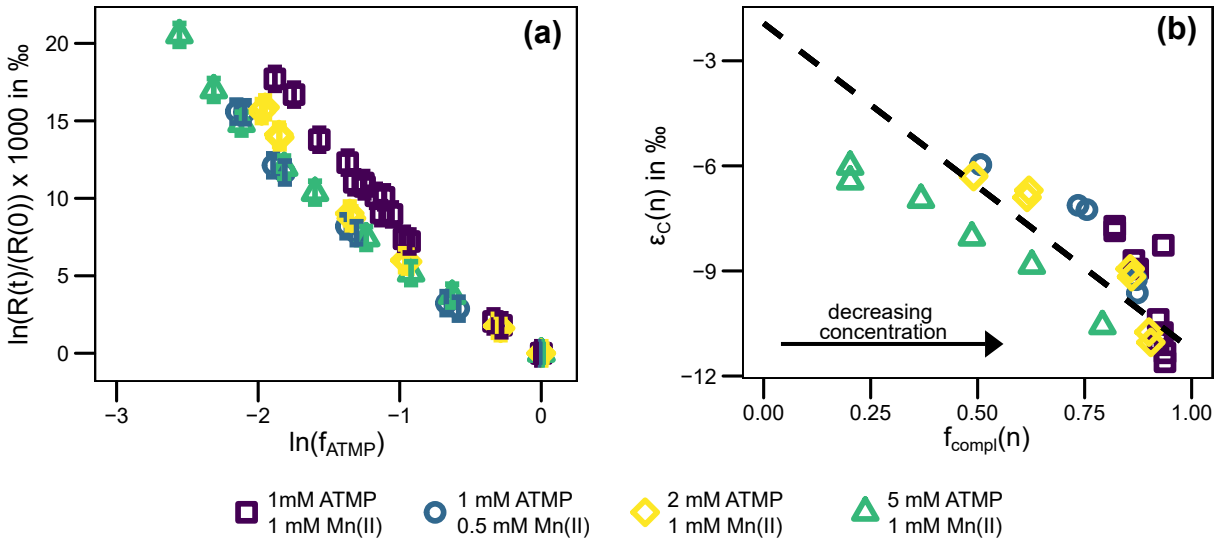

Figure B.8: (**a**) Linearized Rayleigh plot for experiments at pH 6.8 ± 0.1 with initial Mn(II):ATMP ratios of 1:5, 1:2 and 1:1. Error bars were calculated by means of Gaussian error propagation assuming an error of the δ^{13}C–value of 0.5 ‰. (**b**) Stepwise calculated enrichment factors (obtained from linear regressions of three consecutive data points) vs. the complexed fraction of ATMP at the start of the segment (i.e., the first point of the regression) for experiments at pH 6.8 ± 0.1 with Mn(II):ATMP(0) of 1:5, 1:2 and 1:1. The black dashed line represents the linear regression taken from Figure 3.3.

Table B.1: Dependency of the carbon isotope enrichment factor on the complexed ATMP fraction for the reassessed experiments (initial Mn:ATMP ratios of 1:5, 1:2 and 1:1), as well as the overall trend for all experiments. Shown is the spanned range of complexed ATMP fractions ($\Delta f_{\mathrm{compl}}$), the slope of the linear regression ($d\varepsilon_C/df_{\mathrm{compl}}$) including its 95 % confidence interval, the coefficient of determination and the number of experimental data points n.

Starting ATMP and Mn(II) concentration	$\Delta f_{\mathrm{compl}}$	$d\varepsilon_C/df_{\mathrm{compl}}$ (95 % CI) in ‰	R^2	n
1 mM ATMP 1 mM Mn(II)	0.13	-25 ± 15	0.65	10
1 mM ATMP 0.5 mM Mn(II)	0.4	-9 ± 5	0.88	6
2 mM ATMP 1 mM Mn(II)	0.44	-10 ± 3	0.90	8
5 mM ATMP 1 mM Mn(II)	0.73	-7 ± 2	0.97	6
Overall trend (Figure 3.3)	0.82	-9 ± 2	0.92	11

Table B.2: Compilation of stepwise calculated enrichment factors. Shown is the evaluated segment of the Rayleigh plot (n, with a and b representing duplicate experiments), the corresponding range of the data points on the $\ln(f)$–axis, the calculated complexed fraction of ATMP at the beginning of the segment (i.e. for the highest $\ln(f)$–value) and the calculated enrichment factor.

Starting ATMP and Mn(II) concentration	n	range $\ln(f)$	$f_{\mathrm{compl},0}(n)$	$\varepsilon_{\mathrm{C}}(n)$ in ‰
1 mM ATMP	1a	– 0.97 – 0.00	0.82	– 7.7
1 mM Mn(II)	1b	– 0.93 – 0.00	0.82	– 7.9
	2a	– 1.13 – – 0.34	0.87	– 8.7
	2b	– 1.05 – – 0.28	0.87	– 9.0
	3a	– 1.32 – – 0.97	0.92	– 10.4
	3b	– 1.25 – – 0.93	0.92	– 11.1
	4a*	– 1.57 – – 1.11	0.93	– 8.3
	4b*	– 1.75 – – 1.17	0.94	– 11.3
	5a*	– 1.88 – – 1.26	0.93	– 10.8
	5b*	– 2.13 – – 1.37	0.94	– 11.6
1 mM ATMP	1a	– 1.30 – 0.00	0.51	– 6.0
0.5 mM Mn(II)	1b	– 1.38 – 0.00	0.51	– 6.0
	2a	– 1.81 – – 0.58	0.73	– 7.1
	2b	– 1.89 – – 0.67	0.76	– 7.3
	3a	– 2.09 – – 1.30	0.87	– 9.6
	3b	– 2.15 – – 1.38	0.87	– 9.3
2 mM ATMP	1a	– 0.94 – 0.00	0.49	– 6.3
1 mM Mn(II)	1b	– 0.96 – 0.00	0.49	– 6.3
	2a	– 1.34 – – 0.31	0.62	– 6.7
	2b	– 1.35 – – 0.29	0.62	– 6.9
	3a	– 1.85 – – 0.94	0.86	– 9.0
	3b	– 1.85 – – 0.96	0.86	– 9.0
	4a	– 1.98 – – 1.34	0.90	– 10.9
	4b	– 1.95 – – 1.35	0.90	– 11.0
5 mM ATMP	1a	– 1.24 – 0.00	0.20	– 6.0
1 mM Mn(II)	1b	–1.60 – 0.00	0.20	– 6.4
	2a	– 1.82 – – 0.63	0.37	– 7.0
	2b	– 2.12 – – 0.92	0.49	– 8.0
	3a	– 1.82 – – 0.63	0.63	– 8.8
	3b	– 2.56 – – 1.60	0.79	– 10.6

*Calculated for a second, identically treated experiment with longer runtime.

Modeling the effect of a reduced experimental point density on the observed stepwise calculated isotope enrichment factor

Calculations were conducted for a simulated experiment with an ATMP starting concentration of 4.8 mM (i.e., equal to the conducted experiment), a $MnCl_2$ concentration of 1 mM, pH 6.8 and 20 °C.
Speciation of ATMP in the presence of Mn(II) was calculated in the PhreeqC software package,[4] using the wateq4f database, supplemented with the acidity constants for ATMP and the equilibrium constants for mononuclear Mn(II)ATMP complexes.[1,2] The fraction of Mn(II)–complexed ATMP was calculated for remaining ATMP fractions ($f = c(t)/c(0)$) of 0.05 to 1 with $\Delta f = 10^{-3}$. Complexed fractions between these discrete values were interpolated by means of a 4th order regression ($R^2 = 0.9996$).
The expected carbon isotope enrichment factor (ε_C) as a function of the Mn(II)–complexed ATMP fraction(f_{compl}), was calculated by means of the linear regressions obtained by fitting the (ε_C–values of all experiments ($\varepsilon_C = -9.32\,‰ \times f_{compl} - 1.93\,‰$, see **Figure 3.3**).
The nominated isotopic ratio over the remaining ATMP fraction was then calculated stepwise by means of the obtained speciation dependent enrichment factors for a fraction step size (Δf) of 0.001 according to the Rayleigh equation:

$$\ln\left(\frac{R(t)}{R(0)}\right)_n = \left(\ln(f)_n - \ln(f)_{n-1}\right) \times \varepsilon_{C,n-1} + \ln\left(\frac{R(t)}{R(0)}\right)_{n-1} \tag{B.1}$$

From the obtained dataset, data points were subsampled in a way that the modeled ln(f) values matched the experimental ones (absolute averaged error $\pm$ one standard deviation = 0.001 ± 0.002). The stepwise isotope enrichment factors were finally calculated according to the three–point linear regression method described in chapter 3. The averaged absolute error $\pm$ one standard deviation between the calculated and experimental stepwise enrichment factors was equal to 0.6 ± 0.2 ‰.
The results of the model visualized as double–logarithmic Rayleigh plot and stepwise calculated enrichment factors can be found in **Figure B.9**.

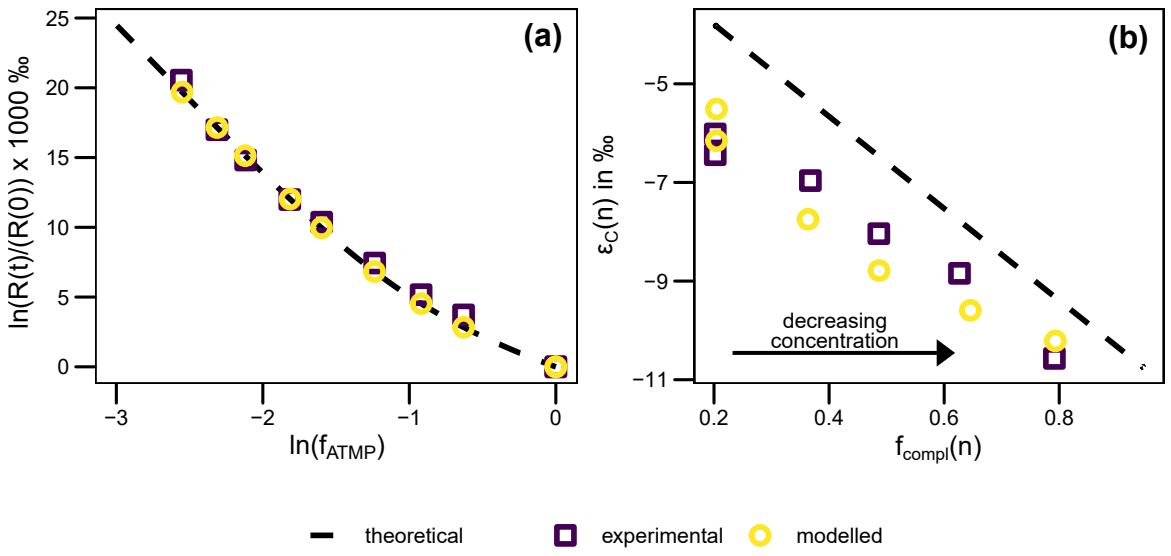

Figure B.9: (**a**) Double–logarithmic Rayleigh plot and (**b**) stepwise calculated carbon isotope enrichment factors ($\varepsilon_C(n)$) as function of the fraction of ATMP complexed with Mn(II) ($f_{\mathrm{compl}}(n)$). Shown as black dashed lines are the modeled theoretical values, based on the assumed dependency of the isotope enrichment factor on the complexed ATMP fraction. Furthermore, the experimental data and the values calculated from the model taking into account the experimental point density are shown.

Estimation of the maximum observable carbon isotope fractionation factor for C–P bond cleavage

The Streitwieser limit for C–P bond cleavage, i.e., the theoretically maximum intrinsic kinetic isotope effect based on vibrational energy differences was calculated according to the following equation:[5,6]

$$KIE = \frac{1}{\exp\left(-100 \times \frac{hc\tilde{v}}{2kT}\left(1 - \sqrt{\frac{\mu_L}{\mu_H}}\right)\right)} \tag{B.2}$$

with the Planck constant $h = 6.626 \times 10^{-34}\,\mathrm{J\,s}$, the speed of light $c = 2.998 \times 10^{8}\,\mathrm{m\,s^{-1}}$, the Boltzmann's constant $k_B = 1.381 \times 10^{-23}\,\mathrm{J\,K^{-1}}$ and the absolute temperature T (298 K). μ_L and μ_H are the reduced masses of ^{12}C and ^{13}C in the C–P bond, respectively. For the vibrational wave number $\tilde{v}$ of the C–P bond a value of $750\,\mathrm{cm^{-1}}$ was used, which lays well in the range, reported for various amino and non–amino phosphonates.[7–9]

With these assumptions, a Streitwieser limit of 1.052 was computed. This value was converted to a maximum observable carbon isotope enrichment factor according to the equation below:[10]

$$\varepsilon_C = \left(\frac{1}{KIE} - 1\right) \times \frac{x}{n}\frac{1}{z} \tag{B.3}$$

With the number of carbon atoms $n = 3$, the number of carbon atoms in the reactive position x and the carbon atoms in intramolecular competition z. Due to the symmetric character of ATMP, $x = z = 3$ was assumed, yielding an enrichment factor of -16.6 ‰.

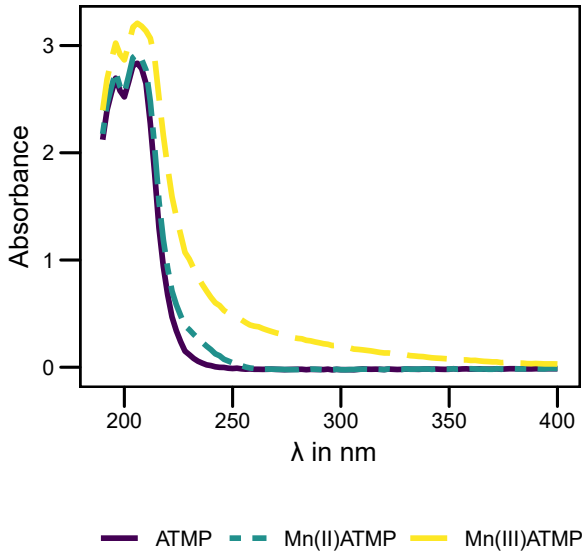

Figure B.10: Absorbance of 1 mM ATMP + 20 mM MES in the absence and presence of 1 mM $MnCl_2$. Mn(III)ATMP represents the absorbance of 1 mM Mn(II)ATMP after the addition of 0.2 mM $KMnO_4$, leading to the oxidation of complexed Mn(II) to Mn(III) as reported earlier for Mn(II)EDTA.[11]

Reference

(1) Lacour, S.; Deluchat, V.; Bollinger, J.-C.; Bernard, S. Complexation of trivalent cations (Al(III), Cr(III), Fe(III)) with two phosphonic acids in the pH range of fresh waters. *Talanta* **1998**, *46*, 999–1009.

(2) Popov, K.; Rönkkömäki, H.; Lajunen, L. H. J. Critical evaluation of stability constants of phosphonic acids (IUPAC Technical Report). *Pure and Applied Chemistry* **2001**, *73*, 1641–1677.

(3) Mundle, S. O.; Vandersteen, A. A.; Lacrampe-Couloume, G.; Kluger, R.; Sherwood Lollar, B. Pressure-monitored headspace analysis combined with compound-specific isotope analysis to measure isotope fractionation in gas-producing reactions. *Rapid Communications in Mass Spectrometry* **2013**, *27*, 1778–1784.

(4) Parkhurst, D.; Appelo, C., *Description of input and examples for PHREEQC version 3–A computer program for speciation, batch-reaction, one-dimensional transport, and inverse geochemical calculations*; Techniques and Methods, Vol. book 6; U.S. Geological Survey: 2013; Chapter A43.

(5) Elsner, M.; Zwank, L.; Hunkeler, D.; Schwarzenbach, R. P. A new concept linking observable stable isotope fractionation to transformation pathways of organic pollutants. *Environmental Science & Technology* **2005**, *39*, 6896–6916.

(6) Jochmann, M. A.; Schmidt, T. C., *Compound-specific stable isotope analysis*; Royal Society of Chemistry: 2015.

(7) Barja, B. C.; Herszage, J.; dos Santos Afonso, M. Iron(III)–phosphonate complexes. *Polyhedron* **2001**, *20*, 1821–1830.

(8) Hameka, H. F.; Carrieri, A. H.; Jensen, J. O. Calculations of the Structure and the Vibrational Infrared Frequencies of Some Methylphosphonates. *Phosphorus, Sulfur, and Silicon and the Related Elements* **2006**, *66*, 1–11.

(9) Juribasic, M.; Tusek-Bozis, L. Spectroscopic and DFT study of 3-quinolyl-α-aminophosphonates. *Journal of Molecular Structure* **2009**, *924-926*, 66–72.

(10) Elsner, M. Stable isotope fractionation to investigate natural transformation mechanisms of organic contaminants: principles, prospects and limitations. *Journal of Environmental Monitoring* **2010**, *12*, 2005–2031.

(11) Schroeder, K. A.; Hamm, R. E. Decomposition of the Ethylenediaminetetraacetate Complex of Manganese(III). *Inorganic Chemistry* **1964**, *3*, 391–395.

C Supporting information to chapter 4

Materials and methods

Preparation of self–synthesized MnO_2

The protocol for the synthesis of $MnO_{2/synth}$ via the reduction of $KMnO_4$ by H_2O_2 under acidic conditions was adapted from Villegas et al..[1] First, 7.2 mL concentrated nitric acid (EMSURE, Merck, Darmstadt, Germany) was added to 72 mL 1 % (v/v, equivalent to 426 mM) hydrogen peroxide (30 %, for analysis, Merck). Afterwards, 75 mL of a 274 mM $KMnO_4$ (EMSURE, Merck) solution was added to the acidic hydrogen peroxide solution with approximately 1.5 mL min^{-1} under constant rapid stirring. After a reaction time of 60 min, stirring was stopped and the particles were allowed to settle for another 60 min. The result was a dark–brown mineral phase and a clear supernatant, indicating complete reduction of the permanganate. The supernatant was discarded and the particles were re–suspended in 160 mL ultrapure water. Afterwards, the suspension was distributed equally into 50 mL glass vials, centrifuged at 1000 rcf for 15 min. The particles were washed with ultrapure water and centrifuged several times until the supernatant was circumneutral and had a conductivity of $\leqslant 1.5\,\mu S\,cm^{-1}$. The washed particles were collected on a 0.45 µm filter (polyamide, Whatman, Dassel, Germany) in a vacuum filtration manifold and dried at 80 °C for 24 h. Finally, the dried mineral was crushed in a mortar and stored in a desiccator over silica gel up to its final use.

Characterization of MnO_2

The point of zero charge was determined on a Zetasizer Nano ZSP (Malvern Pananalytical, Malvern, United Kingdom) in folded capillary zeta cells at 20 °C. Measurements were conducted in triplicates with 10 to 15 runs, each. For analysis, 50 mg L^{-1} MnO_2 suspensions were prepared in 10 mM NaCl + 10 mM MES buffer and the pH was adjusted by 0.1 M or 1 M NaOH and HCl. The point of zero charge was determined by plotting the zeta potential as function of the adjusted pH and subsequent regression of the linear part of the data sets.

BET specific surface area was analyzed on a Gemini VII 2390 (Micrometrics, Norcross, GA, United States) by nitrogen sorption–desorption isotherms. Samples were degassed before analysis over night under vacuum at 120 °C.

Powder X-ray diffraction (*XRD*) was performed using a D8 Discover (Bruker, Billerica, MA, United States) equipped with a Cu–source (Cu–Kα radiation, $\lambda = 1.541\,84$ Å) with a beam voltage and current of 40 kV and 20 mA, respectively.

Mn(III)–content was determined by pyrophosphate (PP)–extraction and subsequent spectroscopic quantification.[2] For extraction of available Mn(III), 1 mM (0.087 g L^{-1}) or 17 mM (1.5 g L^{-1}) MnO_2 was suspended in 20 mM PP (pH 7) and shaken on an overhead shaker for 24 h. Afterwards, the suspension was centrifuged at 14 000 rcf for 15 min and the supernatant was analyzed at 258 nm (UV5Bio, Mettler Toledo, Greifensee, Switzerland). The concentration of Mn(III)PP was calculated based on the molar absorption coefficient at 258 nm of 6750 $M^{-1}cm^{-1}$.[3]

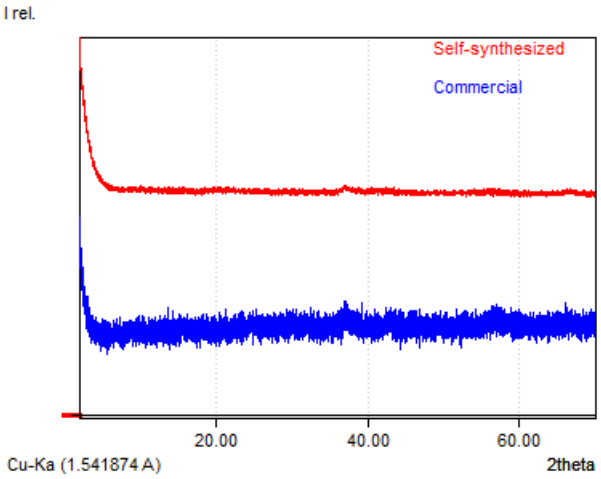

Figure C.1: XRD patterns of the commercial and self–synthesized manganese oxide.

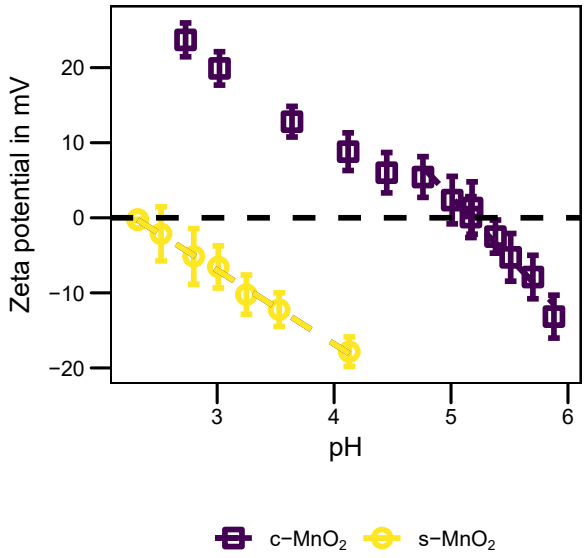

Figure C.2: Zeta potential (ZP) as function of the pH for the commercial and self–synthesized MnO_2 (50 mg L^{-1} in 10 mM NaCl + 10 mM MES). Additionally shown are the linear regressions used for the calculation of the point of zero charge. Error bars were calculated by Gaussian error propagation from the ZP deviations of instrumental triplicate measurements.

Results and discussion

Table C.1: Pseudo first and second order rate constant according to Model PF (k_{PF}, including 95 % confidence interval) and Model ET (k_{ET}), respectively. All experiments were conducted with an initial IDMP concentration of 1 mM at 22 ± 2 °C.

pH	3	6			8		
Buffer	formate	MES			Tris		HEPES
Manganese dioxide ($g\,L^{-1}$)	1.7 com.	1.7 synth.	1.7 com.	3.4 com.	1.7 synth.	1.7 com.	1.7 com.
k_{PF} ± 95 % (CI) ($mM^{-1}h^{-1}$)	$(0.16 \pm 283) \times 10^{-3}$	0.31 ±0.06	$(3 \pm 588) \times 10^{-5}$	0.6 ±0.2	$(10 \pm 2) \times 10^{-3}$	$(1.2 \pm 0.6) \times 10^{-3}$	0.21 ±0.04
k_{ET} ± 95 % (CI) (h^{-1})	0.31 ±0.06	0.32 ±0.03	$(3 \pm 2) \times 10^{-3}$	0.4 ±0.1	$(7 \pm 1) \times 10^{-3}$	$(2.1 \pm 0.4) \times 10^{-3}$	0.16 ±0.03

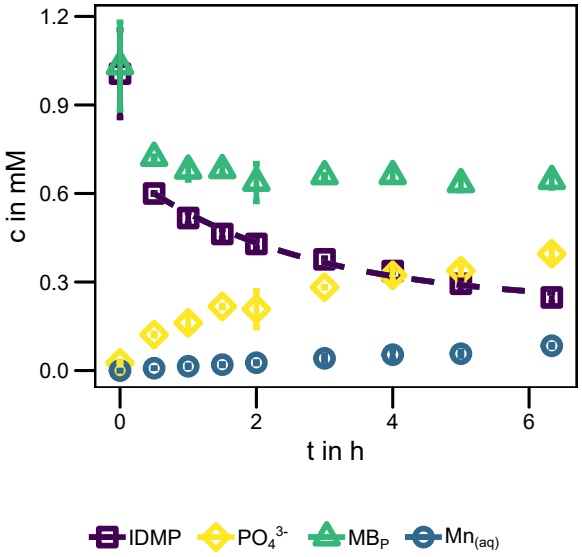

Figure C.3: Temporal profile of IDMP (including the fit according to Model ET), ortho–phosphate, the phosphorus mass balance (MB_P = [IDMP] + [PO_4^{3-}] and dissolved manganese in the presence of 3.4 g L^{-1} commercial MnO_2 at pH 6.0 ± 0.1 (20 mM MES). Shown are the average concentrations of duplicate batch experiments. Error bars represent one standard deviation for the measured concentrations and the error for the MB_P was calculated via Gaussian error propagation, respectively.

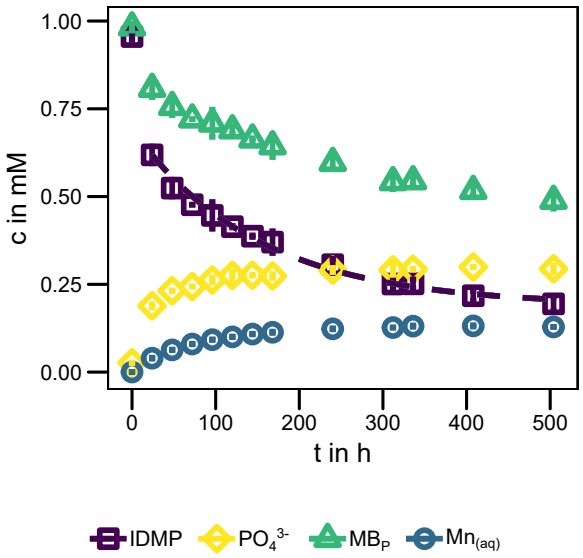

Figure C.4: Temporal profile of IDMP (including the fit according to Model ET), ortho–phosphate, the phosphorus mass balance ($MB_P = [IDMP] + [PO_4^{3-}]$) and dissolved manganese in the presence of $1.7\,g\,L^{-1}$ self–synthesized MnO_2 at pH 8.0 ± 0.1 (20 mM Tris). Shown are the average concentrations of duplicate batch experiments. Error bars represent one standard deviation for the measured concentrations and the error for the MB_P was calculated via Gaussian error propagation, respectively.

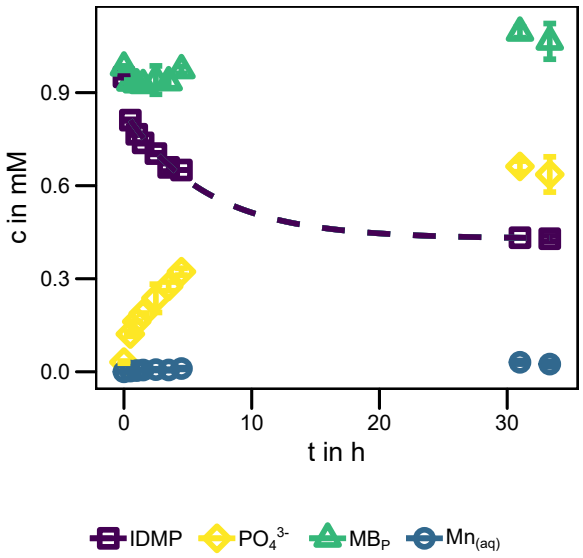

Figure C.5: Temporal profile of IDMP (including the fit according to Model ET), ortho–phosphate, the phosphorus mass balance ($MB_P = [IDMP] + [PO_4^{3-}]$) and dissolved manganese in the presence of $1.7\,g\,L^{-1}$ commercial MnO_2 at pH 8.0 ± 0.1 (20 mM HEPES). Shown are the average concentrations of duplicate batch experiments. Error bars represent one standard deviation for the measured concentrations and the error for the MB_P was calculated via Gaussian error propagation, respectively.

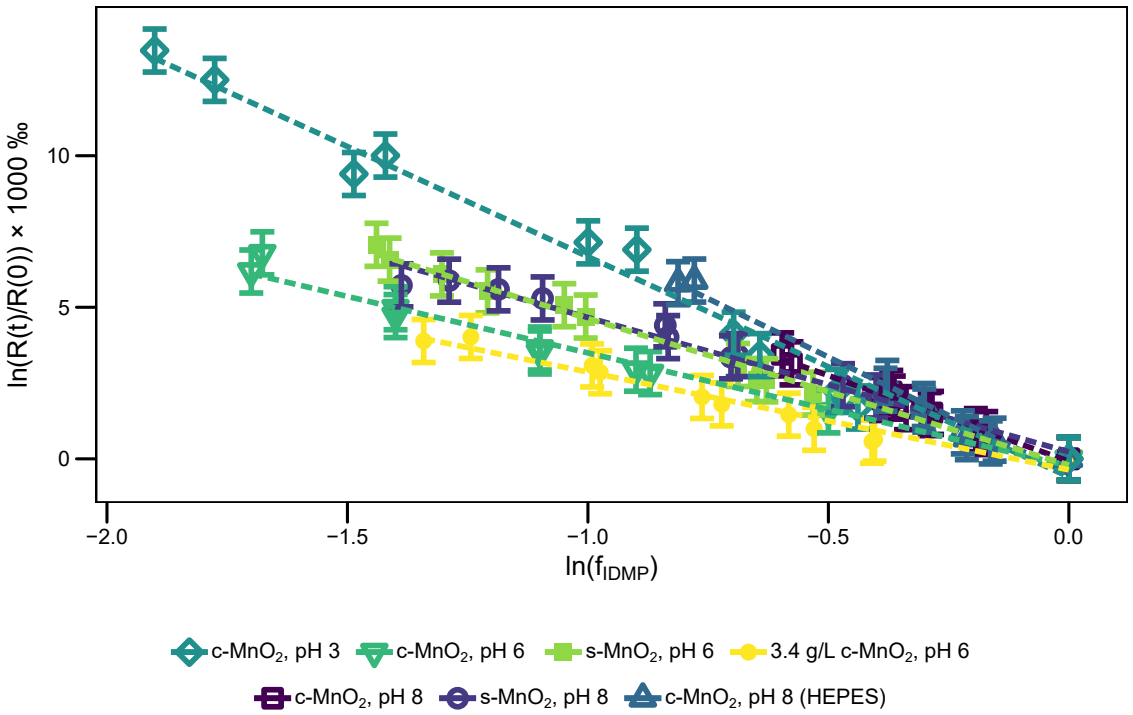

Figure C.6: Double–logarithmic Rayleigh plot showing carbon isotope fractionation of IDMP for varying experimental conditions: Applied mineral, mineral loading ($1.7\,\mathrm{g\,L^{-1}}$ if not stated otherwise), pH and buffer (formate (pH 3), MES (pH 6) and Tris (pH 8) if not stated otherwise. Additionally shown are the linear regressions according to the Rayleigh model normalized to T_0. Error bars were calculated by means of Gaussian error propagation assuming an error of the $\delta^{13}C$ value of 0.5 ‰.

Estimation of the maximum observable carbon isotope fractionation factor for C–P bond cleavage

The Streitwieser limit for C–P bond cleavage, i.e., the theoretically maximum intrinsic kinetic isotope effect based on vibrational energy differences was calculated according to the following equation:[4,5]

$$KIE = \frac{1}{\exp\left(-100 \times \frac{hc\tilde{v}}{2kT}\left(1 - \sqrt{\frac{\mu_L}{\mu_H}}\right)\right)} \tag{C.1}$$

with the Planck constant $h = 6.626 \times 10^{-34}\,\mathrm{J\,s}$, the speed of light $c = 2.998 \times 10^{8}\,\mathrm{m\,s^{-1}}$, the Boltzmann's constant $k_B = 1.381 \times 10^{-23}\,\mathrm{J\,K^{-1}}$ and the absolute temperature T (298 K). μ_L and μ_H are the reduced masses of ^{12}C and ^{13}C in the C–P bond, respectively. For the vibrational wave number $\tilde{v}$ of the C–P bond a value of $750\,\mathrm{cm^{-1}}$ was used, which lays well in the range, reported for various (amino–)phosphonates.[6–8]

With these assumptions, a Streitwieser limit of 1.052 was computed. This value was converted to a maximum observable carbon isotope enrichment factor according to the equation below:[9]

$$\varepsilon_C = \left(\frac{1}{KIE} - 1\right) \times \frac{x}{n}\frac{1}{z} \tag{C.2}$$

With the number of carbon atoms $n = 2$, the number of carbon atoms in the reactive position x and the carbon atoms in intramolecular competition z. Due to the symmetric character of IDMP, $x = z = 2$ was assumed, yielding an enrichment factor of -24.8 ‰.

Reference

(1) Villegas, J. C.; Garces, L. J.; Gomez, S.; Durand, J. P.; Suib, S. L. Particle size control of cryptomelane nanomaterials by use of H2O2 in acidic conditions. *Chemistry of Materials* **2005**, *17*, 1910–1918.

(2) Simanova, A. A.; Kwon, K. D.; Bone, S. E.; Bargar, J. R.; Refson, K.; Sposito, G.; Pena, J. Probing the sorption reactivity of the edge surfaces in birnessite nanoparticles using nickel(II). *Geochimica et Cosmochimica Acta* **2015**, *164*, 191–204.

(3) Liu, W.; Sun, B.; Qiao, J.; Guan, X. Influence of pyrophosphate on the generation of soluble Mn (III) from reactions involving Mn oxides and Mn (VII). *Environmental Science & Technology* **2019**, *53*, 10227–10235.

(4) Elsner, M.; Zwank, L.; Hunkeler, D.; Schwarzenbach, R. P. A new concept linking observable stable isotope fractionation to transformation pathways of organic pollutants. *Environmental Science & Technology* **2005**, *39*, 6896–6916.

(5) Jochmann, M. A.; Schmidt, T. C., *Compound-specific stable isotope analysis*; Royal Society of Chemistry: 2015.

(6) Barja, B. C.; Herszage, J.; dos Santos Afonso, M. Iron(III)–phosphonate complexes. *Polyhedron* **2001**, *20*, 1821–1830.

(7) Hameka, H. F.; Carrieri, A. H.; Jensen, J. O. Calculations of the Structure and the Vibrational Infrared Frequencies of Some Methylphosphonates. *Phosphorus, Sulfur, and Silicon and the Related Elements* **2006**, *66*, 1–11.

(8) Juribasic, M.; Tusek-Bozis, L. Spectroscopic and DFT study of 3-quinolyl-α-aminophosphonates. *Journal of Molecular Structure* **2009**, *924-926*, 66–72.

(9) Elsner, M. Stable isotope fractionation to investigate natural transformation mechanisms of organic contaminants: principles, prospects and limitations. *Journal of Environmental Monitoring* **2010**, *12*, 2005–2031.

Danksagung

Zuallererst möchte ich Prof. Stefan Haderlein für die Möglichkeit danken, meine Doktorarbeit unter seiner Betreuung schreiben zu dürfen. Vielen Dank für das Vertrauen, welches du mir über all die Jahre entgegen gebracht hast, für das Teilen deiner Erfahrung, sowie für die stete Erreichbarkeit und Bereitschaft für Diskussionen von Daten und Texten. All dies hat entscheidend zum erfolgreichen Abschluss meiner Arbeit beigetragen.

Prof. Torsten Schmidt danke ich vielmals für die Übernahme der Zweitbegutachtung meiner Arbeit.

Prof. Olaf Cirpka und Prof. Christian Zwiener möchte ich für die Bereitschaft danken, meiner Verteidigung als Prüfer beizuwohnen.

Dr. Daniel Buchner danke ich vielmals, durch meine Aufnahme in den Club der schweren Isotope und die darauf folgende Ansteckung mit seinem Fable für CSIA und Messgeräte im Allgemeinen, maßgeblich den Weg für diese Arbeit geebnet zu haben. Zudem waren dein Enthusiasmus, deine stete Bereitschaft „nochmal mit aufs Gerät zu schauen“(auch wenn die Zeit knapp war) und deine kritischen Anmerkungen zu Daten und Texten eine außerordentliche Hilfe.

Dr. Maik Jochmann möchte ich zunächst natürlich dafür danken, uns auf die Idee gebracht zu haben, an Phosphonaten zu arbeiten und die sofortige Begeisterung, in das Projekt mit einzusteigen. Darüber hinaus danke ich dir vielmals für deine überragende telefonische Erreichbarkeit und die erhellenden Gespräche, egal ob über Isotopenanalytik, Chemie im Allgemeinen, oder Rick & Morty.

Prof. Martin Elsner danke ich vielmals für die äußerst angenehme und sehr lehrreiche Zusammenarbeit am (nicht enden–wollenden) „Mangan2“–Kapitel.

Ganz besonderen Dank an meinen (wie du es so schön in deiner Danksagung nanntest) Weggefährten Dr. Johannes Scheckenbach. Da ich es nicht passender als du damals ausdrücken könnte, möchte ich dir in Kürze einfach nur für die TOP Zeit zusammen danken, egal ob im Labor beim Reparieren von Geräten, bei den Mittagspausen mit obligatorischer Käseseele und (viel zu starkem) Kaffee, bei der Umschulung zur Gründung von *Büsing & Martin Umzüge GmbH*, oder beim Feierabend–/ Konzertbier.

Vielen Dank an alle Studentinnen, die ich im Laufe meiner Arbeit betreuen durfte und mir bei der Durchführung der Versuche eine große Hilfe waren: Melanie Schüßler, Stefanie Graaf, Swarada Badwe, Tamara Pruneddu und Larissa Werle.

Allen aktuellen und ehemaligen Mitgliedern der Umweltmineralogie und –chemie Arbeitsgruppe, vor allem Monika Hertel, danke ich für die angenehme Arbeitsatmosphäre und Hilfsbereitschaft in den letzten Jahren.

Des Weiteren möchte ich allen (ehemaligen) Mitgliedern des Laborteams der Ebene 4 danken: Sara Cafisso, Bernice Nisch, Stefanie Nowack, Renate Seelig, Annegret Walz und Dr. Thomas Wendel. Vielen Dank, dass ihr immer mit Rat & Tat zur Stelle wart und somit das Arbeiten im Labor wesentlich erleichtert habt.

Daniel Köster, Tobias Hesse und Robert Marks (Instrumentelle Analytische Chemie, Essen) danke ich vielmals für die Einführung in die LC–IRMS Kopplung, das Bereitstellen von Säulen & Standards, die Durchführung der EA–IRMS Messungen und natürlich nicht zuletzt für spannende und hilfreiche Diskussionen. Vielen Dank an Natalia Jakus und Lars Grimm (Geomikrobiologie, Tübingen) für die Durchführung der XRD und BET Messungen.

Meiner Lebensgefährtin Charlotte Henkel danke ich über alle Maßen für die mentale Unterstützung in den letzten Jahren, welche maßgeblich zur Aufrechterhaltung meiner Motivation beigetragen haben. Zudem danke ich dir vielmals für das Korrekturlesen der Arbeit.

Zuletzt gilt mein herzlicher Dank natürlich meinen Eltern Elke Bruns & Uli Martin, sowie meiner Großmutter Lissy Weinert für die stete Unterstützung vor und während meiner Zeit in Tübingen.